TUDelft

Delft University of Technology

Mitigating the autogenous shrinkage of ultra-high performance concrete by using rice husk ash

Huang, H.

Important note
To cite this publication, please use the final published version (if applicable).
Please check the document version above.

Mitigating the Autogenous Shrinkage of Ultra-high Performance Concrete by Using Rice Husk Ash

Dissertation

for the purpose of obtaining the degree of doctor
at Delft University of Technology
by the authority of the Reactor Magnificus prof.dr.ir. T.H.J.J. van der Hagen
chair of the Board for Doctorates
to be defended publicly on
Monday 19 June 2023 at 15:00 o'clock

by

Hao HUANG

Master of Engineering in Materials Engineering, Wuhan University of Technology, China
born in Hubei, China

This dissertation has been approved by the promotors:

Composition of the doctoral committee:
Rector Magnificus,   chairperson
Prof. dr. ir. K. Van Breugel   Delft University of Technology, promotor
Dr. G. Ye   Delft University of Technology, promotor

Independent members:
Prof. W. Chen   Wuhan University of Technology, China
Prof. dr.ir. G. De Schutter   Ghent University, Belgium
Prof. dr.ir. E. Schlangen   Delft University of Technology
Dr. ir. M. Lukovic   Delft University of Technology
Dr. T. Nguyễn Văn   Hanoi University of Civil Engineering, Vietnam
Prof. dr. H.M. Jonkers   Delft University of Technology, reserve member

Printed in the Netherlands

May you pursue the truth throughout the whole lifetime.

Acknowledgements

Yang), Dr. Wenjuan Lyu, Dr. Zhenming Li, Dr. Shizhe Zhang, Dr. Boyu Chen, Yun Chen, Luiz Cezar Miranda de Lima Junior, Albina Kostiuchenko, Xuhui Liang, Zhiyuan Xu, Chen Liu, Yu Zeng, Hu Shi, Dr. Marija Nedeljkovic, Dr. Natalie Mühleisen, Renée Mors, Patrick Holthuizen, Dr. Farhad Pargar, Dr. Ze Chang, Dr. Shi Xu, Dr. Yu Chen, Dr. Shan He, for those cherished moments and supporting.

I would also like to thank Na Zhu and Henk van Koppen for their endless concern and support. Special thanks to Prof. dr. ir. Jansen, K.M.B. (TU Delft), for his helps in desorption isotherm test.

I am deeply thankful to my parents, for their love, support, and sacrifices. Without them, I cannot finish my dissertation. This last word of acknowledgment I have saved for my dear wife Naheya and my lovely sons Xi He Huang and Muyan Huang, who shared my tear and happiness, gave me encouragement to finish my PhD work.

Hao Huang (黄 浩)

Delft, the Netherlands,

May 2023

Table of Contents

List of Figures

List of Tables

List of Symbols

Roman lower case letters

a, b	Constant	[-]
n, c	Rosin-Rammler distribution parameters	[-]
d	Diameter of pore	[μm]
d_0	Size of the smallest capillary pore	[μm]
$d_{w,j}$	Diameter of the maximum water-filled pore at time t_j	[m]
m_C	Mass of cement in a unit volume of cement paste	[g]
m_{CH}	Content of CH	[g]
m_{H_2O}	Weight loss comes from the loss of water	[g]
m_{RHA}	Initial mass of RHA in cement-RHA mixture	[g]
p_{Hg}	Pressure of mercury	[MPa]
p_j	Capillary pressure	[Pa]
t_j	Time at step j	[h]

Roman capital case letters

A, B	Constant	[-]
C_{CH}	Amount of CH in a mixture	[g/g]
$C_{CH,hyd}$	Amount of CH formed in the hydration process	[g/g]
$C_{CH,poz}$	CH-content consumed in the pozzolanic reaction	[g/g]
$C_{CH,mea}$	Amount of CH measured by TGA	[g/g]
C_{SiO_2}	Silica content of RHA	[-]
D_{50}	Mean particle size	[μm]
E_S	Elastic modulus of the steel ring	[GPa]
K_0	Initial penetration rate of the reaction front of a hydrating cement particle	[μm/hour]
M_{dry}	Mass of RHA sample after drying	[g]
M_{wet}	Mass of wet RHA sample	[g]
M_S	Molar mass of SiO_2	[g/mol]

M_{CH}	Molar mass of $Ca(OH)_2$	[g/mol]
Q	Water absorption capacity of RHA	[-]
R^2	Coefficient of determination	[-]
RH_j	Relative humidity at time t_j	[%]
R	Universal gas constant	[J/mol/K]
R_{IC}	Inner radius of the specimen	[cm]
R_{IS}	Inner radius of the steel ring	[cm]
R_{OC}	Outer radius of the specimen	[cm]
RH_D	Relative humidity of the pore solution without the effect of dissolution of salts (like deionized water)	[%]
$RH_{pa,j+1}$	Relative humidity of the cement paste after the moisture transport at time t_{j+1}	[%]
$RH_{RHA,j+1}$	Relative humidity of RHA after the moisture transport at time t_{j+1}	[%]
RH_S	Relative humidity of the pore solution due to the dissolution of salts	[%]
S_{cap}	Water saturation level in capillary pores	[-]
$S_{cap,pa,j+1}$	Water saturation degree in the capillary pores of the cement paste at time t_{j+1}	[-]
$S_{RHA,j}$	Water saturation degree in the still unreacted cores or remaining RHA particles at time t_j	[-]
T	Temperature	[K]
T_0	Mid-point on the temperature axis in the TG curve	[°C]
$V_{cap\_wat,pa,j+1}$	Amount of capillary water in cement paste after moisture transport at time t_{j+1}	[cm^3]
$V_{ce}(0)$	Original volume of cement	[cm^3]
$V_{ce}(t)$	Volume of unreacted clinker from the image analysis at the age t	[cm^3]
$V_{\leq d}$	Capillary pore volume with size less than d	[cm^3]
V_m	Molar volume of water	[m^3/mol]
$V_{por,pa,j}$	Capillary pore volume at time t_j	[cm^3]
$V_{por,RHA,j+1}$	Pore volume of still unreacted RHA particles	[cm^3]
V_{RHA}	Original volume of RHA particles	[cm^3]
$V_{wat,pa,j}$	Total amount of water in cement paste at time t_j	[cm^3]
$V_{wat,poz}$	Water consumption in the pozzolanic reaction for 1 g fully reacted RHA	[cm^3]

$V_{wat,poz,j}$	Amount of water consumed in the pozzolanic reaction at time t_j	[cm^3]
$V_{wat,RHA,j+1}$	Remaining amount of water in RHA particles after moisture transport at time t_{j+1}	[cm^3]
$V_{wat \leq d_w,j}$	Amount of water in capillary pores with diameter $\leq d_{w,j}$ at time t_j	[cm^3]

Greek letters

α_C	Degree of hydration of cement	[-]
$\alpha_c(t)$	Degree of hydration of cement at the age t	[-]
$\dot{\alpha}$	rate of hydration	[-]
α_j	Degree of hydration of cement at time t_j	[-]
$\dot{\alpha}_{j+1}$	Rate of hydration during the time step t_{j+1}	[-]
$\alpha_{RHA}(t)$	Degree of pozzolanic reaction of RHA at the age t	[-]
β_j	Degree of pozzolanic reaction of RHA at time t_j	[-]
γ	Surface tension of water	[N/m]
γ_{Hg}	Surface tension of the mercury	[mN/m]
δ_{tr}	Transition thickness of the shell of hydration products	[μm]
$\Delta\alpha_{j+1}$	Hydration increments of cement in time step Δt_{j+1}	[-]
$\Delta\beta_{j+1}$	Reaction increments of RHA in time step Δt_{j+1}	[-]
Δt_{j+1}	Time step $j+1$	[h]
$\Delta V_{wat,hyd,j+1}$	Water decrement in the cement paste due to cement hydration in time step Δt_{j+1}	[cm^3]
$\Delta V_{wat,j+1}$	Amount of water for moisture transport in time step Δt_{j+1}	[cm^3]
$\Delta V_{wat,pa,j+1}$	Change of amount of water in cement paste in time step Δt_{j+1}	[cm^3]
$\Delta V_{wat,poz,j+1}$	Water decrement in RHA particles due to pozzolanic reaction in time step Δt_{j+1}	[cm^3]
$\Delta V_{wat,pozC,j+1}$	Amount of water consumed by chemical reaction (pozzolanic reaction) in time step Δt_{j+1}	[cm^3]
$\Delta V_{wat,rec}$	Amount of water received by the system with low RH	[cm^3]
$\Delta V_{wat,rec,j+1}$	Amount of water received by the system with low RH in time step Δt_{j+1}	[cm^3]
$\Delta V_{wat,rel}$	Amount of water released by the system with high RH	[cm^3]

$\Delta V_{wat,\,rel,j+1}$	Amount of water released by the system with high RH in time step Δt_{j+1}	$[\text{cm}^3]$
$\Delta V_{wat,reRHA,j+1}$	Amount of water entrained in the volume of RHA that has reacted in time step Δt_{j+1}	$[\text{cm}^3]$
$\Delta V_{wat,\,RHA,j+1}$	Total decrease of the amount of water in remaining RHA particles in time step Δt_{j+1}	$[\text{cm}^3]$
$\Delta \delta_{in,x_i,j+1}$	Incremental increase of the penetration depth of the reaction front of cement particle x_i during a time increment Δt_{j+1}	$[\mu m]$
$\varepsilon_s(t)$	Strain measured in the steel ring at time t	$[\text{mm/m}]$
θ	Contact angle	$[\text{-}]$
θ_{Hg}	Contact angle between the mercury and the pore wall surface of the cement paste	$[\text{-}]$
λ	Coefficient to control the types of reaction	$[\text{-}]$
ρ_{ce}	Density of cement	$[\text{g/cm}^3]$
ρ_w	Density of water	$[\text{g/cm}^3]$
$\sigma_{c,max}$	Maximum tensile stress in shrinking specimen	$[\text{MPa}]$
$\emptyset_{pore,RHA}$	Porosity of RHA particles	$[\text{-}]$
$\Omega_1, \Omega_2, \Omega_3$	Reduction factors allowing for the change of water distribution and change in pore water chemistry in the system	$[\text{-}]$

List of abbreviations

ACI	American Concrete Institute
ASTM	American Society for Testing and Materials
BET	Brunauer-Emmett-Teller
BSE	Back-scattered electrons
CEN	European Committee for Standardization
CH	Calcium hydroxide
C-A-H	Calcium aluminate hydrate
C-S-H	Calcium silicate hydrate
DoH	Degree of hydration
EN	European standards
ESEM	Environmental Scanning Electron Microscope
HP	Hydration products
HPC	High performance concrete
LOI	Loss on ignition
LVDTs	Linear variable differential transformers
MIP	Mercury intrusion porosimetry
PCSIR	Pakistan Council of Specific and Industrial Research
RH	Relative humidity
RHA	Rice husk ash
RPC	Reactive powder concrete
SAPs	Super-absorbent polymers
SF	Silica fume
SP	Superplasticizer
TGA	Thermogravimetric analysis
TSTM	Temperature Stress Testing Machine
UHPC	Ultra-high performance concrete
UPV	Ultrasonic pulse velocity
wt%	Weight percentage
w/b	Water-binder ratio
w/c	Water-cement ratio
XRD	X-Ray diffraction

Chapter 1

Introduction

1.1 Research background

Ultra-high performance concrete (UHPC) shows excellent ductility, high compressive strength and durability. However, it can develop large shrinkage strains. A very high autogenous shrinkage may already develop in the first one or two days after mixing. This points to a considerable probability of cracking at early ages. Such early-age cracking due to restrained autogenous shrinkage tends to negate the many advantageous properties of UHPC and significantly limits its utilization in construction. The very high autogenous shrinkage of this concrete is caused by the very low water-binder ratio and very high amount of silica fume (SF) used, which cause a significant drop in the internal relative humidity (RH) in the cement paste during hardening. The self-desiccation occurs in the absence of any exchange of moisture with the environment.

   Reducing or limiting the autogenous shrinkage of UHPC is very important for the engineering practice. A report by Castro et al. [1] shows that mitigation of autogenous shrinkage using external water curing is not effective, since the very dense microstructure of HPC/UHPC enables only a very small amount of water to penetrate into the interior of concrete members (see also Figure 1.1). With internal curing, whole concrete members can be cured by well-distributed water reservoirs inside the concrete. Thus, internal water curing is considered to be an effective solution to counteract self-desiccation and autogenous shrinkage, thereby reducing the likelihood of early-age cracking.
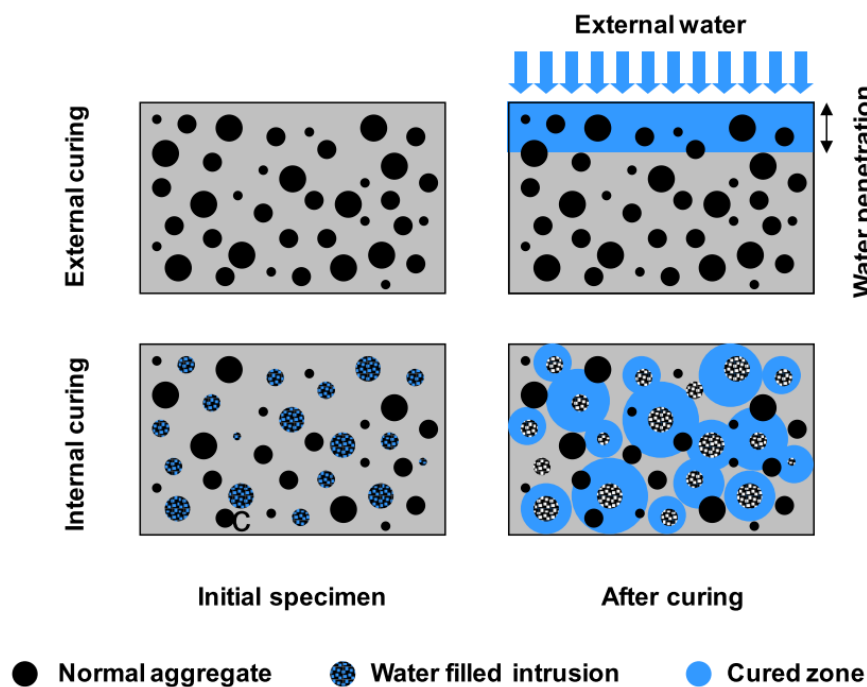
Figure 1.1 The difference between external curing and internal curing [1]

The most common methods for internal curing of concrete are the use of saturated light-weight aggregates and super-absorbent polymers (SAPs). Unfortunately, because of the strict requirements on mechanical properties and maximum size of aggregate, light-weight aggregates are not applicable in UHPC. Only SAP has been proposed as an efficient internal curing agent to mitigate the autogenous shrinkage of UHPC. It has been shown that the use of SAPs also works in practice. However, SAPs make the concrete more heterogeneous,

because it will leave voids in the matrix as big as 600 μm [2], equal to the maximum size of fine aggregate of UHPC [3], which might negatively influence the properties of UHPC.

Searching for an alternative internal curing method of UHPC remains a challenge. One of the very interesting questions is whether any material could play 'a duplex role', to replace both SF and SAPs to make UHPC. Finding such a material would mean a great breakthrough from both the technological and sustainability point of view.

One possibility is to use rice husk ash (RHA), an agricultural waste, which is obtained by burning rice husk. Rice husk constitutes about one-fifth of the 759.6 million metric tons of rice paddy produced annually in the world (2018) [4]. When the husk is incinerated completely under appropriate conditions [5, 6] the residue, RHA, contains 90-96% amorphous silica. RHA is also classified in the same category of highly active pozzolans like SF [7]. RHA has a very high specific surface area ranging from 20 to 260 m^2/g [5], which is attributed to its porous structure [8, 9]. Although using RHA as supplementary material in cementitious mixtures has been proposed decades ago already [7], the research on its application for internal curing is still scarce.

From the perspective of reducing CO_2 emission, using RHA is also beneficial for the concrete industry. RHA itself is an environment-friendly material. RHA is obtained by ignition of rice husk following self-combustion. Although the incineration of rice husk releases CO_2, photosynthesis during rice production recycles the CO_2 into new crops. Besides, the replacement of cement by RHA lowers the clinker content of cement-based products, which reduces the CO_2 footprint of the concrete mix.

1.2 Aim and objective

In this research the possibility is investigated of using rice husk ash to substantially mitigate the autogenous shrinkage of UHPC and reduce its probability of cracking. With this aim, the objectives of this research are listed as follows:
1. To evaluate the effect of rice husk ash on autogenous shrinkage of cement pastes with the low water-binder ratio.
2. To investigate the mechanism of mitigating autogenous shrinkage of cement pastes with RHA.
3. To perform numerical simulations of internal curing in cement pastes with RHA.
4. To investigate the effect of rice husk ash on proneness to cracking due to autogenous shrinkage in UHPC.

1.3 Research strategy

To achieve these objectives, the strategy of this research is as follows:

There is a continuous debate on the onset of autogenous shrinkage. In view of its relevance to the practice, the onset of autogenous shrinkage will be re-evaluated. Plain Portland cement mixtures with different water-cement ratios will be used for experimental investigation.

The effect of the fineness and dosage of RHA on autogenous shrinkage of cementitious mixtures will be studied experimentally. The mechanism behind the effect of RHA on autogenous shrinkage will be explored.

To reveal the mechanism of mitigating autogenous shrinkage with RHA, several influencing parameters will be evaluated. These are: self-desiccation, sorption properties of RHA and the pozzolanic reaction of RHA.

A mesoscopic model will be established to simulate the internal curing process in cement pastes with RHA. Experimental results will be used for the evaluation of the proposed model.

The optimized dosage and particle size of RHA, which substantially mitigates the autogenous shrinkage of cement pastes, will be used in UHPC. The relevant properties, like autogenous shrinkage and proneness of cracking, will be evaluated.

1.4 Outline of this study

This thesis consists of eight chapters. The structure is shown in Figure 1.2.

1. Introduction and literature survey (Chapter 1-2)
2. Onset of autogenous shrinkage (Chapter 3)
3. Experimental and numerical study of the effect of RHA on the autogenous shrinkage of cement pastes (Chapter 4-6)
4. Effectiveness of RHA for mitigating autogenous shrinkage-induced cracking tendency in UHPC (Chapter 7)
5. Conclusions (Chapter 8)

In chapter 1 a brief introduction including background, objective, strategy and outline of this research is given.

In chapter 2 a literature survey is presented regarding UHPC, basic properties of RHA, autogenous shrinkage and internal curing mechanisms in cementitious materials.

In chapter 3 the onset of autogenous shrinkage is analysed in plain cement mixtures. Improved internal relative humidity measurements provide a clearer view on the development of self-desiccation.

In chapter 4 experimental results are presented showing the effect of content and particle size of RHA on the autogenous shrinkage of cement pastes. Information on materials and mixture design is provided.

In chapter 5, based on the experimental results, the pozzolanic reaction and the internal curing effect of RHA are discussed for revealing the mechanism of mitigating autogenous shrinkage in cement pastes.

In chapter 6 numerical simulations are performed to describe the internal curing process in the cement pastes with RHA. The results of numerical simulations are validated by the experimental results presented in chapter 4.

In chapter 7 the effect of RHA on the proneness to cracking in UHPC is evaluated. The results of internal relative humidity, autogenous shrinkage, strain development by ring test and compressive strength are presented.

In chapter 8 conclusions and prospects are drawn. Some suggestions for further work are presented.
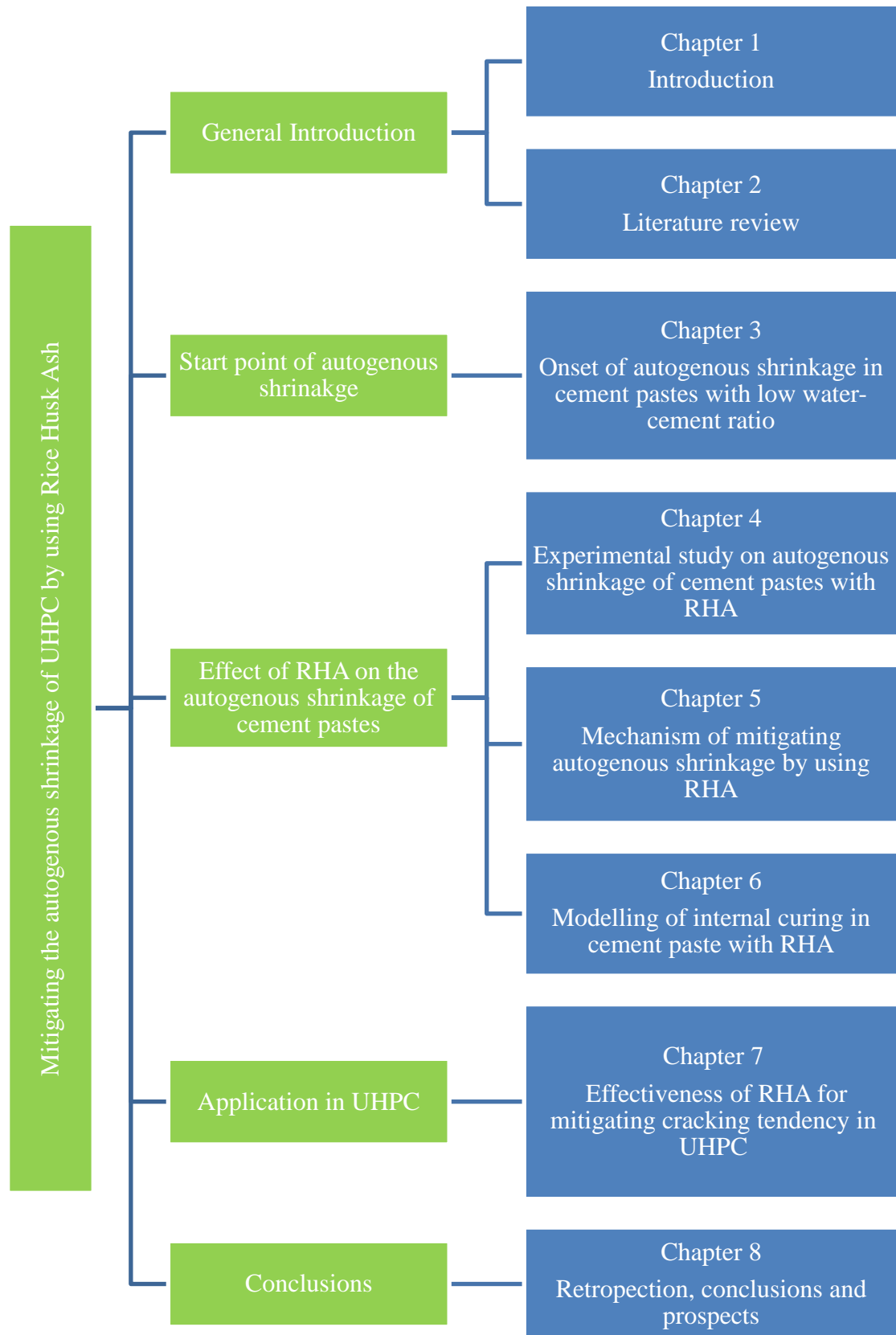
Figure 1.2 Outline of the thesis

Chapter 2

Literature review

2.1 Introduction

Since the development of Portland cement in England by Joseph Aspdin, in the early 19th century, it has become the most common material around the world as basic ingredient of concrete. Concrete made with Portland cement has good behaviour under compressive stress, but it is weak in tension. Cracking caused by tension is a typical problem in concrete practice. High shrinkage at early ages is one of the most common causes of cracking. In that stage shrinkage is strongly related to the decrease of relative humidity (RH) inside the concrete. For conventional concrete, moist curing from the exterior can ensure a high internal RH, thereby reducing the shrinkage. However, mixtures designed for high strength and long durability mostly have a low water-cement ratio (w/c) and dense microstructure. Thus, moisture from external curing cannot easily reach the interior of the concrete. Especially in high/ultra-high performance concrete, cracking caused by autogenous shrinkage can be a severe problem [10]. To minimize the cracking probability induced by autogenous shrinkage, internal curing has been proposed [11]. Several internal curing agents are utilized in high performance concrete and have shown good results for mitigating autogenous shrinkage [12]. Still finding alternative internal curing methods for ultra-high performance concrete remains a challenge. Rice husk ash (RHA), as a porous material, is a possible candidate for reducing the autogenous shrinkage in ultra-high performance concrete.

In this chapter, a literature review is presented regarding ultra-high performance concrete, the properties of RHA, autogenous shrinkage and internal curing.

2.2 Ultra-high performance concrete (UHPC)

2.2.1 Definition

Ultra-high performance concrete (UHPC) is a new class of concrete that has been developed in recent decades for its high strength and good durability. It is defined worldwide as a concrete with a compressive strength exceeding 150 MPa [13, 14]. Typically, the term UHPC has been used to describe a fibre-reinforced, silica fume-cement mixture with a very low water-cement ratio (w/c) produced with the use of superplasticizers, very fine quartz sand (0.15-0.60 mm) instead of ordinary aggregate.

The history of UHPC can be traced back to the early 1990s. Richard et al. [15] used components with increased fineness and reactivity to develop reactive powder concrete (RPC) via thermal treatment. RPC exhibits excellent mechanical properties. According to the author, it can achieve a compressive strength of up to 810 MPa and a flexural strength of up to 141 MPa. In 1994, De Larrard [16] formally introduced the term ''ultra-high-performance concrete''. Until now, the applications of UHPC (150-200 MPa) are widely available in Europe, North America, Oceania and Asia [13, 17, 18].

The basic principles used in UHPC have been identified by several authors [13, 15, 19, 20], and can be summarized as follows:
1. Increase of homogeneity by excluding coarse aggregates.
2. Increase of the packing density by ensuring a balanced particle size distribution of the powder.
3. Improvement of the properties of the matrix by adding a pozzolanic admixture, such as silica fume.
4. The use of a low water-binder (w/b) ratio.
5. Densification of the microstructure of the matrix by post-set heat treatment under pressure.
6. Increase of ductility by incorporating small-sized steel fibres.

Application of the above principles can lead to a concrete with a compressive strength exceeding 150 MPa. The addition of steel fibres improves both the tensile strength and the ductility [15].

2.2.2 Composition of UHPC

As mentioned in Section 2.2.1, UHPC is composed of the following materials: cement, sand, silica fume, fibers, water and superplasticizer. In this thesis the study concentrates on the characteristics of UHPC without fibers and heat curing. In the following the constituents of UHPC mixtures are described.

Cement A typical Portland cement (e.g., CEM I in Europe) or blended cements (e.g., CEM III in Europe) can be used in UHPC.

Sand Quartz sand is usually used in UHPC because of its wide availability, low cost and excellent bond with cement paste. The maximum particle size of sand is limited to 600 µm. Particle sizes below 150 µm are avoided in order to prevent interference with the largest cement particles (80-l00 µm) [15].

Mineral admixtures The addition of fine-grained minerals can improve many properties of concrete. The typical effects are denser packing and pozzolanic reactions. In both cases, the final impact on the pore structure of the mixture is similar: the concrete porosity decreases and the pore size distribution shifts towards smaller pore sizes.

Silica fume (SF) is an amorphous type of silica dust mostly collected in baghouse filters as a by-product of silicon and ferrosilicon production. SF is an ultra-fine powder with perfectly spherical particles. SF is the principal constituent of the new generation HPC and UHPC.

Despite its outstanding properties, SF also has several drawbacks. Firstly, SF is an industrial waste. However, its availability is limited, especially in developing countries. Secondly, SF also causes an aesthetic problem as it sometimes gives a dark colour to the concrete due to the unburned coal in it. Thirdly, because of the fine particle size (about 0.1-1 µm), SF is generally considered nuisance dust of low toxicity. The use and transport of SF require stringent safety measures to ensure human health.

The drawbacks of SF give a motivation for seeking other materials to replace it, especially in developing countries. To date, many micro-powders other than SF, such as pulverized fly ash, ground granulated blast furnace slag, metakaolin, limestone micro-filler and rice husk ash (RHA) have been studied to make UHPC [6, 21-24].

Superplasticizer Superplasticizers, also known as high-range water reducers, are additives used in the concrete industry. They are composed of powerful organic polymers that act as dispersers of particles in suspension to improve the rheological properties of concrete [25]. The addition of superplasticizer to concrete or mortar allows the reduction of the water-cement ratio without sacrificing the workability of the mixture. Since the water-binder ratio of UHPC is very low, the optimum amount of superplasticizer is relatively high, with a solid content of approximately 1.6 wt% of the cement content [15].

2.2.3 Shrinkage of UHPC

Shrinkage of concrete is caused by loss of water due to evaporation or by chemical reactions occurring during the hydration of cement [26]. It is one of the most common reasons for cracking of concrete. Autogenous shrinkage and drying shrinkage are two main types of shrinkage in concrete. Autogenous shrinkage is defined as 'the bulk strain of a sealed specimen of a cementitious mixture, not subjected to external forces and under constant temperature, measured from the time of final setting until a specified age' [27]. Drying

shrinkage refers to the volume reduction in the cement matrix or concrete element resulting from an overall loss of water to the environment through evaporation.

UHPC exhibits large shrinkage values, but, unlike normal concrete, autogenous shrinkage constitutes a bigger fraction of total shrinkage in UHPC compared with drying shrinkage [10].Drying shrinkage of UHPC can be mitigated effectively by exposure to a high external RH [28]. However, using external curing is inappropriate to reduce autogenous shrinkage. Because of the dense microstructure of the paste, only a small amount of water is able to penetrate into the interior of concrete [1]. UHPC shows a very high autogenous shrinkage already in the first few days after mixing (Figure 2.1), which may lead to cracking at early ages. Such early-age cracking due to restrained autogenous shrinkage may negate the numerous advantageous properties of UHPC and significantly limits its utilization in construction. The high autogenous shrinkage of UHPC is caused by a significant drop in the internal relative humidity (RH) during the hardening [11].
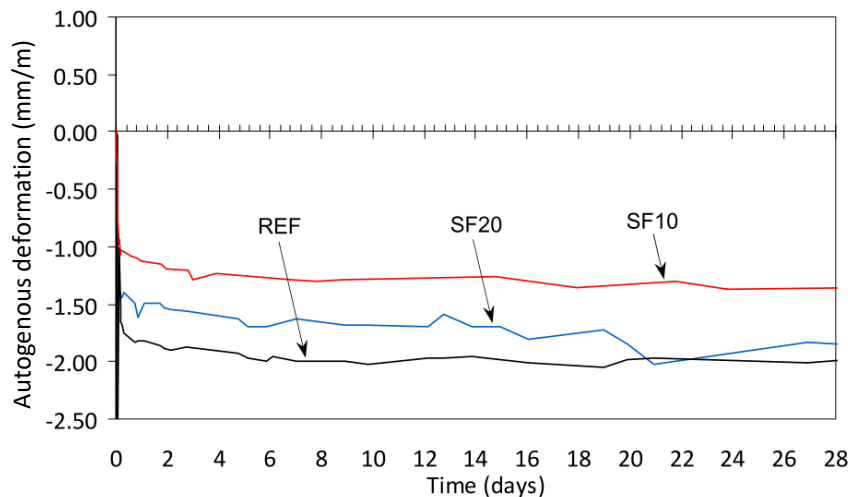
Figure 2.1 Autogenous shrinkage of UHPC mixtures containing different amounts of SF measured from the final setting time, w/b = 0.18 [6]

2.3 Rice husk ash (RHA)

Rice is one of the major crops grown throughout the world, sharing equal importance with wheat as the principal staple food and provider of nourishment for the world's population. Rice husks are the hard protective coverings of rice grains that are separated from the grains during the milling process. The husk constitutes about one-fifth of the 759.6 million metric tons of rice paddy produced annually in the world (2018) [4]. During rice cultivation, the bulky nature of rice husk could cause difficulty for storage and transportation. If the rice husk is not appropriately treated, such as dumping into ponds or streams, it becomes a massive quantity of waste and a severe polluter of the environment. One of the solutions is to burn the rice husks and use the ash as a mineral admixture in concrete. As a result, problems and costs associated with the environmentally safe disposal of this waste can be reduced or sometimes eliminated. The socio-economic benefits, achieved by the utilization of RHA as a mineral admixture in concrete, is now well recognized by all those concerned with the production, disposal and utilization of this waste. In this section, a brief overview of the properties of RHA and its the potential utilization in concrete will be presented.

2.3.1 RHA production

The utilization of RHA as a cementitious material in concrete industry depends on its pozzolanic properties. The pozzolanic activity of the ash depends on the form of silica present and the carbon content. Since the physico-chemical properties of silica in RHA are strongly affected by the temperature and the duration of thermal treatment, the yield of highly reactive ash requires a burning method that can maintain at low firing temperature and a short retention period to generate ash with low carbon content and high surface area [5, 29].

From every 100 kg of rice husk, about 25 kg (25%) of ash is generated when this husk is completely burnt. Rice husk contains about 50% cellulose, 25-30% lignin, 15-20% silica, and 10%-15% moisture [30]. After burning, cellulose and lignin are removed, leaving behind silica ash. Because the crystalline phase of silica has a negligible reactivity with lime, using RHA as a supplementary cementitious material requires that it contains amorphous silica. The amorphous silica content and the porous structure of RHA depend on the temperature and duration of burning, and the pre-treatment (acidification or alkalinization) of husk before combustion [5, 31]. Analysis of several reports, [5, 32], suggests that temperatures below 700°C will be sufficiently safe to produce rice husk ash with high reactivity.

There are several methods to incinerate rice husks to ash, such as the cyclone-type furnace developed by Mehta-Pitt in 1976, the fluidized bed system by Takuma, the tub-in basket type rice husk burner designed by Kapur in 1981, a brick incinerator by the Cement Research Institute of India, drum incinerator by the Pakistan Council of Specific and Industrial Research (PCSIR) in 1979, an annular kiln enclosure by Nair in 2006, and cylinder furnace by the National University of Malaysia (UKM) in 2011 [5, 33-36]. For using at a laboratory scale, Bui [5] utilized a modified drum incinerator similar to the one designed by PCSIR [33], which is also used by Tuan [6], to produce rice husk ash. It takes almost 15-18 hours for complete burning to generate quantities in the range of tens of kilograms of RHA. The husks burn by themselves once ignited. No control is required during the burning process. RHA samples are collected after the complete cooling of ash samples. An impression of the incinerator used by Tuan [6] is shown in Figure 2.2. The drum and detachable chimney of the incinerator were made from galvanized iron sheets. The husks are ignited from the bottom of the incinerator by using pieces of wastepaper. The highest temperature recorded in this incinerator was 600 ℃. The carbon content of the ashes was found to fluctuate from 2 to 6%.
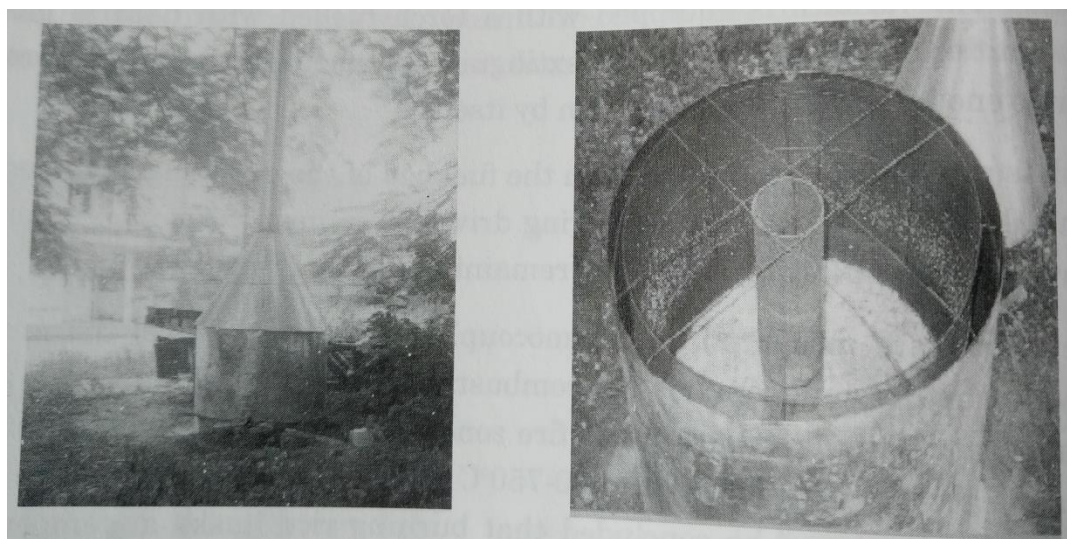
Figure 2.2 Modified PCSIR drum incinerator [5]

2.3.2 Microstructure and fineness of RHA

Upon combustion, the cellulose-lignin matrix of the rice husk is released, leaving behind a porous silica skeleton. The highly porous structure (see Figure 2.3) of the ash displays a large surface area. The specific surface area of RHA, determined by the Brunauer-Emmett-Teller (BET) nitrogen absorption method, ranges from 20 to 270 m^2/g [5], while that of SF is in the range of 18 - 23 m^2/g [37].
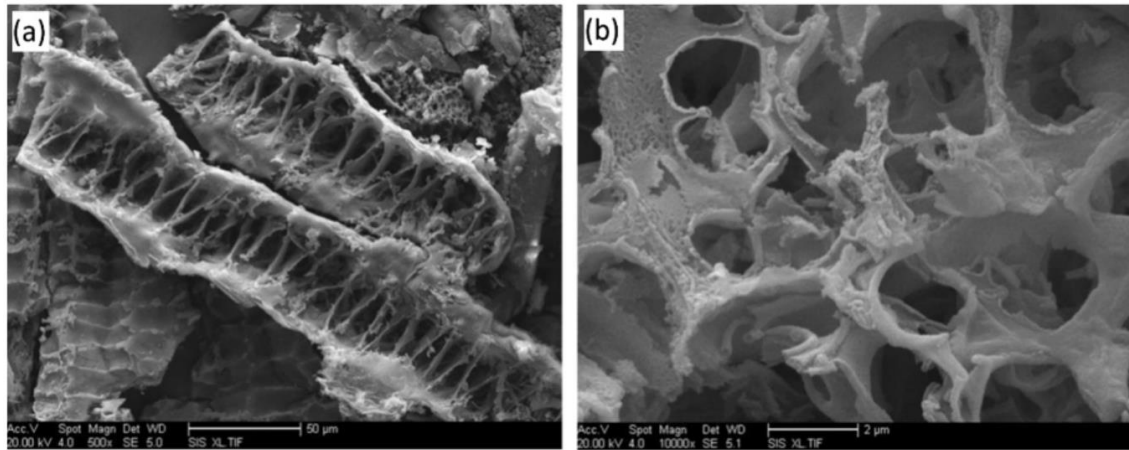
Figure 2.3 Scanning electron micrograph of RHA. (a) 500× magnification and (b)10000 × magnification [38]

Coupled with its high surface area, rice husk ash also displays a relatively big average particle size. While SF has a mean particle size of 0.1-1 µm [37], RHA has a particle size around 45 µm and a much higher surface area [39]. Mehta [9] suggested that, since the pozzolanic reactivity of RHA comes from its high internal surface area, grinding RHA to a high degree of fineness should be avoided. Intensive grinding causes a partial collapse of the porous structure of RHA particles, which leads to a reduction of the total pore volume [6]. Additionally, long periods of grinding reduce the economic benefits, especially in developing countries where electricity is relatively expensive and sometimes intermittent in supply [33]. This indicates that there is an appropriate fineness of RHA which is not only enhancing its pozzolanic reactivity, but also economically beneficial.

Concerning the porous structure of RHA, Sugita et al. [40] showed that the specific pore volume of coarse RHA is as high as 0.16 cm^3/g with pore sizes in the range of 2-40 nm, and an average radius of 12.3 nm. Tuan [6] found that the total pore volume of RHA with a mean particle size 5.6 µm is 0.086 cm^3/g determined by mercury intrusion porosimetry (MIP). The author reported that the size of pores is from 5 to 60 nm. Because of the high porosity, RHA has a high capacity for water absorption, which may adversely affect the fresh properties of mortar or concrete containing RHA.

2.3.3 Physical and chemical composition of RHA

The physical properties and chemical composition of RHA, as reported by several authors, are presented in Table 2.1 and Table 2.2, respectively.

Table 2.2 shows that RHA is very rich in silica and has a high alkali content (mainly K_2O). To use it as a pozzolan in cement and concrete, RHA should satisfy requirements for the

Table 2.1 Physical properties of RHA

Properties	Unit	Mehta 1992 [41]	Zhang 1996 [42]	Bui 2005 [43]	Ganesan 2008 [44]	Tuan 2011 [6]
Specific gravity	g/cm^3	2.06	2.06	2.10	2.06	2.10
Mean particle size	µm	-	-	5.0	3.8	7.30
Fineness (passing 45 µm sieve)	%	99	99	-	99	-
Specific area	m^2/g	-	-	-	36.47	19.2

Table 2.2 Chemical composition of RHA

Chemical component	[%] by weight			
	Mehta 1992 [41]	Zhang 1996 [42]	Bui 2005 [43]	Tuan 2011 [6]
SiO_2	87.2	87.3	86.98	87.96
Al_2O_3	0.15	0.15	0.84	0.3
Fe_2O_3	0.16	0.16	0.73	0.52
CaO	0.55	0.55	1.4	1.14
MgO	0.35	0.35	0.57	-
Na_2O	1.12	1.12	0.11	-
K_2O	3.68	3.68	2.46	3.29
SO_3	0.24	0.24	-	0.47
Loss on ignition (L.O.I)	8.55	8.55	5.14	3.81

chemical composition of pozzolans as stated in ASTM C618. For example, the total proportion of silicon dioxide (SiO_2), aluminium oxide (Al_2O_3) and iron oxide (Fe_2O_3) in the ash should be more than 70 wt%, and the loss on ignition (L.O.I) should not exceed 12% [45].

2.3.4 Hydration process of cement blended with RHA

The use of RHA will change the hydration process and microstructure development of Portland cement. Many researchers have explored the hydration mechanisms of cement blended with RHA [46-51]. They showed that RHA, containing a considerable amount of amorphous silica, can react with calcium hydroxide (CH) to form calcium silicate hydrate (C-S-H) gel. Due to the pozzolanic reaction, cement paste containing RHA has a lower CH content than plain cement paste. The hydration mechanism of cement paste with RHA has been illustrated as shown in Figure 2.4 (Hwang et al. [52]). The mechanism is described below.
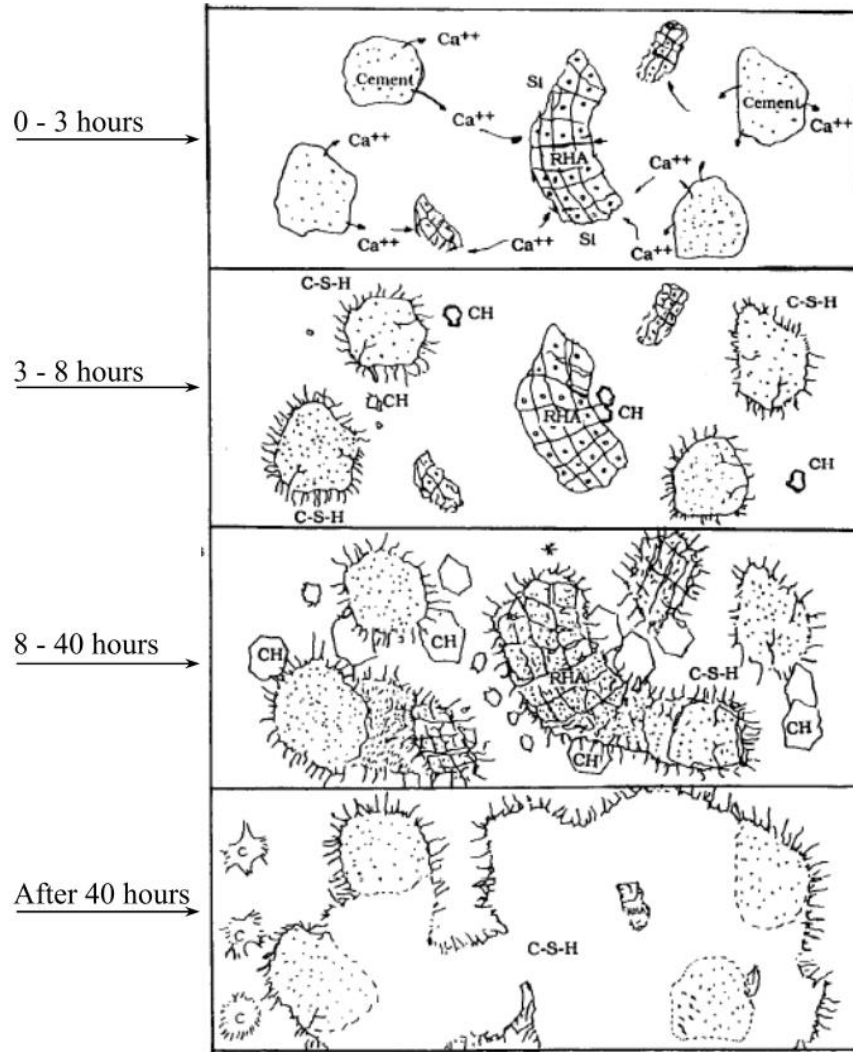
Figure 2.4 Schematic drawing of the hydration of cement paste containing RHA [52]

Similar to what is observed in hydrating Portland cement paste, a cement paste with RHA starts to stiffen in the early stage of hydration. Up to 8 hours the penetration resistance of the fresh cement paste with RHA measured in a Vicat test [52] goes along with the growth of CH. The early resistance against penetration of the Vicat needle is obtained primarily due to the formation of CH crystals. The formation of such crystals at the surface of RHA particles may be due to the adsorption of liquid at the surface of the cellular microstructure of RHA, followed by the pozzolanic reaction inside the cellular spaces of RHA. After 40 hours, the pozzolanic reaction further binds Si in RHA with CH to form the C-S-H gel. The reaction product of RHA fills the finer capillary pores and reduces the permeability, which may be beneficial for durability.

Because the chemical compositions of SF and RHA are similar (more than 90% is reactive silica), Tuan [6] assumed that the pozzolanic reaction of RHA is the same as that of SF. For the pozzolanic reaction it holds [53]:

$$1.1CH + S + 2.8H \rightarrow C_{1.1}SH_{3.9} \tag{2.1}$$

2.4 Autogenous shrinkage

Autogenous shrinkage of concrete is a phenomenon known since 1900 [54]. For a long time, autogenous shrinkage has always been considered negligible compared to drying shrinkage [55]. In the last three decades, much attention is given to autogenous shrinkage due to the increasing use of concretes with low water-binder ratios. Since then, autogenous shrinkage has become one of the main research topics.

2.4.1 Driving force of autogenous shrinkage

There is a general agreement about the existence of a relationship between autogenous shrinkage and RH changes in hardening cement paste [56-58].

When cement paste is in the liquid state, the chemical shrinkage due to cement hydration is fully transformed into external volume change [56]. This volume change does not induce a significant probability of cracking of the material [59, 60]. With ongoing hydration of cement, a "stable" solid skeleton is formed in the hardening paste. From then on, in sealed conditions, the chemical shrinkage cannot totally be transformed into an external volume change. Empty pores are thus formed inside the paste and water will withdraw into smaller pores. The menisci occur at the interface between air and water [61]. As the water is consumed by cement hydration, bigger pores inside the paste empty first [56]. This process is known as self-desiccation, which goes along with a drop in relative humidity.

Over the years, three principal driving forces of autogenous shrinkage have been proposed [62]. The three driving forces are listed below:

1. Change in the surface tension of the solid gel particles
2. Disjoining pressure
3. Tension in capillary water

2.4.1.1 Surface tension of solid particles

Surface tension results from the asymmetry of attractive forces on atoms or molecules in the vicinity of the solid surface [63]. Surface tension of solid particles is affected by the thickness of the water layer adsorbed on them. In general, adsorption of water at the particle surface causes relaxation of the surface tension of the hydration products and results in expansion. Reversely, removal of adsorbed water increases the surface tension and compresses the solid particles. Surface tension can induce compressive stresses of around 250 MPa and noticeable bulk shrinkage in small cement gel particles with large specific surface area [64]. Only the first three layers of adsorbed water play an important role in surface tension of the solid. The effect of layers of adsorbed water, i.e. 4th layer and 5th etc. layer, is almost negligible. The linear relationship between deformation and change of surface tension seems to exist as long as the relative humidity is below 40% [65]. This phenomenon is also observed by other researchers [66, 67]. In the construction practice, this mechanism may not play a major role in autogenous deformation, where normally the RH does not drop under 75% [68].

2.4.1.2 Disjoining pressure

The disjoining pressure is the distance-dependent pressure between two surfaces. It can be either attractive or repulsive. It is active in areas of hindered adsorption, i.e. where the distances between the solid surfaces are smaller than twice the thickness of the free adsorbed water layer, as shown in Figure 2.5.
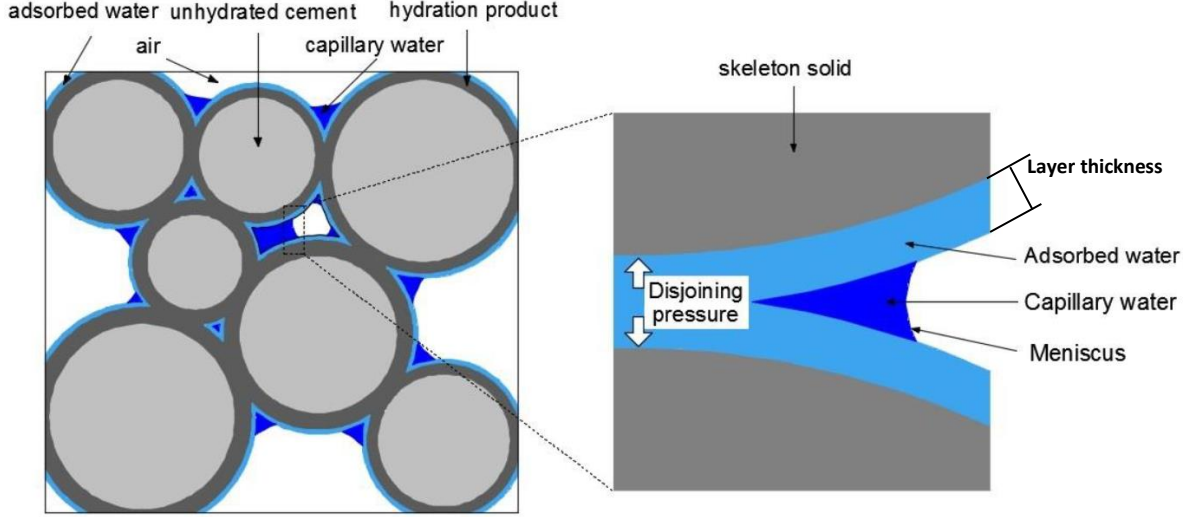
Figure 2.5 Surfaces of hindered adsorption and distribution of disjoining pressure [69]

The disjoining pressure between the solid particles is the result of van der Waals forces, double layer repulsion and structural forces [70]. Among these, van der Waals forces are always contractive, while double-layer repulsion and structural forces are always repulsive. Disjoining pressure changes with the thickness of the adsorbed water layer. This thickness is determined by the RH in the pore system. When the RH drops, the magnitude of disjoining pressure decreases, leading to shrinkage of the materials. For cement-based materials, the disjoining pressure also varies with the concentration of Ca^{2+} ions in the pore fluid [71].

Quantification of disjoining pressure is not easy. For simple geometries, it can be determined by contacting regular-shaped solid particles [72]. However, for the hardening cement paste at early ages, the continuous transformation of the microstructure and the shape of the particles complicates the quantification of the disjoining pressure and its associated volume changes. At which relative humidity range disjoining pressure is responsible for autogenous shrinkage is still a subject of debate [63, 73].

2.4.1.3 Capillary tension

The capillary tension in the pore fluid is related to the relative humidity in the partly empty pores. With the drop of internal RH, the radius of menisci between the liquid and the gas in capillary pores decreases and the capillary tension increases. The capillary tension in the capillary pores brings the surrounding solid into a state of compression. This compressive stress will result in a decrease of the volume of the cement paste. According to Soroka [64], the capillary tension mechanism for autogenous shrinkage is effective in the upper RH range, above about 45% RH.

From the diameter of the maximum water-filled pore $d_{w,j}$ at time t_j, the relative humidity RH_j and the capillary pressure p_j in the pore system of cement paste can be described by the Kelvin equation (Eq. (2.2)) and Young-Laplace equation (Eq. (2.3)), respectively. The equations are list below,

$$ln\, RH_j = \frac{4\gamma V_m \cos\theta}{d_{w,j}RT} \qquad (2.2)$$

$$p_j = \frac{4\gamma}{d_{w,j}} \qquad (2.3)$$

where γ is the surface tension of water (= $72.86 \times 10^{-3} \ N/m$), V_m is the molar volume of water (= $1.8 \times 10^{-5} \ m^3/mol$), $d_{w,j}$ is the pore diameter, R is the universal gas constant (= $8.314 \ J \cdot mol^{-1} \cdot K^{-1}$), T [K] is the temperature, θ is the contact angle, $\cos\theta = 1$ when perfect wetting is assumed.

Combine the Eq. (2.2) and Eq. (2.3), the relationship between relative humidity and capillary pressure at time t_j can be described by:

$$p_j = \ln RH_j \cdot \frac{RT}{V_m \cos\theta} \qquad (2.4)$$

2.4.2 Early age expansion

If a cement paste hydrates in saturated conditions, the reaction can go along with an external expansion, as observed already since 1900 by Le Chatelier [54]. According to Neville [74], values of 1000-2000 microstrain are measured for cement pastes cured under water. In those mixtures, generally with high water-cement ratio, the pore system of cement paste is supposed to remain saturated throughout hydration [74]. The expansion mechanism is complicated and unrevealed. Several possible mechanisms have been proposed in the past few decades to explain this expansion.

Crystal pressure. Crystal pressure generated by the crystallization of salts in capillary pores is a critical factor for the decay of rock, stone and concrete in urban areas [75]. In capillary pores filled with supersaturated solution, a crystal will grow and come into contact with a pore wall. The crystal will then stop growing or repel the pore wall while generating stresses. Crystal pressure is one mechanism proposed to explain the early-age expansion of cement paste. The most common solutes in the pore solution of hardening cement paste are portlandite (CH) and ettringite. The growth of these solutes (ettringite crystals [76, 77] and CH [78]) are considered a possible cause of early-age expansion in cement paste.

Structure change. Budnikov & Strelkov [79] proposed a different mechanism to explain early-age expansion. During hydration, the macroscopic cement particles convert into a number of much smaller hydrated particles through topochemical reactions. These smaller reaction products tend to occupy a larger volume than the original unhydrated particle, generating an internal pressure that produces macroscopic swelling.

Shape of hydration products and the formation of ettringite. Hydration products of cement are found with many shapes, like needles, rods and tree-shaped [80]. Due to the morphology of hydration products, a new network is formed with a total surface area larger than the reactants. The repulsive forces between the solid particles act on a growing surface area and cause an expansion [81]. The formation of ettringite has also been considered a principal reason for early-age expansion [82]. For a discussion of mechanisms causing early-age expansion, see also [83].

2.4.3 Onset of autogenous shrinkage

The schematic development of volume change in a sealed hydrating cement paste is presented in Figure 2.6. When cement paste is in the liquid state, the chemical shrinkage due to cement hydration is fully transformed into external volume change [56]. With ongoing hydration of cement, a "stable" solid skeleton is formed in the hardening paste. From that moment on, most of the chemical shrinkage is converted into voids inside cement paste and autogenous

shrinkage starts to develop. It can be seen in Figure 2.6 that the curves of chemical shrinkage and autogenous deformation start to deviate after the knee point.

In the past the knee point in the deformation curve has been termed "time-zero", and has been considered the onset of autogenous shrinkage. This "time-zero" has been assumed the time when the cement paste develops a "stable" solid skeleton to resist tensile stress [59]. However, there is a continuous debate on the methods for determining the "time-zero" in literature.
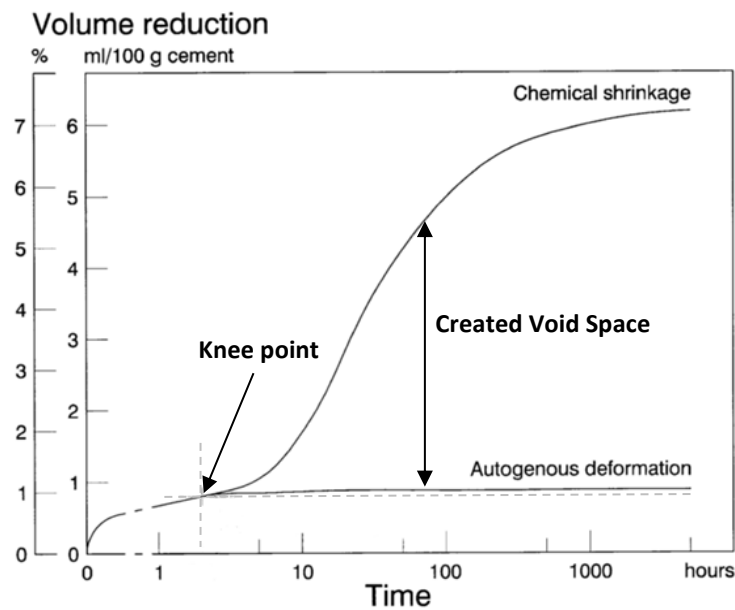
Figure 2.6 Schematic development of volume changes, which take place in a sealed cement paste system [56]

The ASTM C1698 [27] suggests to adopt the final setting time determined by Vicat apparatus as the "time-zero". Due to the arbitrariness of the Vicat penetration method, several researchers [84-87] have questioned the appropriateness of the final setting time as the "time-zero" for autogenous shrinkage. They believe that the penetration method like Vicat test cannot help to determine the "time-zero". Bentur [84] found the "time-zero" is roughly equal, but not identical, to the final setting time.

Researchers also tried to determine the time-zero by other approaches, like internal RH measurement. However, as the material is still in the super hygroscopic state (approximately in the range of 98%-100% of internal RH), measuring the RH change in early-age concrete by conventional hygrometer methods is very difficult. Thus, Miao et al. [85] developed a specific device for measuring the capillary tension within the paste or concrete and determined the "time-zero" from the observed capillary depression [85]. Besides the determination of "time-zero" by RH measurement, Darquennes et al. [86] proposed to adopt the moment of the second strain rate peak as "time-zero" (Figure 2.7). This moment would coincide with the moment stresses started to develop in a hardening concrete test in a TSTM (Temperature Stress Testing Machine).
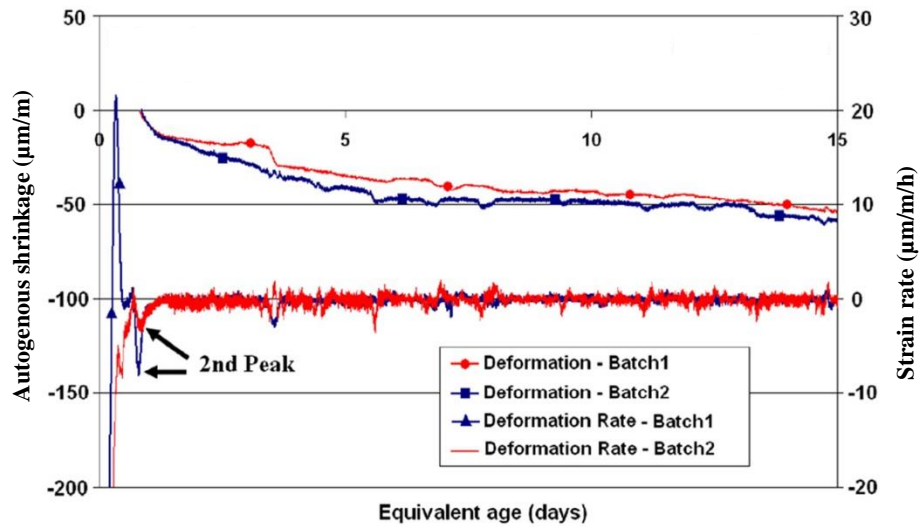
Figure 2.7 Evolution of the strain rate since casting time and the autogenous shrinkage expressed from the second maximal value of the strain rate of the CEM I mix [86]

The issue to the 'correct' moment from which autogenous shrinkage shall be measured will be further discussed in Chapter 3.

2.5 Internal curing

2.5.1 Introduction

Seeking methods to reduce or limit the autogenous shrinkage of HPC/UHPC is becoming very important for the engineering practice. Reports [1, 12] have shown that mitigation of autogenous shrinkage by applying *external* curing is not efficient (Figure 2.8), since the very dense microstructure of HPC/UHPC almost completely prevents water to reach the interior of concrete elements. Instead of external curing, *internal* curing is proposed to reduce autogenous shrinkage of low w/b ratio cementitious system. The definition of internal curing by of the American Concrete Institute (ACI) is: "supplying water throughout a freshly placed cementitious mixture using reservoirs, via pre-wetted lightweight aggregates, that readily release water as needed for hydration or to replace moisture lost through evaporation or self-desiccation [88]". The definition succinctly identifies the primary objective of internal curing is minimizing self-desiccation.
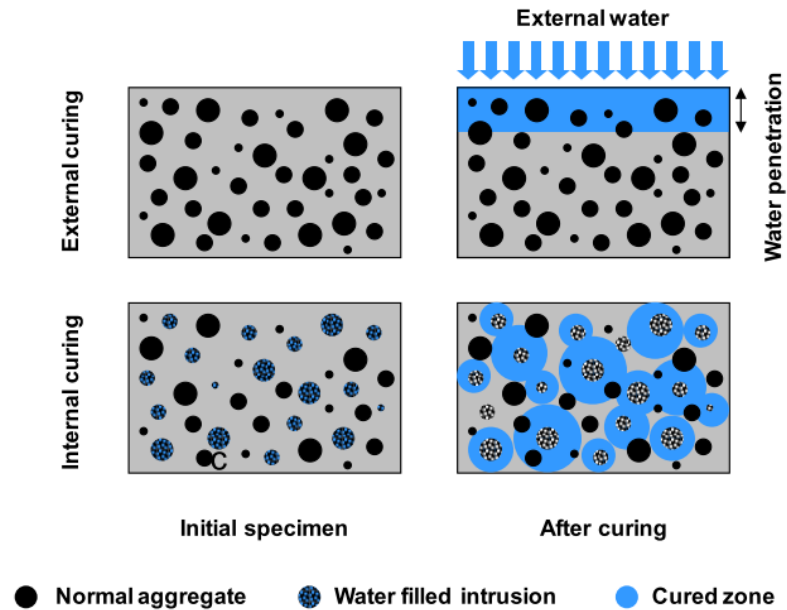
Figure 2.8 Illustration of the difference between external curing and internal curing [1]

2.5.2 Internal curing agent

The most common internal curing agents for concrete used in practice are saturated lightweight aggregates and super-absorbent polymers (SAPs) [89].

The application of natural lightweight aggregate in lightweight concrete dates back to Roman times [90]. However, the first published recognition of the internal curing potential of lightweight aggregates was likely that of Paul Klieger in 1957 [12]. By the mid-1990s, several research groups [91-93] investigated internal curing via the use of pre-wetted lightweight aggregates. In the years soon after that, implementation of other internal water reservoirs, such as super-absorbent polymers (SAP) [94] and pre-wetted wood fibres [95], was also investigated.

Both saturated lightweight aggregate [96] and SAP [94] can effectively reduce the self-desiccation of cementitious mixtures, hence mitigating autogenous shrinkage. However, because of strict requirements on mechanical properties and maximum aggregate size, lightweight aggregates are not always appropriate to be used as internal curing agent in UHPC. For that reason, to this date only SAP has been investigated as an internal curing agent in such class of concrete [2, 97]. Although the autogenous shrinkage of UHPC can almost be eliminated [98] by the addition of SAP, it may easily result in a heterogeneous concrete, leaving voids as big as 600 μm [2] (similar to the size of large sand particles), which might negatively influence the properties of UHPC.

Searching for internal curing methods of UHPC remains a challenge for researchers. A challenging question is whether or not a material can play 'a duplex role' to replace both SF and SAPs to make UHPC. If possible, such a material would yield a significant advantage in producing UHPC. As discussed in section 2.3, RHA is a potential candidate for this concrete class due to its porous structure and pozzolanic reactivity. Investigating the potential of RHA for mitigating autogenous shrinkage by internal curing is the research objective in this thesis.

2.5.3 Simulation of internal curing (conceptual)

To promote a wider application of internal curing of concrete in the engineering practice, a better understanding of phenomena taking place during internal curing is desired. Besides

various experimental methods [99], also numerical modelling has been employed to explore the mechanisms of water migration from internal water reservoirs to the surrounding maturing cement paste, thus improving the understanding of internal curing.

Research on numerical modelling of internal curing is still scarce. By utilizing a hygro-thermo-chemo-mechanical model [100], Wyrykowski et.al [101] simulated internal curing at the macroscopic level (e.g., strains of the material) from the point of view of water transport phenomena. In his simulations the assumption was made that in hydrating cement pastes self-desiccation is practically instantaneously compensated by water supplied from SAP in the hydrating paste. The results of his simulations suggest that the effect of SAP addition on reducing self-desiccation and autogenous shrinkage is adequately described by his model, both from a qualitative and a quantitative viewpoint. Note that SAP acts as water containers and that the material from which these 'containers' are made does not take place in the chemical reactions in the paste during hydration and are, therefore, not considered in Wyryskowski's model. However, if the material from which the water reservoirs are made are chemically reactive, as is the case with RHA that exhibits pozzolanic reactivity, the efficiency of internal curing will be influenced by the reaction of the material from which the water reservoirs are made. In that case, the simulation of internal curing should include the reactivity of the reservoir material.

2.6 Concluding remarks

This chapter provided a brief literature survey regarding autogenous shrinkage of UHPC, internal curing methods and a potential internal curing agent (RHA). Based on the currently available literature, the following state of the art can be made up.

- UHPC exhibits large autogenous shrinkage at early age because of its low w/b ratio and significant drop of RH during hydration. Such large autogenous shrinkage may lead to early-age cracking, which tends to negate the many advantageous properties of UHPC and a significant limitation for its utilization in construction.

- A relationship between autogenous shrinkage and self-desiccation in hardening cement paste is widely accepted.

- The time after mixing or casting, from which autogenous shrinkage becomes relevant, also called "time-zero" of autogenous shrinkage, is still under debate and needs further consideration.

- Internal curing is an efficient method to reduce autogenous shrinkage by counteracting the self-desiccation in hardening cement paste or concrete. Saturated lightweight aggregates and super-absorbent polymers are the two most commonly used internal curing agents in conventional concrete, but have limitations for application in UHPC.

- The porous structure of RHA allows its use as a water reservoir for internal curing, and its pozzolanic reactivity can act as a strength-enhancing agent in UHPC mixtures.

- Wyrykowski's modelling work shows that the internal curing process in cement mixture with SAP can be modelled quite accurately and could serve as a starting point for modelling internal curing using RHA.

Chapter 3

Onset of autogenous shrinkage in cement pastes with low water-cement ratio

3.1 Introduction

Autogenous shrinkage and self-desiccation of concrete are known phenomena since the year 1900 [54], but their practical importance has only been recognized in the last three decades. Although the main driving force of autogenous shrinkage is still in debate [62], a relationship between autogenous shrinkage and self-desiccation in hardening cement paste is widely accepted [56-58].

The term "time-zero" is introduced by researchers to represent the onset of autogenous shrinkage, which is defined as the time when the cement paste develops a "stable" solid skeleton to resist tensile stress [59]. However, there is a continuous debate on the methods for determining the "time-zero".

The ASTM C1698 [27] mentions a set of standard methods to determine autogenous shrinkage and suggests to use the final setting time determined by Vicat apparatus as the "time-zero", i.e. the time from which autogenous shrinkage should be measured. As discussed in Chapter 2, several researchers [84-87] have questioned the appropriateness of the final setting time as the "time-zero" for autogenous shrinkage. Darquennes et al. [86] proposed to use the second peak in the strain rate – time diagram (see Figure 2.7) as "time-zero", and found that this "time zero" coincided with the time of first build-up of stresses in concrete specimens tested in the Temperature Stress Testing Machine (TSTM).
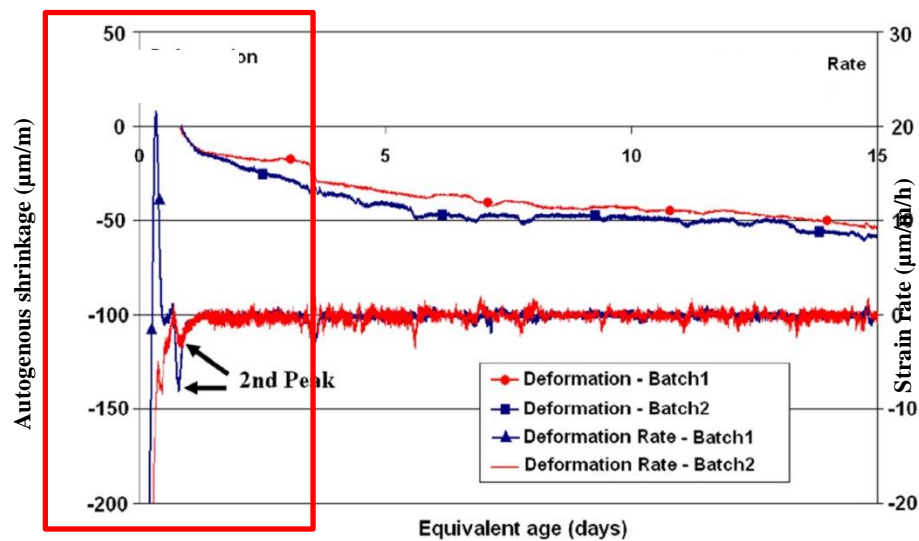
Figure 3.1 Evolution of the strain rate since casting time and the autogenous shrinkage expressed from the second maximal value of the strain rate of the CEM I mix [86]

Assuming a relationship between autogenous shrinkage and self-desiccation, measuring and monitoring the self-desiccation process and changes of the RH (relative humidity) might be helpful in the study of the onset of autogenous shrinkage. Measuring the RH in a hydrating cement paste, however, is not easy. In this study a modified hygrometer method[1] was used

---

[1] The typical procedure for measuring the internal RH is to place cement paste in a small, sealed, and thermostatic container. The internal RH of the cement paste is assumed to equilibrate with the air inside the container, which in turn is measured by a humidity sensor [56]. In practical terms, 100% internal RH is easily reached very soon after casting, that is, up to several hours after mixing. According to Raoult's law, the presence

for monitoring self-desiccation of the hydrating paste from a very early age (i.e., the stage before the final setting). In parallel the free strain of cement paste specimens cast in corrugated plastic tubes is measured according the procedure described in ASTM C1698-09 [27]. The hydration process of cement paste and stiffness development are determined by isothermal calorimetry and ultrasonic pulse velocity measurements, respectively.

3.2 Materials and methods

3.2.1 Materials

The materials used in this study were Portland cement (CEM I 52.5N) and a polycarboxylate-based superplasticizer (Glenium 51, Solid mass content 35%). Table 3.1 shows the properties of the cement. The mineral composition of cement was calculated by the modified Bogue equation [103] and is presented in Table 3.2. The particle size distribution of the cement is shown in Table 3.3. A superplasticizer was used for proper workability of the mixtures with low water-cement ratio. Four types of cement paste mixtures were made. The mixture proportion is listed in Table 3.4.

Table 3.1 Properties of cement

Components	Cement*
Chemical properties, % by weight	
CaO	64.0
SiO_2	24.0
Al_2O_3	5.0
Fe_2O_3	3.0
SO_3	2.4
Na_2O	0.3
K_2O	-
Loss on ignition (LOI)	1.3

* Data provided from the company

Table 3.2 The mineral composition of cement CEM I 52.5N, % by weight (calculated by the modified Bogue equation [103])

Compound	C_3S	C_2S	C_3A	C_4AF
Weight (%)	63.77	9.24	8.18	9.13

of ions decreases the saturated vapour pressure of the solution [62]. Hence, the internal RH of the pore solution in cement paste will not reach 100%. Moreover, the internal RH is extremely sensitive to temperature changes. According to the Bulletin of the American Meteorological Society [102], when RH is above 50%, every 1 °C difference in the dew point and dry bulb temperatures, the relative humidity decreases by 5%, starting with RH = 100% when the dew point equals to the dry-bulb temperature. It means that, in high RH environments, water vapour can easily condense (RH=100%) on the surface of a colder object. Assuming that the internal RH of cement pastes is 98% during the first few hours after mixing (which is also observed in experiments in this study), condensation can happen on the humidity sensor when the temperature of the humidity sensor is 0.4 °C lower than that of the water vapour. Because of this, the measurement of RH at a very early age is challenging. Especially if the hydration heat of cement is taken into account, the probability of condensation is even higher.

Table 3.3 Particle size distribution of cement

Cumulative passing, % by volume	Particle size, μm
0	0.14
10	1.95
20	4.26
30	6.58
40	9.47
50	12.93
60	16.98
70	22.18
80	29.12
90	41.25
100	59.17

Table 3.4 Mixture proportion of cement pastes

Sample	Water-cement mass ratio	Superplasticizer-cement mass ratio
Ref 0.28	0.28	0
Ref 0.28 SP	0.28	0.4%
Ref 0.25 SP	0.25	1.6%
Ref 0.18 SP	0.18	2.6%

3.2.2 Methods

3.2.2.1 Autogenous deformation test

The autogenous deformation of mixtures was measured following ASTM C1698-09 standard [27], inspired by the work of Jensen and Hansen [104]. Figure 3.2 shows the autogenous shrinkage test setup. After cement mixing, a corrugated tube of 440 mm (Ø28.5 mm) was carefully filled with fresh paste and sealed by plugs and sealing glue. Specimens and test instruments were immersed in a box filled with glycol, of which the temperature was regulated at 20 ± 0.1°C. The autogenous shrinkage of the specimens was recorded every 5 min with linear variable differential transformers (LVDTs). Three parallel samples were measured for each mixture. In all the tests, the autogenous deformation of parallel specimens had a similar trend with a deviation of less than 50 microstrains.

3.2.2.2 Internal RH measurement

The internal RH of cement paste was monitored by two Rotronic hygroscopic DT stations equipped with HC2-AW measuring cells. Similar devices were also used by Jensen [68]. The sample is poured into plastic vessels (dimension is 30 mm); the thickness of the test sample is less than 7 mm.
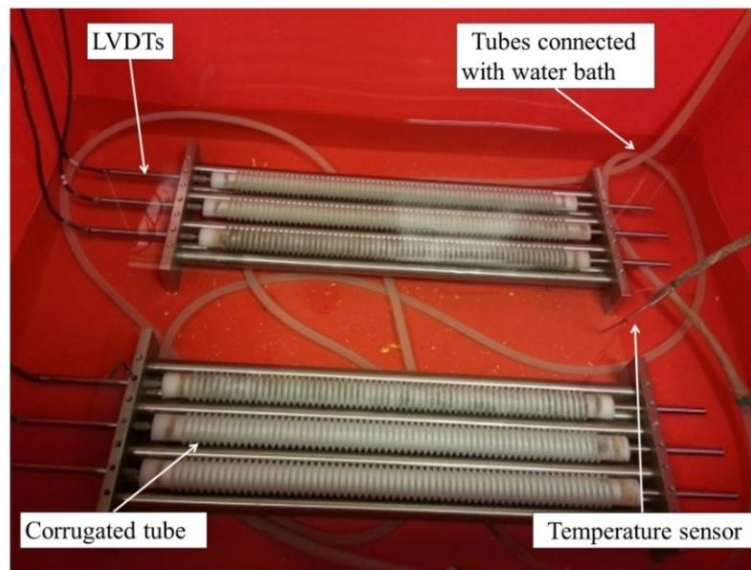
Figure 3.2 Autogenous deformation measurement (after [104])
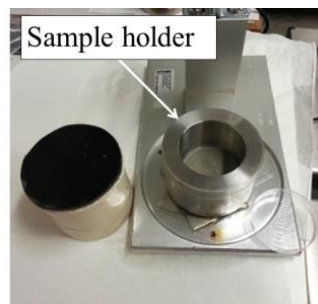
(a)
Casting in the sample holder
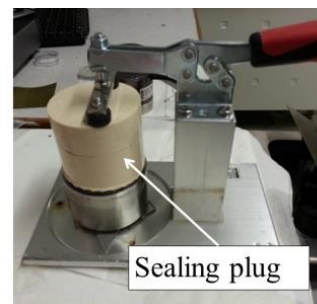
(b)
Sealing the sample holder and curing in
the test room at 20 °C for 0.5 h

(c)
Placing the sample holder in the water bath
for at least 0.5 h

(d)
Placing the humidity sensor (with slightly
higher temperature (20.3 °C)) on the
sample holder

Figure 3.3 Internal relative humidity test procedure

To avoid condensation on the humidity sensor in the very early stage (within one hour after mixing), a test procedure of internal RH measurement is developed. Subsequent steps of the test procedure are shown in Figure 3.3. The specimen was sealed in a sample holder by a sealing plug and put in a test room with a temperature of 20 °C for 0.5 h to achieve temperature equilibrium after mixing (Figure 3.3 (b)). The sample holder was kept in a sealed condition to prevent moisture loss. Due to the hydration heat of cement, the temperature of water vapour from cement pastes is a little higher than the temperature of the humidity sensor. Thus, the temperature of water bath is set at 19.0-19.5 °C (depending on the size of sample) for pre-cooling the cement pastes. Afterwards, the sealed sample and the sample holder were placed in the water bath for at least 0.5 h to achieve temperature equilibrium (Figure 3.3 (c)). Then the sealing plug was replaced by the humidity sensor to start the test (Figure 3.3 (d)).The humidity sensor was kept in a climate chamber at a slightly higher temperature (slightly higher than 20 °C, for example, 20.3 °C) before the test to avoid vapour condensation immediately after placing the sensor. The total time for the preparations before the test is about one hour. During the measurement, the humidity sensor was placed above the water bath, and the sample holder was immersed in the water bath. The temperature surrounding the humidity sensor was kept precisely at 20 ± 0.1 °C in a test room. So, the temperature of the humidity sensor is always higher than that of the pre-cooled pastes in the sample holder. The temperature variation of the humidity sensor is less than 0.1 °C during the whole measurement (Figure 3.4). In this way, the internal RH changes can be observed from the first hour after mixing, which was very hard to realize in test methods used by Jensen et al [68].
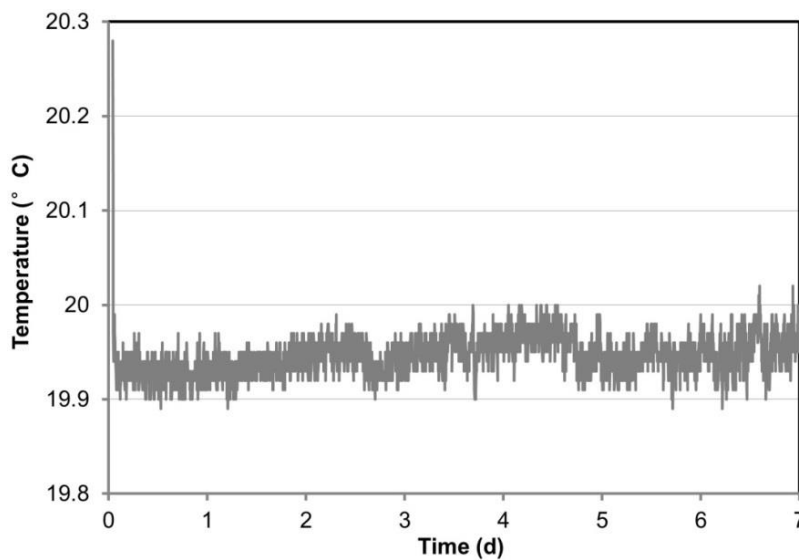
Figure 3.4 The variation of the temperature of humidity sensor in the internal RH test

The internal RH and the temperature of the water vapour in the specimen were continuously measured (every 3 min) for one week after mixing. For each mixture two samples were measured in parallel. The variation of RH measured in parallel samples was less than 0.5%. The results are presented as the average value of two parallel samples for each mixture. For calibrating the RH sensors three saturated salt solutions in the range of 65-95% RH were used before and after each test. The maximum measurement error of the RH sensors was $\pm 0.5\%$.

3.2.2.3   Setting time measurement

The final setting time of sealed specimens was determined with a Vicat apparatus (penetration method) according to the procedure described in standard EN 196-3 [105]. The diameters of the upper and bottom surface of the sample were 70 ± 1 mm and 80 ± 1mm, respectively. The height of the sample was 40 ± 0.2 mm. For avoiding moisture loss, both the sample and the mould were put in a sealed plastic box and stored in a chamber at 20 ± 0.1 °C during the period between the measurements in the Vicat apparatus.

3.2.2.4   Ultrasonic pulse velocity measurement

Ultrasonic pulse velocity (UPV) measurements were performed to monitor the development of a solid skeleton inside cement paste. The UPV technique is based on a pulse generating and transmitting transducer and a receiving transducer. When cement paste is subjected to a pulse vibration load, the longitudinal pulse transmitted to the paste is reflected at various solid-liquid interfaces or passes through the solid phase until it reaches the receiving transducer. With the development of cement hydration, the connection between cement particles leads to clusters that form a solid skeleton. The UPV increases with the development of this solid skeleton, as the stiffness of the cement paste largely depends on the connection of the solid phase [106].

The ultrasonic pulse velocity measurement was conducted with a portable ultrasonic non-destructive digital indicating tester. The ultrasonic transducers were integrated into a $150 \times 150 \times 200$ mm^3 steel mould. The frequency of the transducers was 54 kHz. The time was automatically recorded, and the ultrasonic pulse transition time was measured every 2 minutes for five days. The temperature of the steel mould with the sample is regulated at 20 ± 0.1 °C by using a cooling steel jacket. Two parallel samples were measured for each mixture. The test setup and test procedure are described in [107].

3.2.2.5   Heat evolution

The rate of heat evolution of cement paste was measured with an isothermal conduction calorimeter at 20 °C for five days. For each mixture three samples were measured in parallel. The test procedure followed the method proposed by CEN [108].

3.2.2.6   Mixing procedure

The mixing procedure followed the instruction given in ASTM C305-14. The measurements of autogenous shrinkage, internal RH and final setting time were performed on the same batch of cement pastes.

3.3   Experimental results and discussion

3.3.1   Free (autogenous) strain and internal RH change

The measured free (autogenous) strain of the reference mixture Ref 0.28 is shown in Figure 3.5. The strain was recorded starting one hour after mixing and then zeroed at the final setting time (t = 2.97 h, measured with the Vicat apparatus). From the measured strain in Figure 3.5 the *strain rate* is calculated and shown in Figure 3.6, together with the measured evolution of the internal relative humidity (RH) of cement paste.

Figure 3.5 shows that a significant part (more than 50%) of the autogenous shrinkage of mixture Ref 0.28 measured since final setting time (t = 2.97 h) in the first seven days occurred before the age of the specimen of 12 h. As shown in Figure 3.5, the autogenous shrinkage

curve shows a distinct "knee" at the age of about 12 h. At this knee point, the slope of the free strain curve changes significantly from very steep to more flat. This trend is further illustrated in Figure 3.6. After the second peak of the strain rate curve, the strain rate decreases to nearly zero, fluctuating within a narrow range between ± 50 (μm/m/h) at later ages. Similar results have been observed by Darquennes et al. [86].
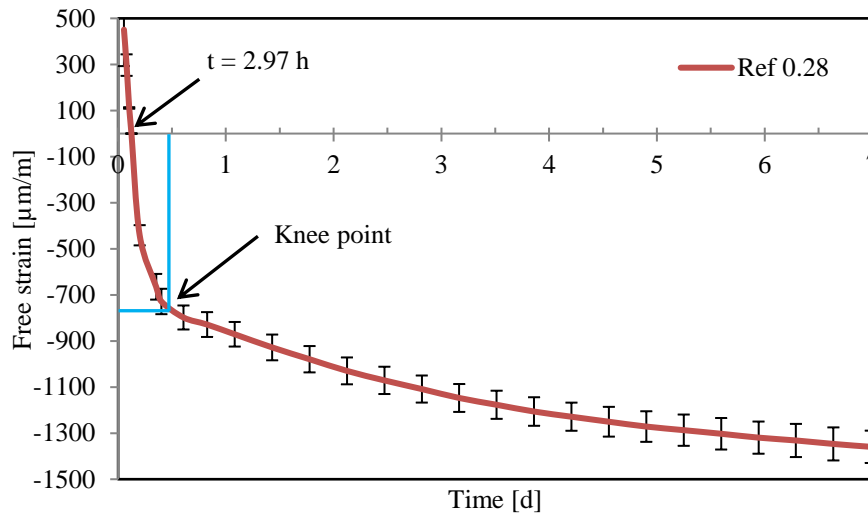
Figure 3.5 Free strain measured on the mixture (Ref 0.28) after casting. (The strain is zeroed at the final setting time, t = 2.97 h)
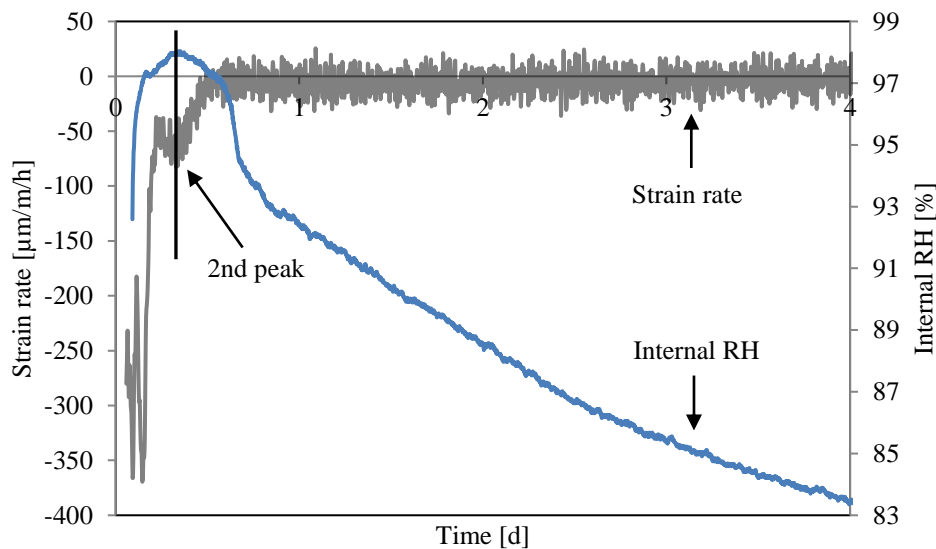
Figure 3.6 Comparison between the deformation rate of the free strain and the internal RH in the mixture (Ref 0.28), measured after casting

According to ASTM C1698 the final setting time should be considered as the onset of autogenous shrinkage ("zero time"), and would also represent the time at which a "stable" solid skeleton of reacted product in the cement paste has formed. After this "time-zero", the rigid skeleton is assumed to have sufficient stiffness to prevent chemical shrinkage from being fully transformed into external volume change. It was expected that the slope of the

deformation curve, shown in Figure 3.5, exhibits some changes due to change in the microstructure around the final setting time. However, Figure 3.5 shows that at that time the strain curve does not show any change. A substantial change in the slope of the strain curve is observed around a distinct "knee point in the strain curve in Figure 3.5 and at the 2nd peak of the strain rate curve in Figure 3.6. This indicates that at the final setting time (at t = 2.76 h), determined by the penetration method, does not reflect a significant microstructure change in the cement paste. Obviously, the skeleton of reaction products formed at the final setting time cannot be considered as a stable skeleton yet.

The precise internal RH measurement (without condensation) records the internal RH when the pastes are still in the super hygroscopic range (approximately 98% to 100% RH). As can be seen in Figure 3.6, the onset of the decrease of internal RH coincides quite well with the 2nd peak of the rate of free strain. According to the result of TSTM tests performed by Darquennes et al. [86], this 2nd peak represents the time of the first build-up of tensile stress to shrink. Because self-desiccation is the main cause of the autogenous shrinkage, the time of the first build-up of tensile stress in cement paste should coincide with the start time of self-desiccation. The observation in Figure 3.6 corroborates this point.

Figure 3.7 shows the evolutions of free strain and the internal RH of mixture Ref 0.28. The internal RH does not decrease until several hours after the final set, but remained at a high value. The internal RH starts to decrease at about 8.5 h after casting, which is very close to the "knee point" on the free strain curve.
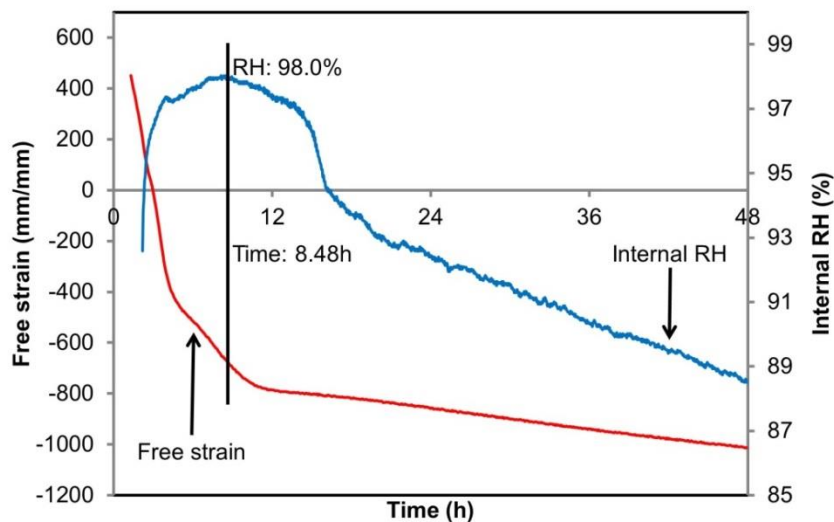
Figure 3.7 Comparison between the free strain and the internal RH of the mixture – (Ref 0.28), measured after casting. (The strain is zeroed at the final setting time, t = 2.97 h)

3.3.2 UPV and heat evolution

The results of ultrasonic pulse velocity measurements and the rate change of the ultrasonic pulse velocity of mixture Ref 0.28 are shown in Figure 3.8.

Figure 3.8 (a) shows that the UPV of mixture Ref 0.28 increases rapidly in the first 9 h after casting and then reaches a plateau. The rate change of the UPV in the first 24 h after casting, shown in Figure 3.8 (b), provides a clearer view for the plateau after 9h. The rate change of UPV slowly decreased until about 9 h after casting. After that, the rate of change of the UPV fluctuated within a narrow range between $\pm\ 0.05\ m/s^2$, which corresponds to the plateau of the UPV curve. The content and the connectivity of the solid phase in hydrating

(a) UPV for 120 h   (b) Rate of UPV for 24 h
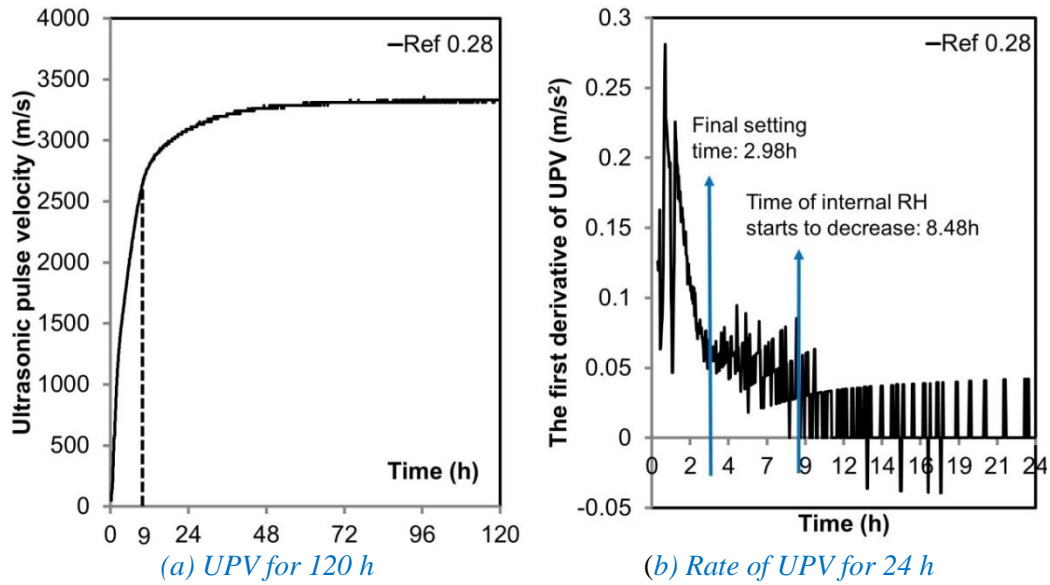
Figure 3.8 (a) Ultrasonic pulse velocity measured on the mixture (Ref 0.28) for 120 h after casting; (b) the rate of change of ultrasonic pulse velocity measured on the mixture (Ref 0.28) for 24 h after casting

cement paste determines the magnitude of UPV at early ages [106]. The result in Figure 3.8 indicates that a solid percolation path through the whole matrix has been formed after about 9 h hydration. After the formation of the solid path, the UPV can still further increase as shown in Figure 3.8 (a). However, the rate (first derivative) of UPV gradually approaches zero after 9 h hydration in Figure 3.8 (b).

The UPV result indicates that after a certain time of hydration a solid skeleton of cement paste has formed. At later hydration, this solid skeleton will give the cement matrix its stiffness and strength, and it can resist internal pore pressure caused by self-desiccation. However, whether this solid skeleton at certain time is a "stable" solid skeleton is not easy to determine with existing experimental tools. While considering the experimental difficulties, modelling of the connectivity of the solid phase in hydrating cement paste can be used as a reference. The modelling work will be performed in the next section.

3.4 Connectivity modelling

3.4.1 HYMOSTRUC 3D

The HYMOSTRUC 3D model [107, 109, 110] is developed to simulate the reaction process and microstructure formation in hydrating Portland cement. In this model, the degree of hydration is simulated as a function of the particle size distribution and chemical composition of cement, water-cement ratio and reaction temperature. With the help of HYMOSTRUC 3D, the microstructure development of cement pastes was simulated.

The hydration process and the microstructural development of a $100 \times 100 \times 100 \ \mu m^3$ cubic sample of cement paste was simulated. The water-cement ratio of the sample is 0.28, and the curing temperature is 20 °C. The simulated degree of hydration in HYMOSTRUC 3D was compared with the degree of hydration calculated from the heat evolution measurements. The rate of heat evolution of mixture Ref 0.28 is shown in Figure 3.9 (a). The
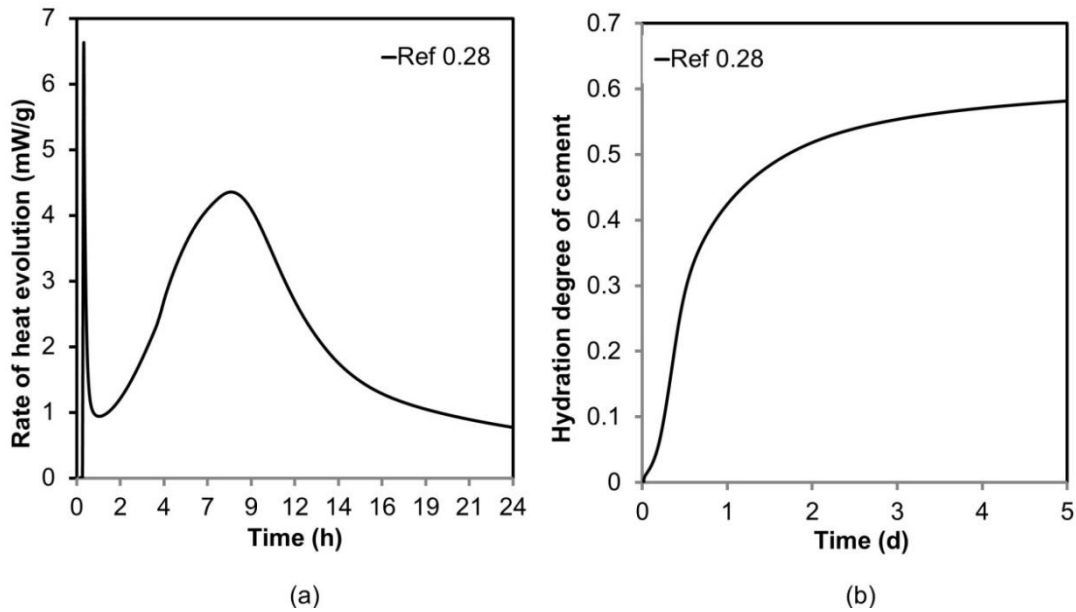
Figure 3.9 (a) Rate of heat evolution measured on the mixture Ref 0.28 in 24 h after casting; (b) hydration degree of cement in the mixture Ref 0.28 calculated from the cumulative heat of hydration during the first 5 days after casting.

cement in this study is assumed to have a potential heat of hydration of 425 J/g calculated from [62]. From the cumulative heat evolution, the hydration degree of the cement is calculated and shown in Figure 3.9 (b).

From a statistic analysis, the size of $100 \times 100 \times 100$ μm^3 cubic sample of cement paste was proven to be sufficiently big to represent the cement paste [111]. A "burning algorithm" [112] was employed to determine the connectivity of the microstructure simulated by HYMOSTRUC 3D at different ages. This algorithm searches for a solid path across the 3D microstructure generated by HYMOSTRUC 3D. Firstly, the simulated 3D microstructure of cement paste is digitized with the information of solid phase and non-solid phase positions. Then, the burning algorithm proceeds iteratively from each solid phase to its nearest neighbours and stops at the solid phase with no other solid phase around. In the simulation, the burning starts at the top of the 3D microstructure and continues until no more 'fuel' remains. Then it is checked whether the bottom of the microstructure has been reached. The connectivity of the cement matrix at different time steps of the HYMOSTRUC 3D simulation is shown in Table 3.5. The 2D images of the microstructure at the age of 3.16 h and 8.91 h are illustrated in Figure 3.10.

The connectivity of cement paste obtained from the simulation shows a so-called "stable" solid skeleton formed between 7.94h and 8.91h. However, at the final setting time (2.98h), when the degree of hydration is 0.03 (Figure 3.9 (b)), the system is more like a dispersion of solid phases in a liquid (Figure 3.10 (a)). At this time, the cement matrix is still in the plastic stage, internal stresses are not generated, and the chemical shrinkage can be transferred entirely into a bulk volume change of the paste. It is not reasonable to choose the final setting time as the "time-zero" for autogenous shrinkage when the "stable" skeleton inside the pastes has not formed. However, when the hydration time reaches 8.91 h (Figure 3.10 (b)), the simulation result shows that a "stable" solid skeleton has formed. The formation of the "stable" solid skeleton reflects the critical point of microstructure change. This point corresponds with the knee point of the autogenous shrinkage curve (see Figure 3.5).

Table 3.5 Connectivity of cement matrix at different time steps from HYMOSTRUC

Calculation step	Hydration time (h)	Connectivity (Y/N)
1	1.00	N
…	…	...
10	2.82	N
11	3.16	N
...	...	...
19	7.94	N
20	8.91	Y
21	10.00	Y

(a) 3.16 h hydration   *(b) 8.91 h hydration*
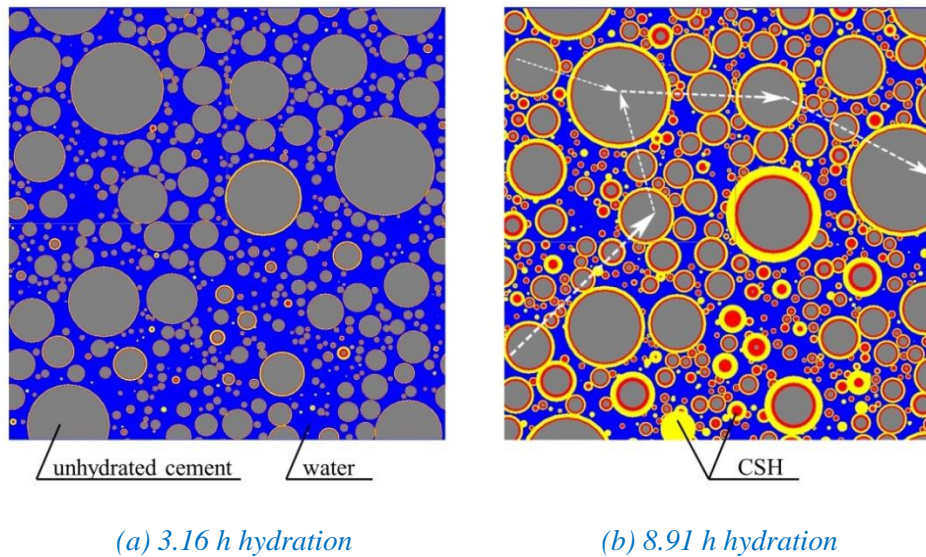
Figure 3.10 2D images of the microstructure from HYMOSTRUC in the mixture Ref 0.28 at different ages. (a) 3.16 h; (b) 8.91 h

3.4.2 Start time of autogenous shrinkage

The results of the simulation of the connectivity of solid particles discussed in the previous section are in relatively good agreement with the results of UPV measurements. Both the UPV measurements and simulation results illustrate that the "stable" skeleton does not form at the final setting time, but at a later stage in the hydration process. Whether the moment a "stable" solid skeleton is formed is the accurate starting time of autogenous shrinkage will be discussed below.

When the "stable" solid skeleton is formed, empty pores could form inside the pastes due to ongoing hydration and associated chemical shrinkage [56]. When the water in the cement paste is gradually used up, the internal RH begins to decrease, as shown in Figure 3.7. As hydration proceeds, more water is consumed, the pore structure refines, the remaining water withdraws into the smaller pores, and the capillary tension further increases. The solid

skeleton resists the capillary tension and is put in compression [62]. The solid skeleton, and hence the paste, may shrink and, if restrained, may start to crack.

The formation of a "stable" solid skeleton is a precondition for the self-desiccation [61], but it does not mean that the RH must decrease right after the formation of the "stable" solid skeleton. For example, when a "stable" solid skeleton is formed in concrete with a high water-cement ratio (w/c greater than 0.4-0.45) [56], the pores generated from chemical shrinkage are still (almost) full of free water. The RH does not drop immediately at this time and autogenous shrinkage caused by self-desiccation is still negligible. The high efficiency of internal curing to mitigate autogenous shrinkage by Super Absorbent Polymer (SAP) also proves that autogenous shrinkage can be controlled by maintaining a high internal RH [94]. So, the formation time of a "stable" solid skeleton does not represent the start of autogenous shrinkage in mixtures with high water-cement ratios or with internal curing agents. Instead, the start of self-desiccation, i.e., the onset of internal RH drop, represent the start of autogenous shrinkage.

The evolution of the measured free strain and the internal RH of the mixtures Ref 0.25 SP, Ref 0.28 SP, and Ref 0.18 SP are shown in Figure 3.11, Figure 3.12, Figure 3.13, respectively. All these figures show that the knee points in the free (autogenous) strain curves correspond to the onset of the self-desiccation process. The knee point reflects the threshold of solid percolation, which corresponds to the formation of the stable solid skeleton. Once the stable solid skeleton is formed, especially for cement pastes with a low water-cement ratio, the internal RH starts to decrease.
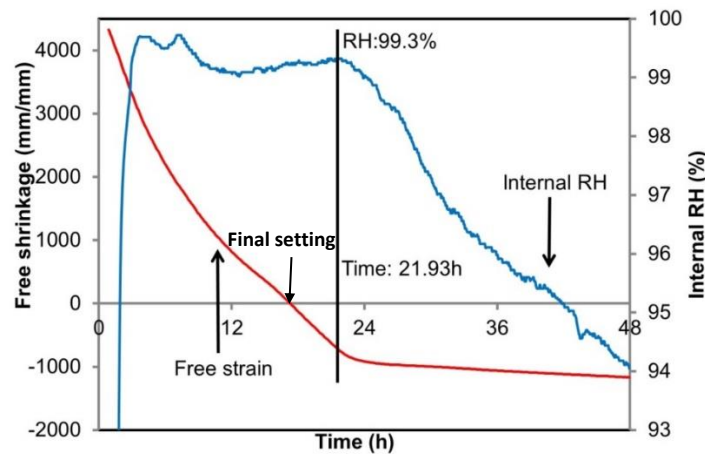
Figure 3.11 Comparison between the free strain and internal RH of the mixture Ref 0.25 SP, measured after casting. (The strain is zeroed at the final setting time, t = 17.28 h)
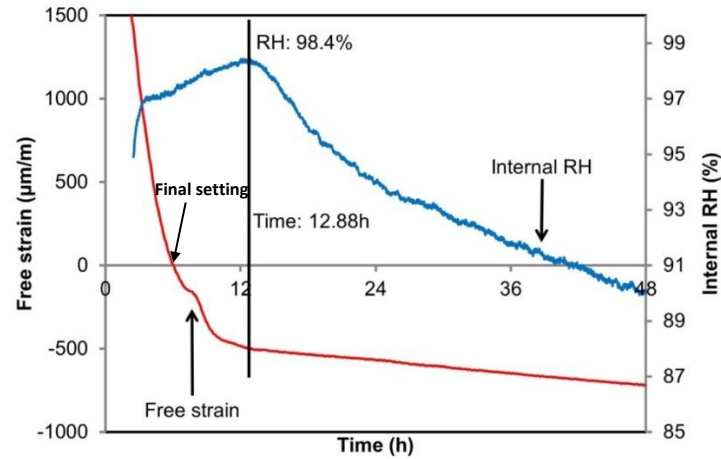
Figure 3.12 Comparison between the free strain and internal RH of the mixture Ref 0.28 SP, measured after casting. (The strain is zeroed at the final setting time, t = 6.02 h)
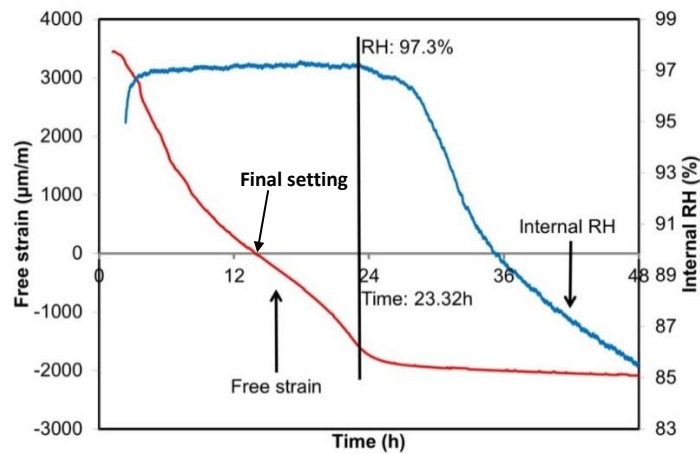
Figure 3.13 Comparison between the free strain and internal RH of the mixture Ref 0.18 SP, measured after casting. (The strain is zeroed at the final setting time, t = 13.87 h)

Figure 3.14 shows the autogenous shrinkage of cement mixtures after the final setting time (Figure 3.14a) and the onset of internal RH drop (Figure 3.14b), respectively. For the three mixtures shown in Figure 3.14 the shrinkage measured from the final setting time is larger than measured after the onset of internal RH drop. In the period between final setting and the onset of internal RH drop a solid skeleton is gradually formed inside cement matrix. In this stage, however, the strength and stiffness of this solid skeleton are still so low that chemical shrinkage is almost completely transformed into an external volume change. In other words, the large volume change observed in this period is not caused by self-desiccation, but the result of free chemical shrinkage.

(a) (Autogenous) shrinkage measured after final setting time

(b) (Autogenous) shrinkage measured from the onset of self-desiccation
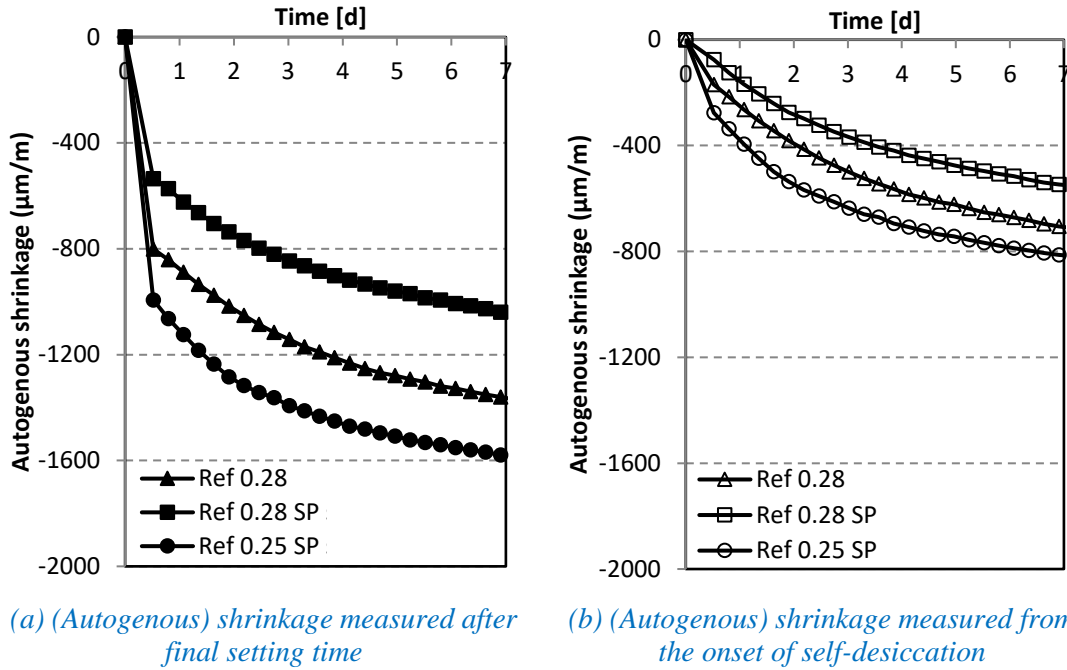
Figure 3.14 Autogenous shrinkage of the cement mixtures measured after the final setting time and after the onset of internal RH drop

3.5 Conclusions

Based on the results and discussion, the following conclusions can be made for the cement mixtures with low water-cement ratio:

- Internal relative humidity of cement pastes does not decrease immediately after the final setting time determined by the Vicat needle test.
- Both UPV measurements and numerical simulation of cement paste illustrate that the percolation path does not form at the final setting time determined by the Vicat apparatus, but formed around the onset of internal RH drop.
- With an improved hygrometer method for monitoring the change of internal RH in cement pastes with low water-cement ratio at very early age, the knee point in the free strain is found to correspond with the onset of self-desiccation.

The onset of internal RH drop is a more plausible start time of autogenous shrinkage for estimating the (autogenous) shrinkage caused by self-desiccation.

Chapter 4

Experimental study on the autogenous shrinkage of cement pastes with RHA

4.1 Introduction

Rice husk is a by-product of the rice paddy milling industry. It is acknowledged that after appropriate incineration the residue, rice husk ash (RHA), has a high content of amorphous silica (85-90%) and a porous structure with a high specific surface area (60-100 m^2/g) [5, 41, 51]. Because of its porous structure, RHA may also act as an internal curing agent to mitigate autogenous shrinkage of HPC/UHPC. It is reported that RHA can decrease the autogenous shrinkage of cement matrices. The efficiency of mitigating shrinkage is affected by the properties of RHA [113-115].

In this chapter, the influence of the fineness and dosage of RHA on autogenous shrinkage and self-desiccation of cement pastes is investigated. The measurements of internal RH, autogenous shrinkage, heat evolution of cement pastes, pore size distribution, and water vapour desorption property of RHA are presented and discussed.

The objective of the experimental studies in this chapter is to optimize the content and particle size of RHA for mitigating autogenous shrinkage and also provide data for validating the numerical modelling of internal curing as reported in Chapter 6.

4.2 Materials

The materials used in this study are Portland cement (CEM I 52.5N), RHA, and a polycarboxylate-based superplasticizer (Solid mass content 35%). The RHA was produced by a drum incinerator, which was introduced by Tuan [6]. The details of the incinerator are shown in Figure 4.1. The husks burn by themselves once ignited. The highest temperature recorded inside the incinerator was 550 °C. The properties of cement and RHA are shown in Table 4.1.

Figure 4.2 shows the X-Ray diffraction patterns of RHA and SF. The RHA sample contains a small amount of quartz, while the bulk of the ash is amorphous, similar to the SF sample.

Figure 4.1 The drum incinerator for RHA production, which is similar to the equipment used by Tuan [6].

Table 4.1 Properties of cement and RHA used in this study

		Cement*	RHA**
Chemical properties	[%] (weight)		
CaO		64.00	1.72
SiO_2		24.00	88.86
Al_2O_3		5.00	0.30
Fe_2O_3		3.00	0.20
SO_3		2.40	0.60
Na_2O		0.30	-
K_2O		-	4.22
Minor components		-	1.59
Loss on ignition (L.O.I)		1.30	2.51
Physical properties			
Specific gravity	[g/cm^3]	3.15	2.10
Specific surface area (Blaine)	[cm^2/g]	4500	-
Specific surface area (BET)	[m^2/g]	-	29.7
Mean particle size	[μm]	13.7	9.0

* Data provided by the company

** Chemical composition determined by X-Ray Fluorescence Spectrometry method
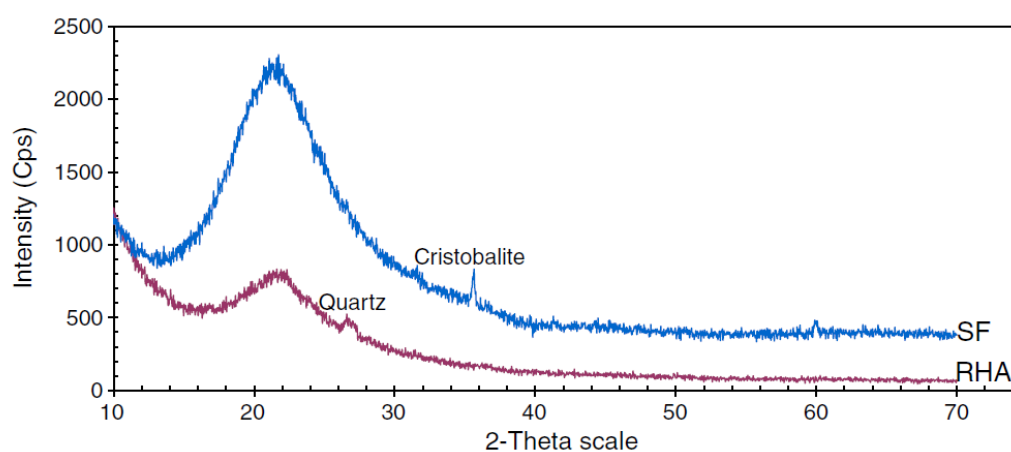
Figure 4.2 XRD patterns of RHA and SF [6]

Table 4.2 Grinding time and mean particle sizes of RHAs

	Unit	RHA-7	RHA-9	RHA-12
Mean particle size (D_{50})	μm	7.1	9.0	12.1
Grinding time	days	7	4	2
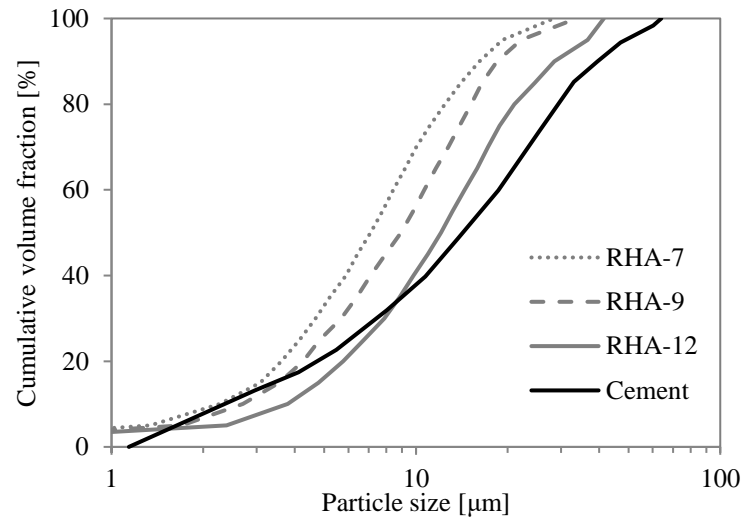
Figure 4.3 Particle size distribution of the cement and RHAs

Mixture design

The well-burned ash was ground to different particle sizes in a ball mill with a speed of around 20 rpm. According to the study of Tuan [6], the cement mixture with 20% coarse RHA, i.e. particle size $> 15~\mu m$, requires a large amount of superplasticizer to achieve sufficient fluidity. Therefore, for obtaining proper workability of the mixtures, the mean particle size of RHA was chosen to be smaller than 15 μm. In order to study the effect of RHA fineness on autogenous shrinkage of cement pastes, three types of RHA with different

Table 4.3 Mixture compositions of cement pastes used in this study

Aspect to be investigated	Mixture name	Mixing-water/binder ratio*	Water-cement ratio**	Superplasticizer -binder ratio	Replacement percentage of RHA	Mean particle size of RHA (μm)
- Effect of the fineness of RHA	Ref 0.25	0.25	0.260	1.6%	0	-
	10% RHA-7	0.25	0.225	1.6%	10%	7.1
	10% RHA-9	0.25	0.225	1.6%	10%	9.0
	10% RHA-12	0.25	0.225	1.6%	10%	12.1
	20% RHA-7	0.25	0.180	1.6%	20%	7.1
	20% RHA-9	0.25	0.180	1.6%	20%	9.0
	20% RHA-12	0.25	0.180	1.6%	20%	12.1
- Effect of the dosage of RHA	10% RHA-9	0.25	0.225	1.6%	10%	9.0
	15% RHA-9	0.25	0.204	1.6%	15%	9.0
	20% RHA-9	0.25	0.180	1.6%	20%	9.0
	25% RHA-9	0.25	0.154	1.6%	25%	9.0

* The mixing-water/binder ratio is the amount of water added for casting per gram dry powders of binder. It does not include the water in the superplasticizer. Binder here refers to the cement and dry RHA powders.

** It refers to water-cement ratio after uptake of water by RHA, and includes the water in the superplasticizer. The water absorption capacity of RHA is 0.58 g/g (section 4.4.1) determined by MIP.

mean particle sizes were chosen. The particle size distribution of the cement and the three RHAs are presented in Figure 4.3. The particle size distribution was determined by laser diffraction. The grinding time and the mean particle size of these RHAs are shown in Table 4.2. The required grinding time increases rapidly when a mean particle size of less than 7 μm is strived at. The smallest mean particle size of RHA in the study is chosen to be 7 μm. Due to the high specific surface area of RHA, the workability of cement pastes is dramatically reduced with increasing of RHA content [6]. In this study the RHA dosage was limited to a maximum of 25%. In all mixtures the same dosage of superplasticizer was used. The fixed dosage is optimized to avoid bleeding and provide relatively good workability for all the mixtures. The mixture compositions of cement pastes are listed in Table 4.3.

4.3 Methods

4.3.1 Autogenous shrinkage and internal RH test

For the autogenous shrinkage and internal RH measurements, the preparation of samples and the test program were the same as those described in section 3.2.

4.3.2 Mercury intrusion porosimetry (MIP)

MIP is a widely used technique to measure the pore size distribution and porosity in cement-based materials [116, 117]. Although it is a fast method to obtain an indication of the pore structure, the result from MIP is influenced by some factors such as pore shape, the ink-bottle effect, damage of the fine structure caused by the applied pressure, surface tension and sample preparation, i.e. drying treatment [117-119].

In this study MIP measurements were performed with Micrometrics PoroSizer® 9320 (Figure 4.4). The PoreSizer-9320 is a 207 MPa mercury intrusion porosimeter, which determines pore sizes in the range from 7 nm to 400 µm. The apparatus has two low-pressure chambers and one high-pressure chamber. The measurement is conducted in two stages: a manual low pressure run from 0 to 0.170 MPa and an automated high pressure run from 0.170 to 205 MPa.

The relation between the pressure p_{Hg} (MPa) and the pore diameter d (µm) is described by the Washburn equation (4.1)[117], based on the assumption of cylindrical pores:

$$p_{Hg} = -\frac{4\gamma_{Hg} \times \cos\theta_{Hg}}{d} \tag{4.1}$$

where γ_{Hg} is the surface tension of the mercury (mN/m) and θ_{Hg} (-) is the contact angle between the mercury and the pore wall surface of the cement paste. In this study, the mercury contact angle and surface tension used were 139˚ and 480 mN/m, respectively [117]. By applying the Washburn equation, mercury intrusion data can be converted into a pore size distribution.

Figure 4.4 Micrometrics PoreSizer-9320

4.3.3 Isothermal calorimetry

The rates of heat evolution of all the cement mixes were measured in a Thermometric isothermal conduction calorimeter (TAM-AIR-314), using 10 ± 0.01 g samples. All the materials were placed in a climate chamber for 24 hours at 20 ˚C before the test. The cement pastes were cast into capped glass vials, and the vials were quickly inserted in the calorimeter. The tests were performed on 2 parallel samples at 20 ˚C and lasted for 7 days.

4.3.4 Vapour sorption isotherm

A dynamic vapour sorption analyser (Figure 4.5) was used for investigating the sorption property of RHAs under the controlled condition of temperature and relative humidity. The RHAs were immersed in water for 10 minutes before the test. Then the 5-10 mg wet RHA sample was placed in the sample holder. The test was carried out to obtain the water vapour desorption isotherm. The desorption RH point of the water vapour isotherm was set at 98%, 95%, 90%, 80%, and 1%, respectively. The test was performed at each RH point until the equilibrium is reached, i.e. the mass change of the sample is less than 0.1%. Each test was performed in parallel on two samples at 20 ˚C.

Figure 4.5 Dynamic vapour sorption analyser (TA Q5000 SA)

4.4 Results and discussion

4.4.1 Effect of the fineness of RHA on autogenous shrinkage of cement paste

4.4.1.1 Mixtures with 10% cement replacement by RHA

The autogenous shrinkage of cement pastes with and without RHA with different particle sizes is presented in Figure 4.6. The replacement percentage of cement is 10%. The measurement of autogenous shrinkage starts at different times and are shown in Figure 4.6a and Figure 4.6b, respectively. Figure 4.6a shows the shrinkage measured from the final setting time, whereas Figures 4.6b shows the shrinkage measured from the onset of self-desiccation.

It is obvious that for the same mixture, different starting times of the measurement mean several hundred microstrain difference in the autogenous shrinkage. This may lead to different conclusions when discussing the effect of RHA on autogenous shrinkage. The strain curves in Figure 4.6a show that the influence of the fineness of RHA on the autogenous shrinkage *cannot* be ignored. However, Figure 4.6b shows that when the measurements start from the onset of self-desiccation, the influence of the fineness is neglectable. As discussed in Chapter 3, the onset of self-desiccation is the preferred starting point for measuring autogenous shrinkage.

Figure 4.6b clearly shows that 10% replacement of cement by RHA can reduce the autogenous shrinkage of the pastes at 7 days from about 810 microstrains to near 280 microstrains.

(a) (Autogenous) shrinkage measured from the final setting time

(b) (Autogenous) shrinkage measured from the onset of self-desiccation
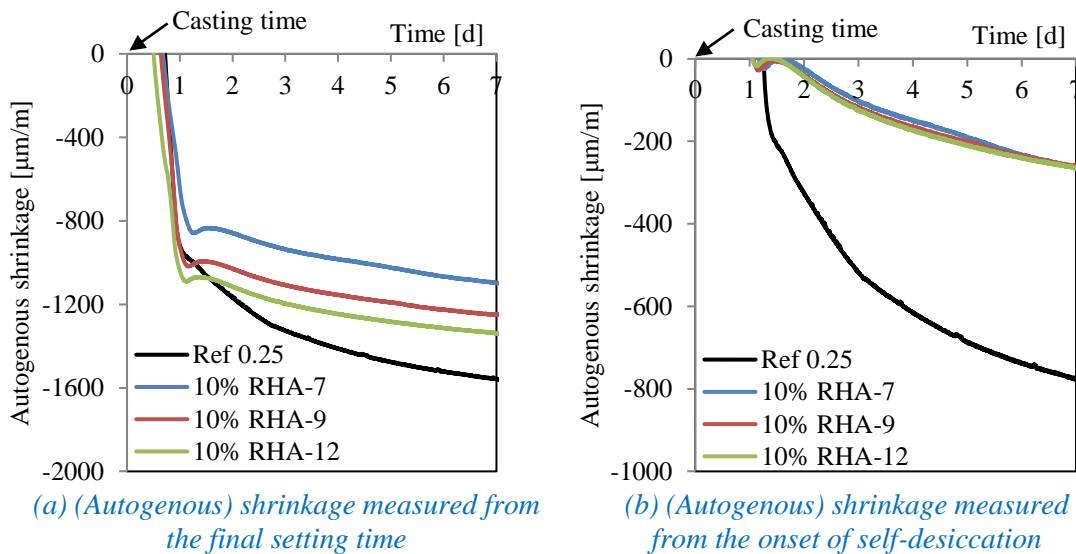
Figure 4.6 (Autogenous) shrinkage of cement pastes with and without RHA with different particle sizes, measured from different times after casting. The replacement percentage of cement is 10%. Please note the different scale of the vertical axis.

Still for the mixtures with 10% RHA, Figure 4.7a shows how the addition of RHA retards the decrease of the internal RH in pastes, leading to less autogenous shrinkage. Figure 4.7b shows the decrease of internal RH of different mixtures since casting time. For comparing the evolution of self-desiccation of different mixtures, Figure 4.7 (c) shows the decrease of the internal RH measured from the onset of self-desiccation. The curves clearly show that the fineness of RHAs does not have a significant effect on the internal RH change.
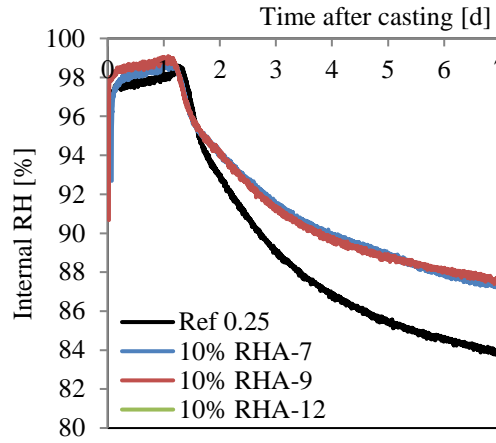
(a) Internal RH change since casting
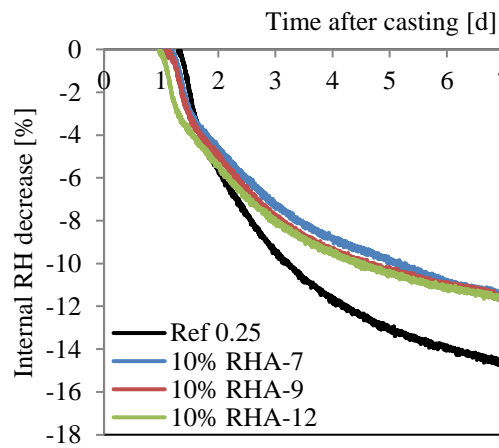
(b) Internal RH decrease since casting
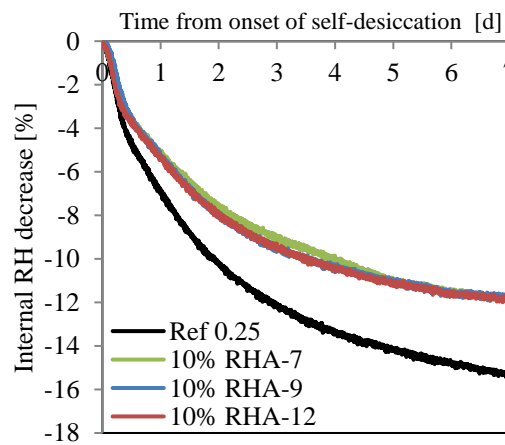
(c) Internal RH decrease since the onset of self-desiccation

Figure 4.7 Internal RH change of cement pastes incorporating RHA with different particle sizes. The replacement percentage of cement is 10%.

4.4.1.2 Mixtures with 20% cement replacement by RHA

The effect of RHA fineness on the mixtures with 20% replacement of cement by RHAs was also investigated. The evolution of autogenous shrinkage and internal RH are presented in Figure 4.8 and Figure 4.9, respectively. It happens again that different starting moments of the measurement result in different magnitude of autogenous shrinkage for the same mixture, which is shown in Figure 4.8a and Figure 4.8b. The difference is more than 1000 microstrain. This indicates again the importance and need of agreement about the starting point for measuring autogenous shrinkage.

When the replacement is 20%, the addition of RHA almost eliminates the autogenous shrinkage of the pastes. The autogenous shrinkage after 7 days of the mixtures with RHAs is less than 80 microstrains, as shown in Figure 4.8b. The mixtures with three kinds of RHAs, i.e. RHA with different fineness, showed a similar trend of the autogenous shrinkage curves, except that the mixture with RHA-12 had slightly larger shrinkage.

The addition of the RHAs with different fineness postponed the internal RH drop as shown in Figure 4.9. While the internal RH of the mixture with RHA-12 decreased faster than the other two mixtures with RHA, the difference between the curves in Figure 4.9 (b) is small.
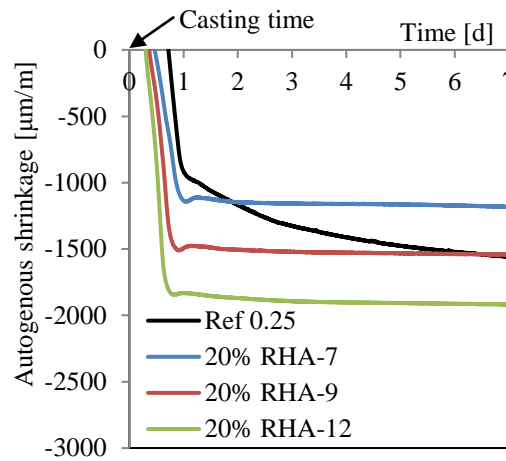
(a) Autogenous shrinkage measured from the final setting time
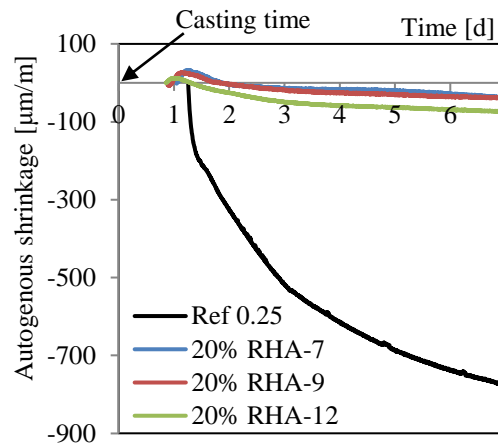
(b) Autogenous shrinkage measured from the onset of self-desiccation
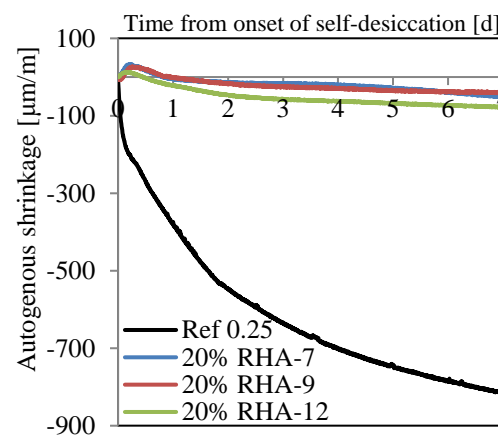
(c) Autogenous shrinkage since the onset of self-desiccation

Figure 4.8 Autogenous shrinkage of cement pastes with and without RHA with different particle sizes. The replacement percentage of cement is 20%.
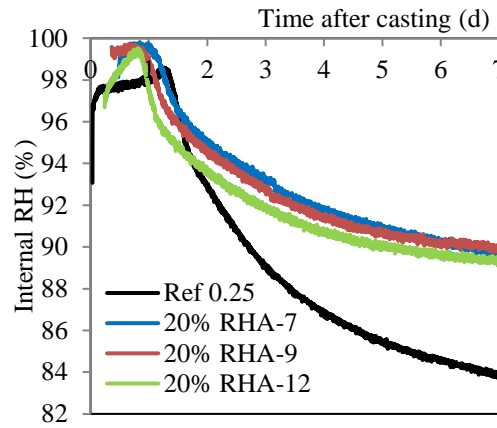
(a) Internal RH change since casting
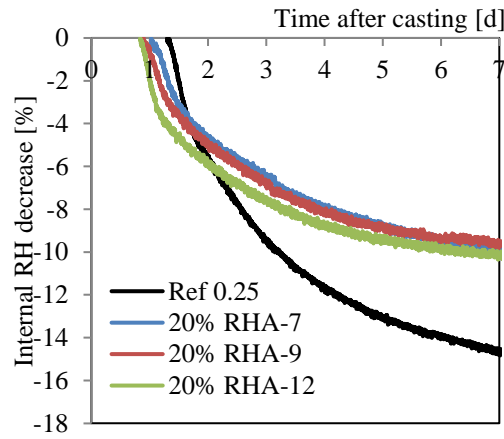
(b) Internal RH decrease since casting
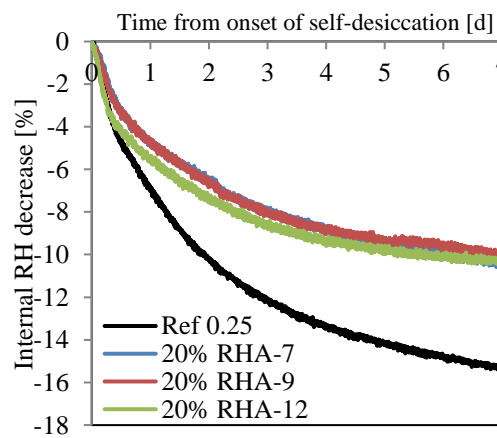
(c) Internal RH decrease since the onset of self-desiccation

Figure 4.9 Internal RH change of cement pastes incorporating RHA with different particle sizes. The replacement percentage of cement is 20%.

4.4.1.3 Discussion on effect of the fineness of RHA

As a potential internal curing agent, the water absorption and pozzolanic reaction of RHA are the two critical factors that determine the efficiency of RHA as internal curing agent.

Water absorption

The water absorption of RHA (powder) stems from its porous structure and depends on the pore volume and pore size distribution. The total pore volume reflects the maximum water absorption capacity of RHA, while the pore size distribution determines whether water can be released fast enough for internal curing. Figure 4.10 shows the pore structure of RHAs characterized by MIP. The total pore volume of RHAs is presented in Figure 4.10b. The curves indicate that the total pore volumes of three kinds of RHA are almost identical (around $0.58\ cm^3/g$), which means the water absorption capacities of the three RHAs are identical ($0.58\ g/g$) as well.

(a) Pore size distribution   *(b) Total pore volume*
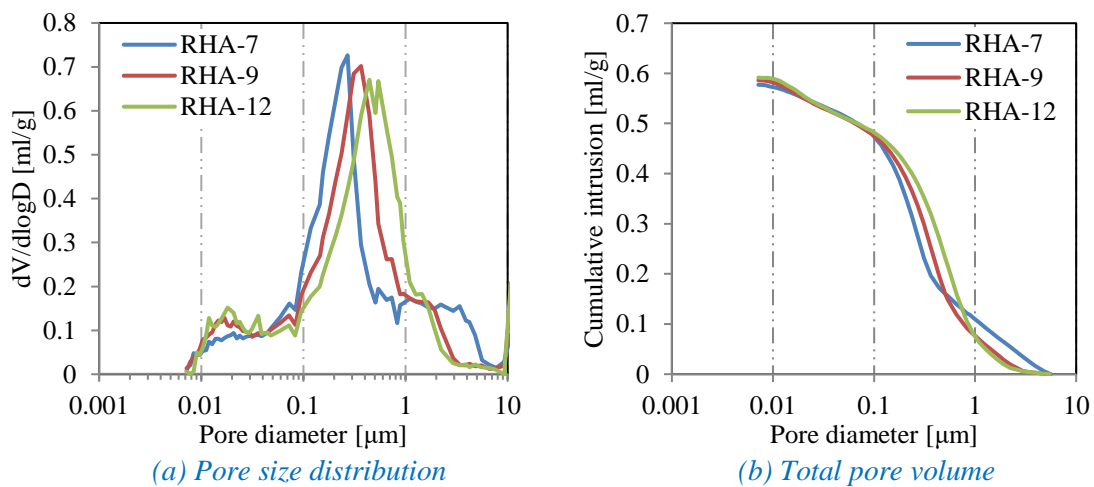
Figure 4.10 Pore structure characterization of RHA with different mean particle sizes from mercury intrusion porosimetry (MIP).

Due to the ink-bottle effect and other factors [117], the pore size distribution in Figure 4.10a from MIP tests does not reflect the realistic pore structure of RHA. The result from MIP cannot help to determine the amount of water released at different RH by RHA. Thus, the water vapour sorption analyser is utilized. For determining the desorption property of saturated RHA particles, the RHA samples were immersed in water for 10 minutes and then put into the device for measuring at 20 ˚C. The desorption RH point of the water vapour isotherm was set at 98%, 95%, 90%, 80%, 50% and 1%, respectively. The result is shown in Figure 4.11. The figure illustrates that the three RHAs have a similar water vapour desorption isotherm. The amounts of released water at different RH in the three RHAs are almost the same. It indicates that three kinds of RHAs have an identical pore structure.
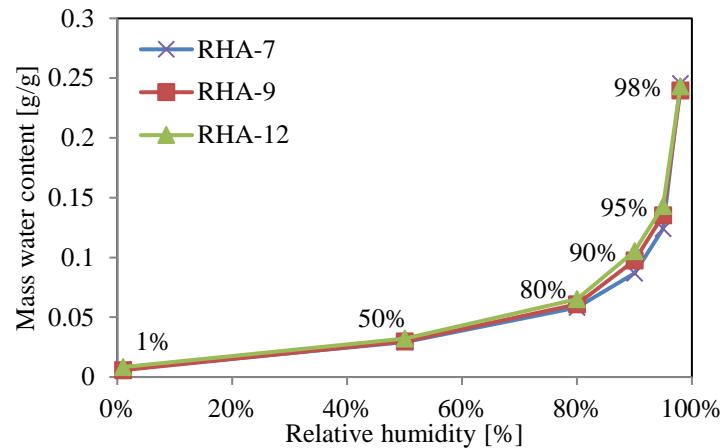
Figure 4.11 Water vapour desorption isotherms of RHA with different mean particle sizes

Pozzolanic reaction

Besides the pore volume and pore structure of RHA, the pozzolanic reaction of RHA in cement pastes also affects the internal curing efficiency. RHA is a pozzolanic material, which contains a large amount of amorphous silica. Due to its porous structure, RHA adsorbs the water when cement paste is cast. With ongoing hydration of cement, calcium hydroxide is generated and that reacts with RHA in a pozzolanic reaction. The porous structure of the reacted RHA will collapse, while the pozzolanic reaction will consume water (see also Chapter 5). For determination of the intensity of the pozzolanic reaction, isothermal calorimeter studies were performed. The heat evolution of the blended cement-RHA pastes with three kinds of RHA is shown in Figure 4.12. The mean particle size of RHA in the three mixtures is 7 µm, 9 µm, and 12 µm, respectively. The replacement percentage of cement by RHA is 20%. It is clear that the curves of three cement mixtures in Figure 4.12a and 4.12b almost overlap. The water-binder ratio and the dosage of RHA are the same in the three cement mixtures. The pore structure of the three RHAs is also identical, as shown in previous section. The overlapping curves in the heat evolution show that three kinds of RHA have a

(a)

(b)
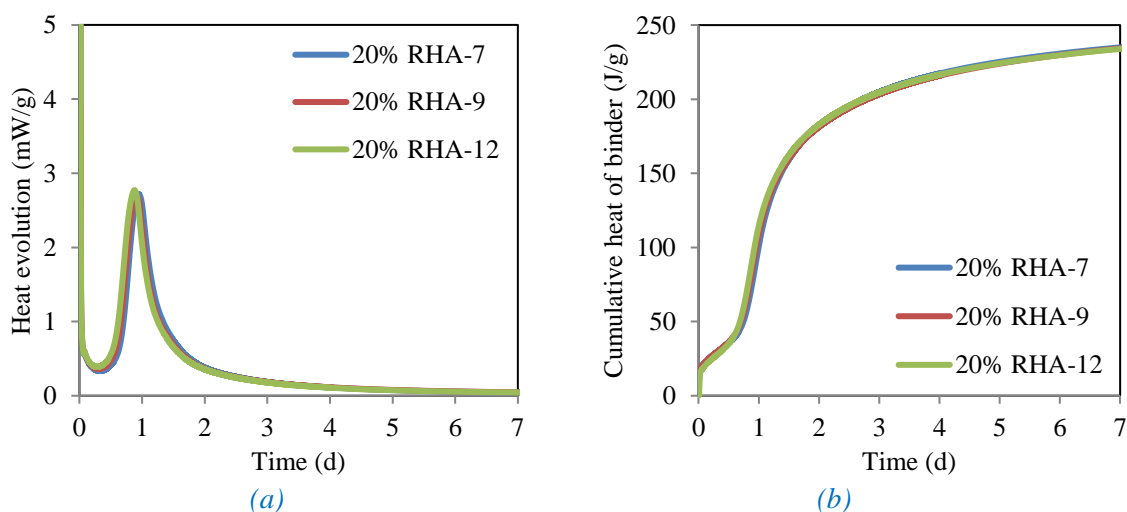
Figure 4.12 Heat evolution of cement pastes incorporating RHA with different particle sizes. The replacement percentage of cement is 20%.

similar effect on the heat evolution of the pastes. This indicates that their pozzolanic reactions proceed at the same rate.

Since both the water absorption capacity and degree of pozzolanic reaction of three different RHAs are almost the same, the internal curing efficiency of three RHAs can be assumed largely identical. This explains why the effect of the RHA fineness on autogenous shrinkage is relatively small. The possible reason for this observation might be that the size range considered in this study is relatively small.

4.4.2 Effect of the dosage of RHA on autogenous shrinkage of cement paste

Figure 4.13 shows the development of autogenous shrinkage of cement pastes with different dosages of RHA. The onset of self-desiccation is chosen as the starting point of autogenous shrinkage. The figure shows that the autogenous shrinkage of cement paste decreases with increasing RHA dosage. This result is in line with the findings of Tuan [113] and Rößler [114]. When the dosage reaches 20%, the value of autogenous shrinkage becomes less than 50 microstrains at 7 days. When the dosage increases to 25%, the autogenous shrinkage is very small (near 70 microstrains at 7 days) and the curve is close to the one for 20% RHA. It can be concluded that the autogenous shrinkage of the mixture is almost eliminated when the RHA dosage is equal to or beyond 20%.
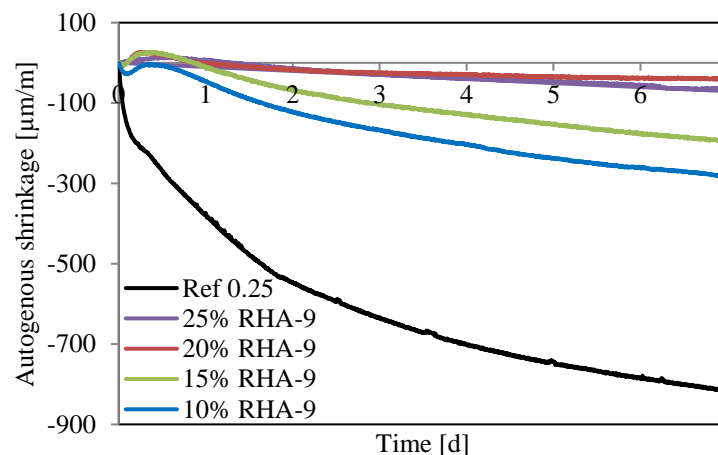
Figure 4.13 Autogenous shrinkage of cement pastes incorporating RHA with different dosages, measured from the onset of self-desiccation

Figure 4.14a presents the evolution of the internal RH of cement pastes incorporating RHA. The addition of RHA reduced the drop of internal RH in hardening cement pastes. Figure 4.14c shows the internal RH decrease after the onset of self-desiccation. It appears that the larger dosage of RHA leads to a smaller drop of internal RH. The decrease of internal RH of pastes becomes smaller when the RHA dosage increases from 5% to 25%. Unlike the SAP, the water absorption capacity of RHA is relatively small. The water content of RHA-9 at RH98% is around 0.24 g/g RHA (Figure 4.11), while the water uptake of SAP in cement pastes is more than 1000% by mass [94]. Because of the big difference in water absorption capacity, the cement pastes need a higher dosage of RHA than SAP to provide enough internal curing water. In the cement paste (w/c=0.3) studied by Jensen [94], adding 0.6% dosage of SAP is enough to eliminate the autogenous shrinkage. However, in the cement-RHA paste, the dosage of RHA needs to be equal or more than 20% to eliminate the autogenous shrinkage (Figure 4.13).
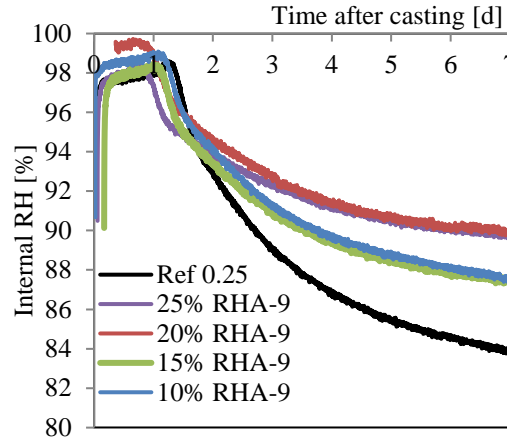
(a) Internal RH change since casting
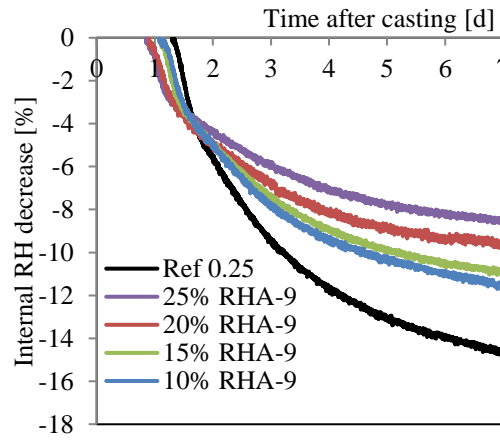
(b) Internal RH decrease since casting
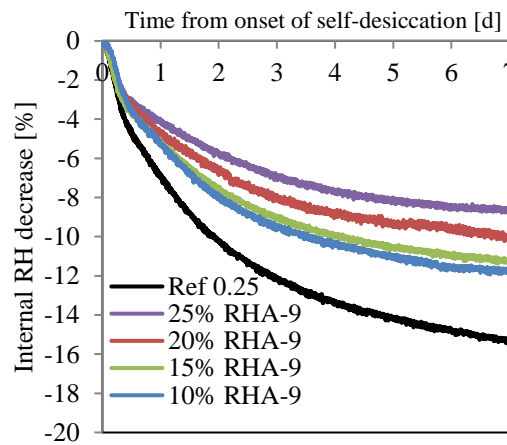
(c) Internal RH decrease since the onset of self-desiccation

Figure 4.14 Internal RH change of cement pastes incorporating RHA with different dosages

4.5 Conclusions

In this chapter, the effects of the fineness and dosage of RHA on self-desiccation and autogenous shrinkage of cement pastes were investigated. RHA turns out to be effective in mitigating autogenous shrinkage of cement pastes. Based on experimental results and the discussion of these results, the following conclusions have been drawn.

- The effect of the fineness of RHA, i.e. the mean particle size from 7.1 µm to 12.1 µm, on the self-desiccation and autogenous shrinkage of cement pastes is neglectable. This is because the water absorption capacity of three different RHAs are almost identical.
- The autogenous shrinkage of cement pastes decreases with increasing dosage of RHA. The larger dosage of RHA leads to a smaller drop of internal RH in cement pastes.
- With the optimized dosage (20%) and mean particle size (9 µm), the autogenous shrinkage of cement pastes (mixture 20% RHA-9) at early age can be eliminated by using RHA.

It needs to mention that the absorption of dry RHA particles on casting water will decrease the water-cement ratio in blended cement-RHA pastes. Thus, the water-cement ratio in cement pastes with different dosage of RHA is different.

The pozzolanic reaction of RHA will consume water and change the porous structure of RHA. This may influence the efficiency of internal curing of RHA, which will be discussed in detail in next chapter.

Chapter 5

Mechanism of mitigating autogenous shrinkage by using RHA

5.1 Introduction

The experimental results in Chapter 4 show that RHA is effective in mitigating autogenous shrinkage of cement pastes. However, the exact mechanism in mitigating autogenous shrinkage by using RHA, that is chemically reactive itself (pozzolanic reaction) is unclear. The objective of this chapter is to study the relevant mechanism of mitigating autogenous shrinkage by RHA.

The American Concrete Institute (ACI) Terminology Guide defined internal curing as "supplying water throughout a freshly placed cementitious mixture using reservoirs, via pre-wetted lightweight aggregates, that readily release water as needed for hydration or to replace moisture lost through evaporation or self-desiccation" [12]. According to this definition, RHA performs as an internal curing agent [56].

The amount of water entrained in the RHA particles can be released during self-desiccation of the hydrating cement paste, mitigating autogenous shrinkage [94]. However, unlike currently used internal curing agents, like superabsorbent polymers (SAPs) or water-saturated aggregate [89], the RHA will react in a pozzolanic reaction. This will result in a change of the pore structure and thus affect water absorption capacity of the RHA. The high content of amorphous silica enables RHA to react with calcium hydroxide from cement hydration. Moreover, this pozzolanic reaction will consume extra water, which would even lead to an increase of self-desiccation.

The internal curing process with a 'reacting' water reservoir, like RHA, is more complex than that with conventional reservoir. For revealing the mechanism of internal curing with chemically reactive water-containing particles, first the absorption capacity of RHA needs to be determined. After that the effect of the pozzolanic reaction on the internal curing effect of RHA will be studied. The materials and methods that will be used for the experimental study of the absorption capacity and the pozzolanic reactivity of RHA will be dealt with in the next two sections.

5.2 Materials

The materials used in this study are Portland cement (CEM I 52.5N), RHA, and a polycarboxylate-based superplasticizer (Solid mass content 35%), which are all the same as those used in Chapter 4.

The cement mixture with the optimized dosage (20 wt%) and mean particle size of RHA (9 µm) as established in chapter 4 is used. The mixture composition is listed in Table 5.1.

Table 5.1 Mixture composition of cement pastes

Mixture name	Mixing-water/binder ratio*	Water-cement ratio**	Superplasticizer-binder ratio	Replacement percentage of RHA	Mean particle size (D_{50}) (µm)
Ref 0.25	0.25	0.26	1.6%	0	-
20% RHA-9	0.25	0.18	1.6%	20%	9.0

* The mixing-water/binder ratio is the amount of water added for casting per gram dry powders of binder. It does not include the water in the superplasticizer.

** The water-cement ratio includes the water in the superplasticizer.

5.3 Methods

5.3.1 Filtration method for determining the absorption capacity of RHA

From the liquid absorption by SAP it is known that the ion concentration of the absorbed liquid strongly affects the liquid uptake of SAP [11]. Such an effect might also occur in the water absorbed by the RHA. It was decided, therefore, to consider two fluids with different ion concentrations for estimating the absorption kinetics of RHA. One is demineralized water and the other is a synthetic pore fluid. The test details are presented below.

The RHA-9 to be used in the experiments was oven-dried at 105 ˚C for 1 day before the test. 200 ml of demineralized water or synthetic pore fluid at 20 ± 1˚C was prepared to which about 5 g of RHA was added. This condition was maintained for 5, 10, 15, 30, and 60 minutes, respectively, while stirring. The sample was vacuum filtered with glass fibre filter paper (Whatman^{TM} 1820-110, pore size 1.6 µm). To avoid the influence of water drops sticking on filter paper, the sample was moved from the filter paper to a small glass dish and weighted. Then the glass dish with the wet sample was oven-dried for obtaining the dry sample mass. The synthetic pore fluid is similar to that used by Jensen [94] for determining the absorption capacity of SAP. The composition of the synthesized pore fluid [$mmol/l$]: [Na^+] = 400, [K$^-$] = 400, [Ca^{2+}] = 1, [SO$_4^{2-}$] = 40, [OH$^-$] = 722.

For each measurement, two parallel samples were used. The absorption capacity (Q) of RHA was calculated with the equation:

$$Q = \frac{M_{wet} - M_{dry}}{M_{dry}} \tag{5.1}$$

where M_{wet} is the mass of wet sample, M_{dry} is the mass of RHA sample after drying.

Because the pore size of filter paper is 1.6 µm, the small RHA particles (<1.6 µm) may pass through the filter paper and get lost in the vacuum filtration process. The pass rate (by mass) of RHA through the filter paper in vacuum filtration process is also measured, i.e. 1.4 $\pm$ 0.1 %. Due to the low penetration rate of RHA during filtration, the liquid absorbed by the 'lost' RHA particles is neglected.

5.3.2 Thermogravimetric analysis (TGA) for determination of CH content

For studying the pozzolanic reactions of RHA it is important to know the CH (calcium hydroxide) content of in hydrating cement-RHA paste. For that purpose, test samples of the mixtures Ref 0.25 and 20% RHA-9 (See Table 5.1) were prepared in a Hobart mixer at room temperature around 20 ± 2 ℃. After 3 minutes mixing, the pastes were poured into plastic bottles (ϕ 33×70 mm) and sealed to prevent moisture loss. All the specimens were stored in a climate room at 20 ± 1 ℃.

At a predefined age, the specimens were demoulded from the plastic bottles and crushed into small pieces. After that, the specimens were immersed in liquid nitrogen (around -195 ℃) for 5 minutes to stop hydration. The specimens were then dried in a freeze-dryer. Water loss was recorded once per day after drying for one week. When the loss of water was less than 0.05% per day, the drying procedure was considered complete.

The dried paste samples were ground by hand until the particle size was smaller than 125 µm. The obtained powder was put in an aluminium oxide (Al$_2$O$_3$) crucible and heated from 40 °C to 1100 °C in a thermoanalyzer TG-449-F3-Jupiter instrument (Figure 5.1). The heating rate is 10 °C per minute. The weight change of the sample was measured with the thermo-analyzer

Figure 5.1 TG-449-F3-Jupiter® for thermogravimetric analysis

and was carried out in Argon atmosphere. The test was performed at the age of 1d, 2d, 3d, 7d, 14d, and 29d.

The amount of CH of the paste was determined by TGA-test according to Midgley [120]. A typical weight-loss versus temperature curve obtained from TGA-measurements for Portland cement paste (w/c=0.4; at 28 days) is shown in Figure 5.2 [121]. Three characteristic endothermic effects are observed. The first endothermic effect, in the temperature range from 100 to 320 °C, is attributed to the dehydration of calcium silicate hydrate (C-S-H) and calcium aluminate hydrate (C-A-H) [122-124]. For determination of the amount of CH in the cement paste the second endothermic temperature peak is of interest that occurs between 420 and 550 °C. The decomposition reaction of CH follows Equation (5.2):

$$Ca(OH)_2(s) \rightarrow CaO(s) + H_2O(g) \tag{5.2}$$

During the decomposition of CH, the weight loss of the sample comes from the loss of water. This weight loss (m_{H_2O}) can be determined by a graphical technique proposed by Marsh [123] (see Figure 5.2). Within the TG curve the onset and offset points of the decomposition curve of CH are determined, which are the intersections of two tangent lines.
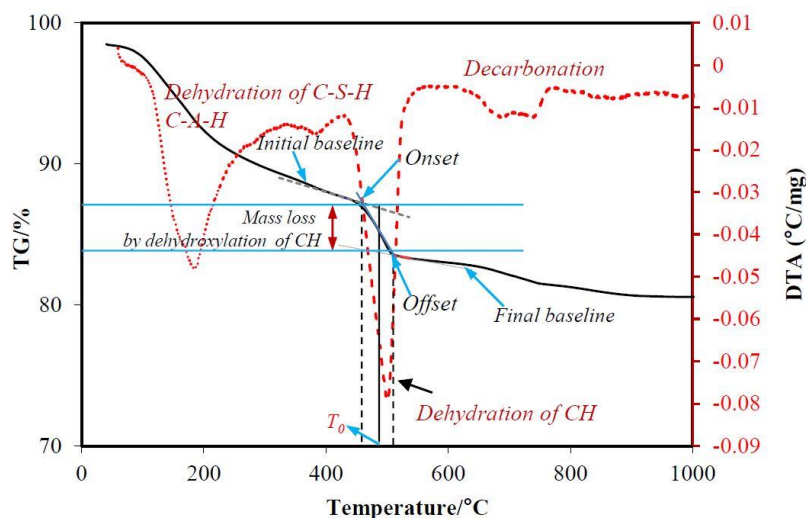
Figure 5.2 Procedure used to calculate the CH content of paste from TGA-test result [121]

They are defined as the initial baseline and final baseline, respectively. By the onset and offset points (Temperature axis), the mid-point T_0 is created. The weight loss m_{H_2O} is defined as the distance between two intersections generated by the vertical line from T_0 with initial and final baselines. Then the content of CH (m_{CH}) is calculated:

$$m_{CH} = m_{H_2O} \times \frac{74}{18} \tag{5.3}$$

where 74 and 18 are the molar weights of $Ca(OH)_2$ and H_2O.

The third endothermic effect around 700 °C indicates the decarbonation of calcium carbonate ($CaCO_3$) in cement paste. Decarbonation of calcium carbonate will not be further dealt with in this study.

5.3.3 ESEM studies for determination of the degree of hydration of cement

For determination of the degree of hydration of the cement ESEM (Environmental Scanning Electron Microscope) studies have been performed. For preparing test samples of cement pastes for ESEM studies the same procedure was followed as used for the TGA test samples as discussed in section 5.3.2.

Several pieces of the dried paste samples (about 20 g) with different sizes were collected in a plastic bottle for ESEM tests. The sample in a plastic bottle was put in a vacuum chamber and degassed at 30 mbar for 1 hour. With the vacuum pump still running, a very low viscosity epoxy resin was infused dropwise from a cup outside the chamber to the top of the samples via a plastic tube. The infusion is stopped when the upper surface of the sample was covered with epoxy. After about 10 minutes, the air was gradually let into the vacuum chamber and the bottle was taken out. The impregnated sample was stored at atmospheric pressure at 20 ºC for 24 hours. Then the samples were ready for grinding and polishing. Figure 5.3 shows an example of the sample ready for the ESEM studies. The ESEM-measurements were performed at the age of 1d, 2d, 3d, 7d, 14d, and 29d.

The microstructure characteristics of the paste samples were studied using the back-scattered electrons (BSE) mode. The observations were conducted with a Philips-XL30-ESEM in a gaseous (water vapour) environment (no conductive coating is needed). An acceleration voltage of 20 kV was used. The size of the reference region in each image is 248 μm in length and 188 μm in width. The magnification is 500× and the image size is 1424 × 968 pixels, so the resolution of each image is 0.18 μm per pixel.

BSE image analysis technique is widely used for determining the hydration degree of cement in cement paste [125]. One must remember that the accuracy of the results depends
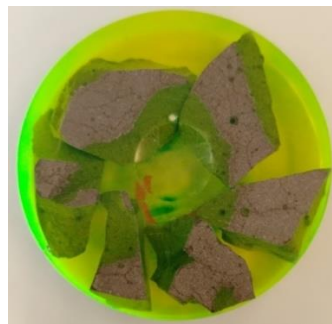
Figure 5.3 Sample for ESEM images analysis

on the resolution of the images. Scrivener et al. [126] found that for a cement paste analysis often fields at a magnification of 400 were sufficient to give a standard error of around 0.6%. Mouret et al. [127] applied a rigorous statistical analysis to show that a magnification of 200 is sufficient to give good results for the anhydrous phase and that 30 images are needed for a mean value with an error of $< 0.2\%$ in pastes and mortars. In this chapter, a magnification of 500 and 20 images were used for the image analysis, following the method used by Ye [117].

A typical BSE image of Portland cement paste (w/c = 0.4; at 7 days) and its grey level histogram are shown in Figure 5.4. Phases with different densities show different grey levels. The grey level histogram indicates that the main phases are unhydrated cement (anhydrous), hydration products (CH, HP), and pores. Figure 5.4 illustrates that the unhydrated cement phase in cement paste can easily be segmented. The degree of hydration of cement, α_C, can be estimated from the area fraction (equivalent to volume fraction) of remaining unhydrated cement. It is the ratio of reacted cement relative to the original amount of cement as indicated in Equation (5.4):

$$\alpha_c(t) = \frac{V_{reacted}}{V_{original}} = 1 - \frac{V_{ce}(t)}{V_{ce}(0)} \qquad (5.4)$$

where $V_{ce}(t)$ is the volume of unreacted clinker from the image analysis at the age t, and $V_{ce}(0)$ the original volume of cement in the mix proportions.
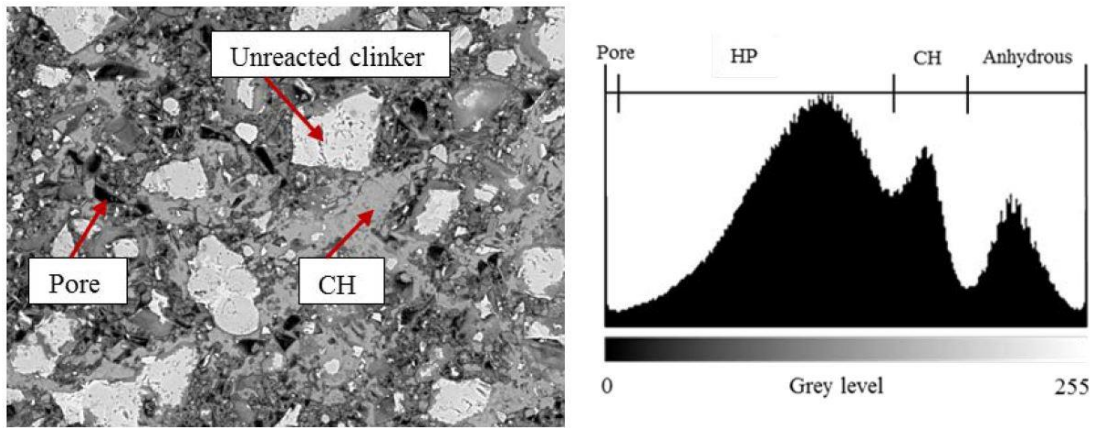
Figure 5.4 A typical BSE image (500×) of cement paste at 7 days and its grey level histogram (Pore: Porosity; HP: hydration products other than Portlandite; CH: Portlandite; Anhydrous: unhydrated cement)[121]

The same segmentation procedure as mentioned before can also be applied for analysing the degree of hydration of cement in cement-RHA blended systems. An example is shown in Figure 5.5. It is not possible, however, to distinguish the RHA particles or portlandite from the grey level histogram in Figure 5.5, because the grey levels of RHA particles overlap those of hydration products (CH, HP). Besides this, the irregular shape of RHA particles also complicates the segmentation of RHA from BSE images. This means that the area selection tool [128] cannot be utilized here. Hence, the reaction degree of RHA is hard to obtain from the BSE images directly, whereas the degree of hydration of cement in blended systems can easily be calculated with Equation (5.4).
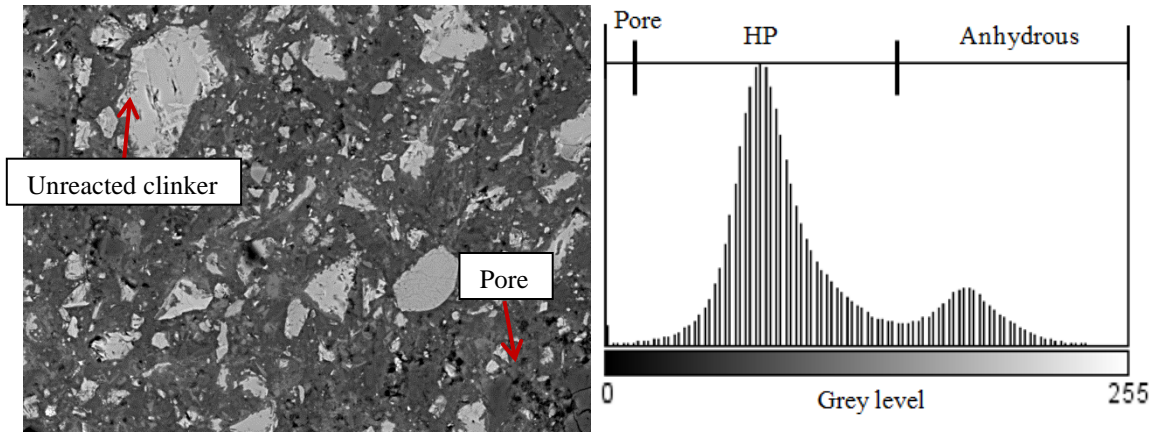
Figure 5.5 A typical BSE image (500×) of cement paste incorporating RHA at 7 days and its grey level histogram (Pore: Porosity; HP: hydration products; Anhydrous: unhydrated cement)

5.3.4 Determination of the degree of reaction of RHA[2] in blended cement

In the pozzolanic reaction $Ca(OH)_2$ is consumed and forms C-S-H. The consumption of $Ca(OH)_2$ can, therefore, be used as an indicator for the pozzolanic reaction in blended cement [131, 135]. Bentz et al. [53] derived $C_{1.1}SH_{3.9}$ to represent the C-S-H gel produced by the pozzolanic reaction of silica fume. Because the chemical composition of silica fume (SF) and RHA is similar (see section 4.2), it is assumed that their pozzolanic reactions are similar as well. The pozzolanic reaction of RHA (represented by "S") is presented below:

$$1.1CH + S + 2.8H \rightarrow C_{1.1}SH_{3.9} \tag{5.5}$$

where CH represents $Ca(OH)_2$; S represents SiO_2; H represents H_2O; C represents CaO.

The amount of CH in a mixture at a certain time t ($C_{CH}(t)$) results from the amount of CH initially present in the cement ($C_{CH,0}$), the CH formed in the hydration reaction of the cement, i.e. $C_{CH,hyd}(\alpha_c(t))$, and the consumption of CH in the pozzolanic reaction ($C_{CH,poz}(t)$). This amount of CH can be measured by TGA ($C_{CH,mea}(t)$) as explained in section 5.3.2. In formula form:

$$C_{CH}(t) = C_{CH,mea}(t) = C_{CH,0} + C_{CH,hyd}(\alpha_c(t)) - C_{CH,poz}(t) \tag{5.6}$$

---

[2] Several authors [[129-132] have used *selective dissolution methods* to measure the reaction degree of slag or fly ash in blended cement. With this method the reaction products are dissolved leaving behind the unreacted pozzolanic materials. However, researchers already noted that the dissolution of reaction products is often incomplete. Taylor and Mohan [133] noted that large corrections must be made for incomplete dissolution of other phases and estimated an error in the results of about ± 10%. For studying the reliability of the selective dissolution, Kocaba et al. [134] examined the residues after selective dissolution by XRD and SEM. The results showed that except ettringite and ferrite, the other anhydrous and hydrated phases were not completely dissolved, and in the residues hydrotalcite was observed by XRD. Ben Haha et al. [132] noted a significant possible error in the result of the selective dissolution method as different assumptions lead to large differences in the quantification of reaction degree of fly ash. Kocaba et al. [134] also pointed out that wildly divergent results are reported for this method by different workers in nominally similar pozzolanic materials.

In the light of the previous work and the scatter of the results in the literature, the selective dissolution method will not be used for quantitative determination of the reaction degree of RHA.

The amount of CH formed during hydration, i.e. $C_{CH,hyd}(\alpha_c(t))$, is assumed to be a linear function of the degree of hydration of the cement $\alpha_c(t)$, viz. [ref]:

$$C_{CH,hyd}(\alpha_c(t)) = A \cdot \alpha_c(t) + B \tag{5.7}$$

where A and B are constants to be determined experimentally. The degree of hydration of the cement, $\alpha_c(t)$, can be determined by SEM as explained in section 5.3.3.

By rewriting Eq. (5.6), the amount of CH consumed in the pozzolanic reaction, $C_{CH,poz}(t)$, g/g binder) it holds:

$$C_{CH,poz}(t) = C_{CH,0} + C_{CH,hyd}(\alpha_c(t)) - C_{CH,mea}(t) \tag{5.8}$$

Once $C_{CH,poz}(t)$ is known, the reacted SiO_2 content can be calculated with Eq. (5.5). The degree of pozzolanic reaction of RHA at the age t, i.e. $\alpha_{RHA}(t)$, (g/g RHA) can then be determined with Eq. (5.9):

$$\alpha_{RHA}(t) = \frac{C_{CH,poz}(t)}{R} * \frac{M_S}{1.1 * M_{CH}} * \frac{1}{C_{SiO_2}} \tag{5.9}$$

where C_{SiO_2} is the SiO_2 content of RHA, (88.86%), $C_{CH,poz}(t)$ is the reacted CH content in the pozzolanic reaction [g/g binder], R is the replacement ratio of cement by RHA in the mixture (here: 20%), M_S is the molar mass of SiO_2(60.08 g/mol) and M_{CH} is the molar mass of $Ca(OH)_2$ (74.093 g/mol).

5.4 Results and discussion

5.4.1 Liquid absorption capacity of RHA

The absorption capacity of RHA was measured in demineralized water and synthetic pore solution, respectively, for different immersion time. The result is shown in Figure 5.6. The figure indicates that the RHA particles can rapidly absorb the liquid in several minutes and reach the maximum absorption capacity after 5 minutes. The reason for this high-speed absorption is capillary action. The pore size of RHA-9 particles is less than 10 µm (result of MIP in Chapter 4, Figure 4.10). With these small pores, a prominent capillary force according to the Young-Laplace equation [12] will form, when RHA particles become in contact with liquids. As a consequence, the liquids were moved quickly into RHA particles under the capillary force.
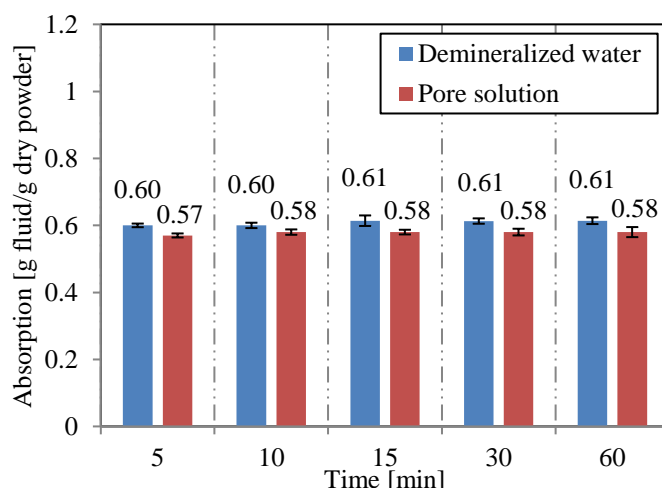
Figure 5.6 Absorption capacity of RHA-9 measured in demineralized water and synthetic pore solution with different immersion time

The results also show that the maximum absorption capacity of RHA in synthetic pore solution is slightly smaller than that in demineralized water. It indicates that the presence of ions in solution has an impact on the maximum absorption capacity of RHA, but this effect is small[3]. Because of the presence of ions in the pore solution of cement pastes, in further studies a maximal liquid uptake of RHA-9 in the mixture will be adopted of 0.58 g/g.

5.4.2 Evolution of reactions in cement and RHA

The evolution of the hydration reaction in the cement and the pozzolanic reaction in the RHA in the mixtures Ref 0.25 and 20% RHA-9 (see Table 5.1) are presented in Table 5.2 and graphically in Figure 5.7 to Figure 5.11.

5.4.2.1 Degree of hydration of cement in mixtures Ref 0.25 and 20%RHA-9

The degree of hydration of the cement in the mixtures Ref 0.25 and 20%RHA-9 is determined from BSE images as discussed in section 5.3.3. Results are presented in Table 5.2 and in Figure 5.7. The figures show that for the same age, the degree of hydration of the cement in mixture '20% RHA-9' is higher than that in mixture 'Ref 0.25', although the effective water/cement ratio in '20% RHA-9' is lower, i.e. 0.18 instead of 0.25 in the reference sample (due to absorption of water by RHA). This may be explained by two mechanisms. First, the hydration product of cement, i.e. CH, is consumed by the pozzolanic reaction, promoting further hydration of cement. Second, the RHA releases the absorbed water gradually, which provides extra water for cement hydration. It is noted that if the degree of pozzolanic reaction

---

[3] The small difference in absorption capacity of RHA in demineralized water and pore solution can be explained by the analogy with SAP-studies. The absorption capacity of SAP amounts to approximately 350 g/g in distilled water and 37 g/g in synthetic pore fluid [94]. The driving forces for absorbing liquid are different between SAP and RHA. The macromolecular matrix of SAP is a polyelectrolyte, i.e. a polymer with ionizable groups that can dissociate in solution. For this reason, a high concentration of ions existing in the solution inside the SAP leading to a water flow into the SAP due to osmosis. The salinity of the aqueous solution has an important effect on the osmosis pressure and influences the swelling of SAPs [11]. However, the water flowing into RHA particles is driven by capillary action. The salinity of the solution has a minor influence on the capillary force in the Young-Laplace equation. This is why the maximum absorption capacities of RHA measured in demineralized water and synthetic pore solution are close.

Table 5.2 Summary of measurement data of degree of hydration and CH-content in mixtures Ref 0.25 and 20% RHA-9, as well as calculated degree of pozzolanic reaction of RHA.

Time t [days]	Ref 0.25		20% RHA-9				
	Degree of hydration $\alpha_c(t)$ [SEM] [--]	CH-content $C_{CH}(t)$ [TGA] [g/g]	Degree of hydration $\alpha_c(t)$ [SEM] [--]	CH-content $C_{CH,mea}(t)$ [TGA] [g/g binder]	$C_{CH,hyd}(\alpha_c(t))$ (calc.) Eq. (5.9) [g/g]	$C_{CH,poz}(t)$ (calc.) Eq. (5.10) [g/g]	Degree of reaction $\alpha_{RHA}(t)$ Eq. (5.11) [%]
1	0.41	0.69	0.46	0.55	0.64	0.09	3.7
2	0.46	0.83	0.52	0.63	0.76	0.13	5.4
3	0.49	0.90	0.62	0.69	0.93	0.24	9.9
7	0.53	0.94	0.63	0.66	0.95	0.29	11.9
14	0.55	0.98	0.64	0.65	0.97	0.32	13.0
29	0.56	1.05	0.64	0.59	0.97	0.38	15.5
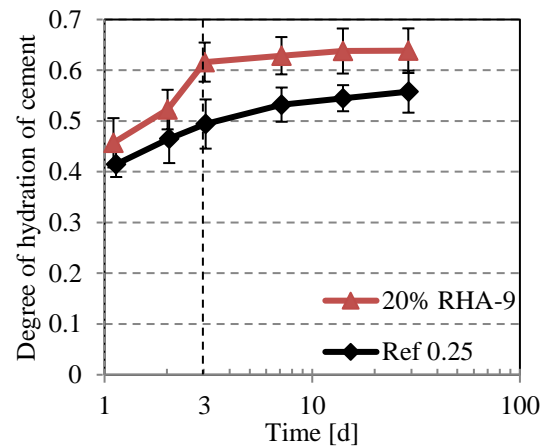
Figure 5.7 Degree of hydration of cement in mixtures Ref 0.25 and 20%RHA-9, determined from BSE images.

is relatively small at certain age, which means the amount of water consumed in the pozzolanic reaction is much less than the amount of water released by RHA particles, the second mechanism will dominate.

5.4.2.2 Evolution of CH content in mixtures Ref 0.25 and 20%RHA-9

The evolution of the CH content in the mixtures Ref 0.25 and 20%RHA-9 was determined experimentally by TGA measurement. Results are shown in Table 5.2 and in Figure 5.8 a and b. In Figure 5.8a the CH content is presented as function of time for both mixtures. For the reference mixtures the CH content increases with time, whereas the amount of CH mixture '20% RHA-9' starts to decrease after about 3 days. Obviously from that time on the pozzolanic reaction starts at noticeable rates.

In Figure 5.8b the CH content is presented as function of the degree of hydration of the reference mixture Ref. 0.25. As shown in this figure there is an almost linear relationship between the CH content and the degree of hydration of the cement after 1 day since casting.

For the relation between the amount of CH formed in the hydration process, i.e. $C_{CH,hyd}(\alpha_c(t))$, it follows (after curve fitting the constants A and B in Eq. (5.7)):

$$C_{CH,hyd}(\alpha_c(t)) = 0.2282 \cdot \alpha_c(t) - 0.0245 \qquad (5.10)$$

From the curve fit analysis, a strong correlation between the degree of hydration and the liberated amount of CH was found: coefficient of determination (R^2) is 0.97.

Now the values of constant A and B in Eq. (5.7) are known, i.e. A = 0.2282 and B = -0.0245, the amount of CH (per gram cement) formed from cement hydration in mixture 20%RHA-9 can be calculated. These calculated values of $C_{CH,hyd}(\alpha_c(t))$ are presented in Table 5.2.

a. Measured CH content vs. time   *b. Measured CH content vs. degree of hydration*
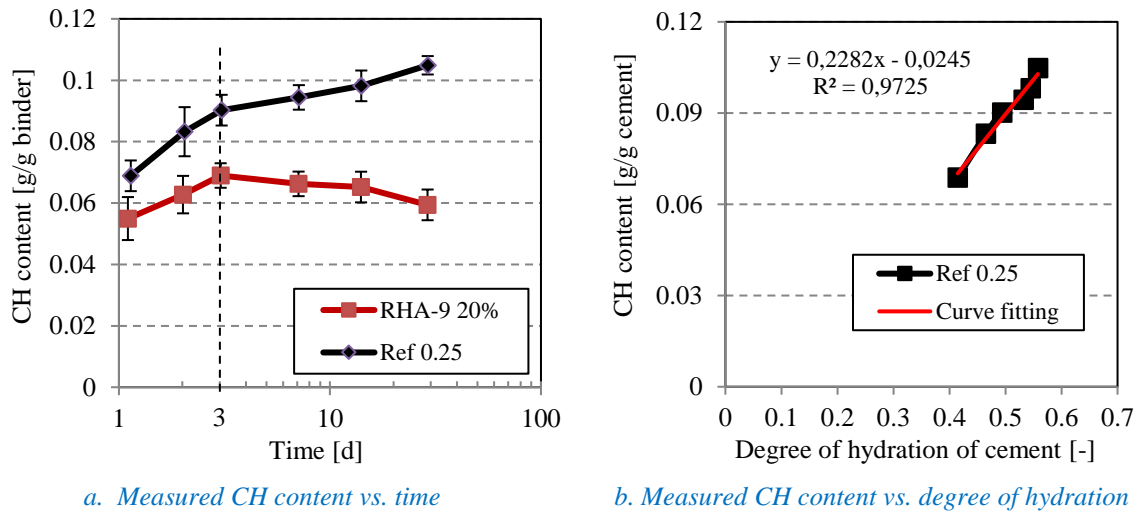
Figure 5.8 Measured CH content, $C_{CH,mea}(t)$, in cement mixtures Ref. 0.25 and 20%RHA-9, determined by TGA. a) CH content vs. time. b) CH content vs. degree of hydration of cement

5.4.2.3 Evolution of the pozzolanic reaction in RHA in mixture 20%RHA-9

The degree of pozzolanic reaction of the RHA in mixture 20%RAH-9 is calculated with Eq. (5.9). The only unknown in Eq. (5.9) is the CH-content consumed in the pozzolanic reaction, i.e. $C_{CH,poz}(t)$. Values of $C_{CH,poz}(t)$ have been calculated with Eq. (5.8) and are presented in Table 5.2. The evolution of the pozzolanic reaction is calculated and presented in Figure 5.9.
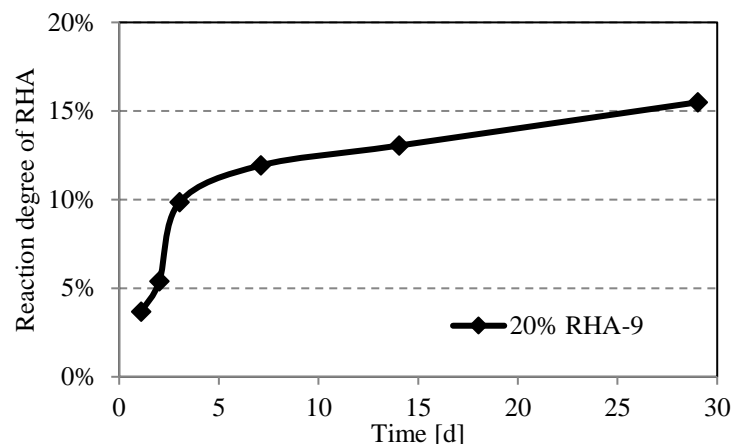
Figure 5.9 Evolution of the pozzolanic reaction of RHA-9 in mixture 20% RHA-9 with time

As shown in Figure 5.9, the degree of pozzolanic reaction of RHA at the age of 29d is only 15.5%. Compared to the high reaction activity of SF at early ages [135], the activity of pozzolanic reaction of RHA is low. Tuan [6] also found that the pozzolanic reaction activity of RHA was much lower than that of SF. Tuan found that for the same replacement percentage, the cement paste with RHA had a higher CH content than a cement paste with SF after 3 days since casting. Obviously the pozzolanic reaction in the mixture with RHA had hardly started, resulting in a high CH content in the paste.

5.4.3 Internal curing with pozzolanic reaction of RHA

In section 5.4.2 the evolution of the degree of hydration of the cement and of the pozzolanic reaction of the RHA in a cement-RHA blended paste have been discussed. In this section the focus will be on the evolution of the internal moisture state during these reactions and how RHA may act as an efficient internal curing agent.

5.4.3.1   Water consumed in pozzolanic reaction

RHA can hold water thanks to its porous structure. In cement pastes the porous structure of RHAs will collapse due to the pozzolanic reaction with CH. The reacted RHA particles can then no longer act like water reservoirs as before. In fact, the initially absorbed water will be needed for the pozzolanic reaction of the RHA. According to Eq. (5.5), 1 g RHA (88.86% SiO_2 content) can react with 0.75 g water. If the amount of entrained water in RHA is 0.58 g/g, 1 g RHA needs 0.17 g *extra* water for a complete pozzolanic reaction. The water will be taken from the cement paste, leading to extra self-desiccation of the paste.

For mixture 20% RHA-9, with an evolution of the pozzolanic reaction as presented in Figure 5.9, the total amount of water needed for the pozzolanic reaction is shown in Figure 5.10.
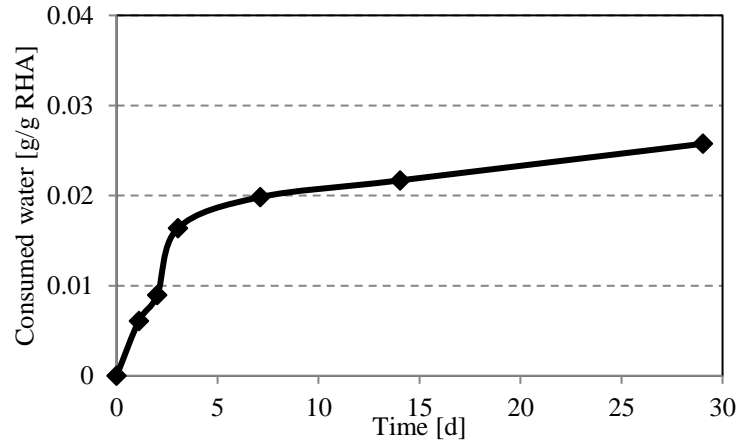
*Figure 5.10 Total amount of water consumed in the pozzolanic reaction of RHA in mixture 20%
RHA-9 (pozzolanic reaction as in Figure 5.9)*

The fact that for the pozzolanic reaction of the RHA more water is needed than absorbed in
its pore structure means that the pozzolanic reaction will intensify the self-desiccation of the
paste and negatively affect the efficiency of the internal curing by RHA. Yet, the
experimental results in Chapter 4 have clearly shown that RHA can efficiently mitigate the
autogenous shrinkage of cement pastes. This suggests that the amount of water released by
the still intact RHA particles is higher than the amount of water needed for the pozzolanic
reaction of the reacting RHA. More details about the influence of pozzolanic reaction on the
efficiency of internal curing by RHA will be discussed in chapter 6.

5.4.3.2   Evolution of RH (relative humidity) in reacting cement-RHA blended systems

The autogenous shrinkage and internal RH measurements shown in Chapter 4 indicated that
RHA has a positive effect on mitigating autogenous shrinkage of cement pastes. The porous
structure makes RHA particles acting as water reservoirs. For estimating the effectiveness of
internal curing of RHA, the amounts of water released at different ages need to be determined.
In chapter 4 the measured internal RH in cement paste at the onset of self-desiccation of
mixture 20%RHA-9 was about 99.5%. The initial RH drop of about 0.5% can be attributed
to dissolved salts in the pore fluid. The effect of dissolved salts on the RH of the pore solution
amounts to several percent in the Portland cement system. For example, for a composition of
the pore fluid of a two-month-old cement paste with w/c ratio 0.45 [136], a value of 96.7%
RH is calculated. Here it will be assumed that the initial RH drop measured in the mixture
20% RHA-9 is only caused by dissolved salts and, furthermore, that effect remains constant
during hydration [57]. With this assumption it is possible to calculate the RH change without
the effect of dissolved salts.
   The RH in the pore systems can be estimated using the following formula [62]:

$$RH = RH_S * RH_D \tag{5.11}$$

where RH_S is the relative humidity of the pore solution due to the dissolution of salts and
RH_D is the relative humidity of the pore solution *without* the effect of dissolution of salts
(like deionized water).
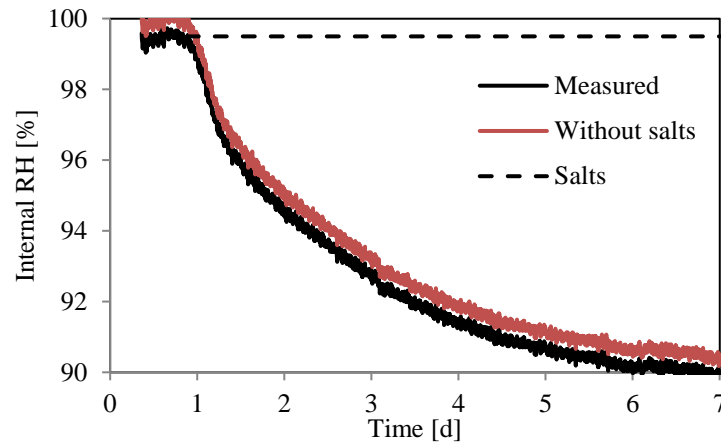
Figure 5.11 Measured internal RH change, RH due to salt dissolution in the pore fluid and internal RH change without salt dissolution in the mixture '20% RHA-9' (Eq. (5.11))

The change of the internal RH of the pore solution without the dissolved salts RH_D, calculated with equation (5.11), is shown in Figure 5.11. Figure 5.12 presents water vapour desorption isotherm of RHA-9 at different RH (partly from Chapter 4). The maximum water absorption capacity of RHA-9 measured in Section 5.4.1 is the water content of RHA at 100% RH. Based on the water content of RHA particles at different RH in measured desorption isotherm and the evolution of internal RH in the mixture '20% RHA-9', the water content in the RHA particles in the mixture '20% RHA-9' at different ages can be determined. As the initial water uptake of RHA-9 is 0.58 g/g, the amount of water released from RHA particles with time is obtained and shown in Figure 5.13.
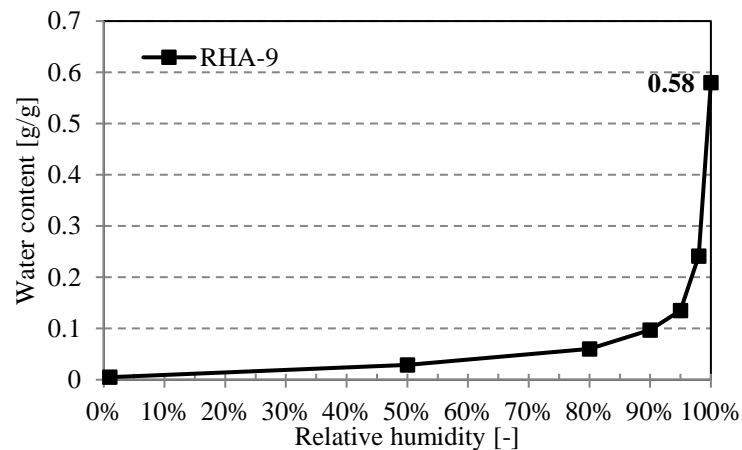
Figure 5.12 Water content of RHA-9 at different RH
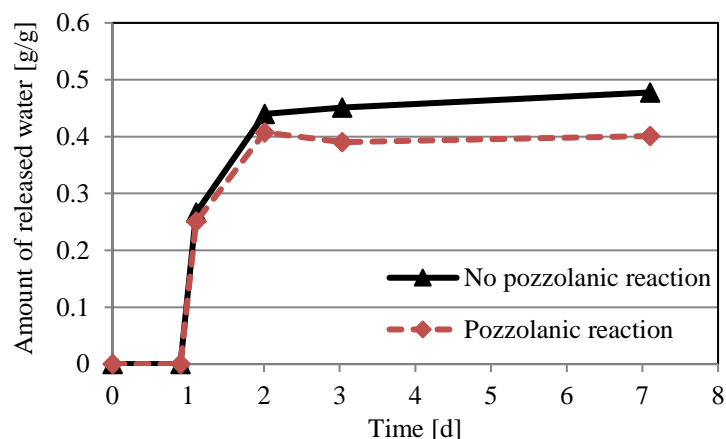
Figure 5.13 Amount of internal curing water released by RHA at different ages in the mixture '20% RHA-9' with and without considering pozzolanic reaction

As discussed in section 5.4.3.1, the pozzolanic reaction consumes a certain amount of entrained water inside RHA and thereby reduce the amount of released water for internal curing. The amounts of released water at different ages with and without considering pozzolanic reaction are presented in Figure 5.13. Due to the relatively low degree of pozzolanic reaction of RHA-9 (15.5% at 29 days in Figure 5.9), the influence of this pozzolanic reaction on the content of released water is limited.

A sketch of internal curing process of RHA in cement pastes is shown in Figure 5.14. Before the onset of self-desiccation, the RH in cement pastes is almost 100% (a bit lower due to the effect of dissolved salts). During this period no RH gradient exists between RHA and cement pastes, thus no water is released from RHA particles before the onset of self-desiccation in the cement paste (see Figure 5.13). In the mixture '20% RHA-9', the internal RH is about 95% at 2 days after casting. According to Figure 5.12, the water content in RHA-9 is 0.58 g/g at RH 100% and 0.135 g/g at RH 95%. Therefore, a major part (77%) of the water stored in RHA-9 is released in 2 days. The phenomenon has also been observed in cementitious mixtures with SAP [94] and lightweight aggregate [57]. These internal curing agents, including RHA, can release most of the entrained water at the early age when the self-desiccation starts while the RH value is still relatively high. This is a critical characteristic of a good internal curing agent. Because at the very early age of a sealed cement paste the stiffness is relatively weak, even moderate capillary tension can induce big autogenous shrinkage and form cracking. It is important to keep the internal RH as high as possible during this period, which means a good internal curing agent should release a large amount of water at a high RH. A typical negative example is using a porous material – zeolite as internal curing agent. It can be found in the literature [137] that zeolite aggregate has a high water absorption capacity, but their fine pore structure hold the absorbed water until the RH is lower than 80%. Most of the water is retained in nm-sized pores and does not help to counteract the effects of self-desiccation.

RHA can provide internal curing at later ages, which is favorable for the long-term properties of cement mixtures. The water content in the RHA-9 after 7 days is calculated at

Figure 5.14 Internal curing in cement paste with RHA. (a) At initial condition, RH equilibrium exists between paste and RHA. (b) Water migrates from RHA to cement pastes due to RH difference. (c) New RH equilibrium is reached after moisture exchange.

about 0.1 g/g. This implies that a certain amount of water still remains in the smaller pores and is gradually released at later ages. Even after 28 days, when the RH has decreased to 78% [138], the water content in the RHA-9 is still about 0.06 g/g (see Figure 5.12). The remaining water can be released to the surrounding cement paste and beneficial for the hydration of cement at later ages. This phenomenon is also observed with high-performance mortar using saturated lightweight aggregates in [139].

5.4.4 RHA as internal curing agent: Summary of findings

5.4.4.1 Mechanism in mitigating autogenous shrinkage

RHA can be considered an excellent agent for mitigating autogenous shrinkage of cement pastes. When dry RHA powder is mixed with cement paste, due to its porous structure and

high pore volume, a part of the added mixing water is rapidly absorbed by RHA. With the evolution of cement hydration, self-desiccation of cement pastes occurs and an RH gradient forms between RHA particles and surrounding cement paste. The initially absorbed water is then gradually released from the RHA particles to the cement pastes. The internal curing by RHA reduces the self-desiccation and maintains the internal RH value at a high level (RH > 90% in 7 days). During the internal curing process, part of the RHA reacts in the pozzolanic reaction which reaction needs extra water. However, since the degree of reaction remains small (15.5% at 29 days), the effect of the pozzolanic reaction on the amount of released water is limited.

5.4.4.2   Comparison with other internal curing agents

Lightweight aggregates and SAPs are the two most commonly used internal curing agents for concrete used in practice. The absorption capacity and particle size of SAPs are the two most critical factors which determine the efficiency of internal curing.

The absorption capacity of RHA-9 (0.58 g/g, Figure 5.6) is bigger than that of normal lightweight aggregates (0.13 ~ 0.27 g/g in [140], 0.26 g/g in [57]), but much smaller than that of SAPs (37 ~ 350 g/g in [94]). To provide a similar amount of curing water, a larger dosage of the internal curing agent with smaller absorption capacity is needed. Therefore, the dosage of RHA in cement mixtures is much larger than that of the SAP (less than 1% [94]). The particle size of RHA-9 (D_{50} = 9 µm) is several orders of magnitude smaller than that of lightweight aggregates (grain size 0.15 ~ 4.75 mm in [140], grain size 4 ~ 8 mm in [57]) and SAPs (D_{50} = 125 ~250 µm in [94]). The 'distribution' of water reservoirs plays an important role in internal curing process, because it determines whether the entire body of the mixture is cured by the water released from these water reservoirs [89]. Computer simulations indicate that the water diffusion in a cement paste is limited to distances of the order of 100-200 µm when the capillary pore space is percolated [141]. In mixtures with a low water/binder ratio, especially in UHPC, the microstructure of cement paste is very dense, which constrains the water movement from reservoirs to the surroundings. This means that water reservoirs should be well dispersed in the paste to ensure the effectiveness of internal curing agents. In this respect, RHA is easier to disperse than SAP because of its smaller particle size.

Due to the strict requirements on mechanical properties and the maximum size of aggregate, lightweight aggregate is not frequently used in UHPC for internal curing. For those mixtures SAP has more often been proposed as internal curing agent to mitigate the autogenous shrinkage. However, SAP makes the concrete heterogeneous, because it will leave voids even as big as 600 µm [2], which has a negative impact on the properties of UHPC.

As discussed above, RHA is a competitive internal curing agent and has an advantage in mixtures with low water/binder ratio, especially for UHPC.

5.5   Conclusions

Based on the experimental results and discussions in this chapter, the following conclusions have been drawn.

1) With the evolution of cement hydration, the self-desiccation occurs in cement paste and an RH gradient is formed between the RHA particle and the surrounding cement paste. Due to capillary suction and moisture diffusion water gradually releases from the RHA to the cement pastes until the new RH equilibrium in the paste is reached.

The amount of released water provides the internal curing for the mixture, thus counteracting self-desiccation and reducing autogenous shrinkage.

2) The pozzolanic reaction of RHA can intensify the self-desiccation and negatively affects the mitigation of autogenous shrinkage of cement pastes, but this influence is limited and will not negate the beneficial effect.

3) Compared to the SAPs and lightweight aggregates, RHA is a competitive internal curing agent, especially for UHPC due to its dense microstructure.

The influence of pozzolanic reaction of RHA on internal curing in the mixture 20% RHA-9 is qualitatively estimated by experiments in this chapter. However, this influence may be differenct in other mixtures which has different dosage of RHA. For further understanding, the quantitive descirption of the effect of pozzolanic reaction by numerical simulation will be performed in next chapter.

Chapter 6

Numerical simulation of internal curing in cement paste with RHA

6.1 Introduction

In Chapter 5, the mechanisms for mitigating autogenous shrinkage by using RHA have been studied experimentally. The internal curing effect of RHA can counteract the self-desiccation and reduce the autogenous shrinkage. At the same time the pozzolanic reaction of RHA can intensify the self-desiccation and increase the autogenous shrinkage. These two effects of RHA jointly determine the efficiency of RHA to mitigate autogenous shrinkage. For a better understanding of these two effects of RHA on mitigating autogenous shrinkage, numerical simulations will be performed in this chapter.

The effect of internal curing and its effect on the rate of cement hydration and the pozzolanic reaction of RHA is evaluated quantitatively by using the numerical simulation model HYMOSTRUC. How this simulation model is used for quantitative simulation of internal curing will be described in this chapter. Parameters that will be focused on in particular are the (evolution of the) degree of saturation and the internal relative humidity of the hardening paste. As output the evolution of the degree of hydration of the cement and the associated internal relative humidity in the paste are shown for different dosages of RHA.

6.2 Moisture transport in hydrating cement pastes with RHA

6.2.1 Mechanism of moisture transport in hardening cement paste with RHA

For the internal curing process, water migration in cement paste is essential. For cement pastes with internal curing agents (water reservoirs), capillary pressure differentials in the pore system are the driving force of water movement [142-145]. When the hydration of cement proceeds, the pores of the paste are gradually emptied, resulting in different values of the RH in the pore systems of the paste and the "reservoirs" [146]. Under capillary pressure water will be drained from the reservoirs to the small pores in the drying cement paste. After receiving extra water from these reservoirs, the hydrating cement paste maintains a higher saturation degree and a higher RH compared to cement pastes without saturated RHA.

For the explanation of simulation, the schematic of the internal curing of cement paste by saturated RHA in section 5.4.4 is shown again in Figure 6.1. Initially the saturation degree and RH of cement paste and RHA are both, roughly, 100%. No difference exists between the RH of the paste and RHA, which means no water movement (Figure 6.1a). With progress of cement hydration, self-desiccation of the paste happens. The RH in the hydrating cement paste becomes lower than 100%. However, the RH in the RHA is still 100% at this moment since the pozzolanic reaction degree of the RHA is still very small in that stage. The capillary pressure gradients drive the water from RHA to the cement paste (Figure 6.1b). The water from the RHA particles enters the drying pore structure of the cement paste and increases the degree of saturation and internal RH in the paste. Due to the movement of water from RHA to the cement paste, the RH in the pores of the RHA particle decreases until a new RH equilibrium is reached (Figure 6.1c). With ongoing hydration of the cement, new equilibriums will be established step by step. The internal curing process continues until the water inside RHA is used up or hydration of cement stops.
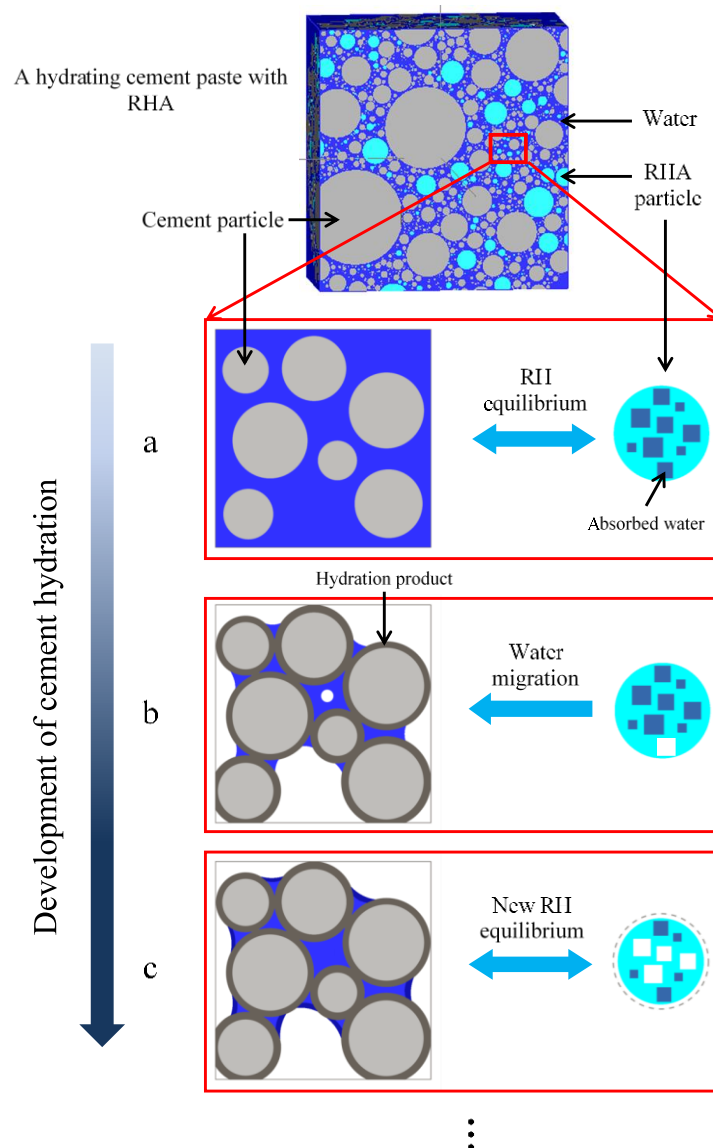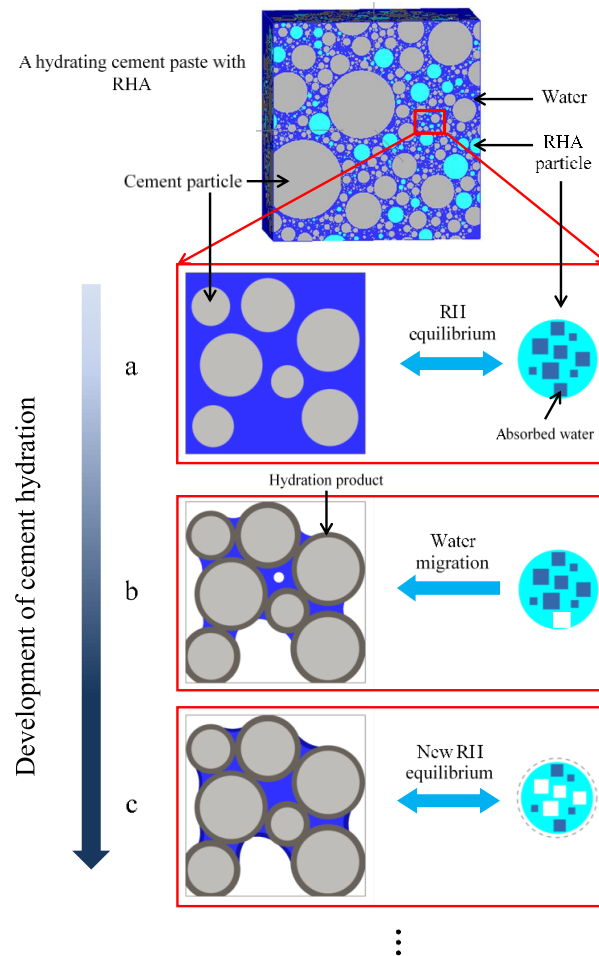
Figure 6.1 Internal curing in cement paste with RHA. (a) At initial condition, RH equilibrium exists between paste and RHA. (b) Water migrates from RHA to cement pastes due to RH difference. (c) New RH equilibrium is reached after moisture exchange.

6.2.2 Aspects to be considered for simulation of internal curing

For modelling the internal moisture transport, as described in the foregoing section, at least the following two aspects have to be considered:
   a. Evolution of the pore structure in hydrating paste
   b. Mechanism driving the moisture transport

In this section these aspects will be briefly discussed, with particular emphasis of modelling constraints.

Ad a. Evolution of the pore structure of RHA-blended cement paste
In an RHA-blended cement paste the ongoing chemical reactions, i.e. cement hydration and pozzolanic reaction of RHA, will cause a continuous change, i.e. densification, of the pore structure and a decrease of the amount of water in the pore system. The decreasing amount of water will concentrate in the smaller pores of the pore system. Gradually the paste dries out (self-desiccation), which goes along with an increase in the capillary pressure in the pore water and a drop of the relative humidity.

   As mentioned in section 2.4.1, the pore pressure and the relative humidity are related to each other via the Kelvin-Laplace equation. In the equations, the magnitude of the relative

humidity (and also of the capillary pressure) is determined by the largest pore still filled with water (pore diameter d_w). It is important, therefore, to know the largest filled pore as accurately as possible in order to make reliable predictions of the evolution of the relative humidity.

Generating detailed information about the pore structure, including the pore size distribution, of a hydrating system is not easy. Already for simple non-blended cement pastes numerical simulation of the evolution of the pore structure is difficult. For blended pastes this is even more complicated. In a cement-RHA mixture the reaction products of cement and RHA gradually merge, resulting in a pore structure *different* from that of a plain cement paste. Without detailed information about the pore structure, however, it will not be possible to determine the largest water-filled pore d_w and the corresponding relative humidity in the pore system.

Since modelling of the evolution of pore structures in blended cement pastes was not the goal of this thesis, an alternative approach will be followed. In this alternative approach the pore structure of cement paste will be described by a mathematical expression applied in the simulation model HYMOSTRUC [9], used for simulating hydration processes in plain cement pastes. This mathematical expression contains two model parameters, *a* and *b,* which depend on, among other things, the type of binder. How to determine a and b for the blended pastes considered in this thesis will be explained further in section 6.3.1. In section 6.2.3 a brief introduction of the HYMOSTRUC model will be given, including further explanation of the description of the pore structure.

Ad b. Moisture transport process from saturated RHA particles to drying cement paste
The simulation of hydration-induced moisture transport in saturated RHA particles to drying cement paste is complicated and computationally time-consuming [147]. From experimental studies Lura et al. [142] inferred that water could travel up to 3 mm in a hardening cement paste (w/c 0.3). Trtik et al. [148] used neutron tomography for studying water migration from large SAP particles to maturing cement paste. They found that during the first day of hydration of a cement paste with w/c 0.25 hardly any gradient of water content could be observed [101]. An almost uniform distribution of water in the hardening paste also became plausible from numerical simulations of water migration performed by Wyrzykowski [146]. For modelling internal curing Wyrzykowski et al. [101] assumed that self-desiccation caused by water consumption of hydrating cement is practically instantaneously compensated by supply of water from mixed-in 'reservoirs'. The results of Wyrzykowski's simulation were in very good agreement with experimental data, i.e. measurements of the evolution of the internal RH. Based on these findings it is considered justified to assume that, for numerical simulation of internal curing, moisture transport induced by self-desiccation takes place almost instantaneously.

In blended cement/RHA mixtures the relatively small RHA particles, i.e. $D_{50} = 9\mu m$, with dosages 10%-20%, are assumed to be well-distributed in the paste. Because of this homogenous distribution the moisture from the RHA particles can easily migrate to the bulk cement matrix. The assumption as proposed by Wyrzykowski et al. [101] regarding the instantaneous water transport will also be considered for the numerical simulations in this study. However, unlike the SAP in the Wyrzykowski's simulation, RHA is *not* an inert water reservoir. The RHA will react with calcium hydroxide generated from cement hydration. For this pozzolanic reaction water is consumed and the volume of unreacted water-containing RHA particles decreases. This pozzolanic reaction should also be considered in the simulation of internal curing in a hydrating cement paste with RHA.

6.2.3 Numerical simulation of internal curing in RHA-blended cement pastes

The blended cement/RHA system considered in this study consists of two powders, i.e. cement paste and RHA. For modelling the reaction processes, these two components of the system will be considered, at first, separately. The hydrating cement paste is called system A, and the RHA is called system B. System B exhibits pozzolanic activity. The hydrating system A consumes water and gradually dries out. When the hydration process starts, water will flow from the saturated RHA particles to the drying cement matrix. From that moment on the rate of hydration of system A will be affected by the water coming from system B (RHA). As soon as the RHA starts to react in a pozzolanic reaction, water transport from the system B to system A will slow down, stops, or even water is taken from the hydrating cement paste, potentially resulting in extra self-desiccation.

In the following sub-sections, some basics features of numerical modelling of cement hydration (system A) and pozzolanic reaction of RHA (system B) will be briefly presented.

6.2.3.1 Hydrating cement paste (System A)

General description of hydration and microstructure development of sealed cement paste
In a sealed hydrating cement paste water is consumed by the reaction with cement, resulting in self-desiccation of the paste. The reaction products form a gel, which contains the solid reaction products and the gel pores. Under normal curing conditions these gel pores are always filled with water, i.e. gel water. Pores with a size beyond the size of gel pores are capillary pores. These pores are partly filled with water and partly with air.

A particular stage in the evolution of the microstructure is schematically shown in Figure 6.2. At the walls of capillary pores a thin layer of adsorbed water is present. The thickness of this layer depends on the relative humidity in the empty pores. For a given pore system there is an equilibrium between the relative humidity in the capillary pore system and the amount of water stored in the smaller capillary pores.
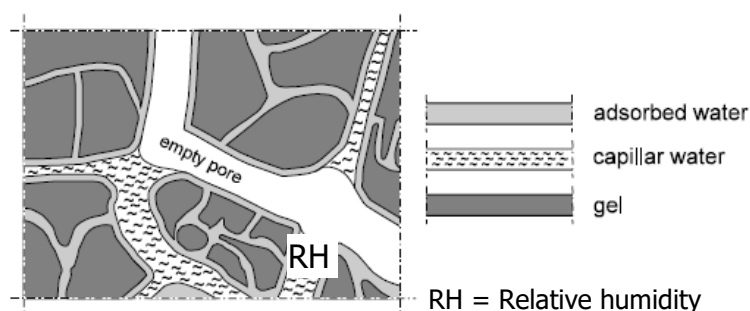
Figure 6.2 Schematic view of state of water in the pores systems of a cement paste [80]
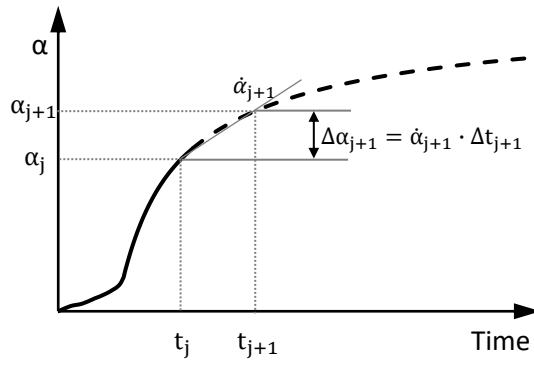
Figure 6.3 Evolution of the hydration process in sealed-cured cement paste - Schematic.

When the reaction proceeds more capillary water is consumed. The paste dries out, the relative humidity will further drop and the reaction proceeds at a slower rate. At an arbitrary time t_j the degree of hydration (DoH) of the cement is α_j. In the subsequent time step Δt_{j+1} the degree of hydration will increase by a hydration increment $\Delta \alpha_{j+1}$. This increment follows from (see also Figure 6.3):

$$\Delta \alpha_{j+1} = \dot{\alpha}_{j+1} \cdot \Delta t_{j+1} \tag{6.1}$$

where $\dot{\alpha}_{j+1}$ is the rate of hydration during the time step t_{j+1}. The rate of hydration $\dot{\alpha}(t)$ is a function of, among other things, the type of cement, the amount of water in the system and the distribution of the water in the pore system of the paste.

Numerical simulation of the sealed-cured cement with HYMOSTRUC
In this study the evolution of the hydration process will be calculated with the numerical simulation program HYMOSTRUC. In HYMOSTRUC, the hydration process of Portland cement is modelled at the particle level. At particle level the reaction is assumed to start as a *phase-boundary reaction* and gradually changes into a *diffusion-controlled reaction [80]*. In HYMOSTRUC these two types of reaction are simulated with a core-shell model, schematically shown in Figure 6.4. At the beginning, the cement particles are modelled as digitized spheres randomly distributed in a three-dimensional body. As cement hydrates, the cement grains gradually dissolve and a porous shell (outer product) of hydration products is formed around the grain, which will lead to an outward growth of the outer shell. When the total thickness of the inner product and outer product reaches a threshold value, the hydration will become a *diffusion-controlled reaction*. This threshold value is defined as *transition thickness*. During the aforementioned reaction period, the reaction rate is affected by the total thickness of the inner product and outer product.

With increasing thickness of outer shell the adjacent small particles will be embedded in the outer shell of bigger particles. The encapsulation of adjacent small particles will result in an extra growth of the outer shell (Figure 6.4). In addition, if the embedded small cement particles are not fully hydrated yet, they will further react, consuming water. In consequence, the rate of reaction of the bigger particles will further decrease.
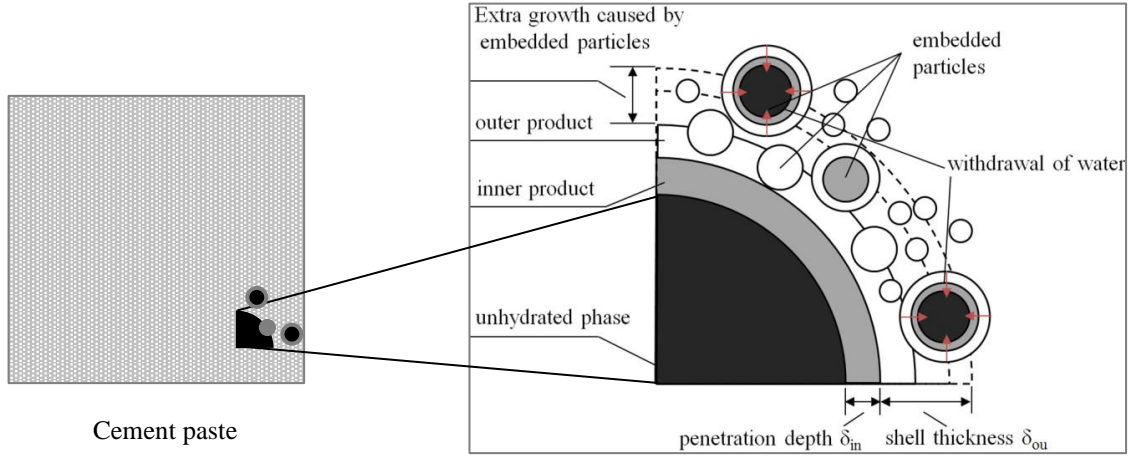
Figure 6.4 Schematic representation of core-shell model of cement particle in HYMOSTRUC

Based on the above growth process, the HYMOSTRUC program [80] calculates the rate of hydration of an individual cement particle with Eq. (6.2) (simplified form):

$$\frac{\Delta\delta_{in,x_i,j+1}}{\Delta t_{j+1}} = K_0 \times \Omega_1(.) \times \Omega_2(.) \times \Omega_3(.) \times \left[\frac{\delta_{tr}}{\delta_{x_i,j}}\right]^\lambda \tag{6.2}$$

where $\Delta\delta_{in,x_i,j+1}$ is an incremental increase of the penetration depth of the reaction front of cement particle x_i during a time increment $\Delta t_{j+1} = t_{j+1} - t_j$. The factor K_0 [µm/hour] is the initial penetration rate of the reaction front of a hydrating cement particle. $\Omega_1(\alpha)$, $\Omega_2(\alpha, S_{cap})$ and $\Omega_3(\alpha, S_{cap})$ are reduction factors allowing for the change of water distribution and change in pore water chemistry in the system. δ_{tr} is the *transition thickness* of the shell of hydration products when the hydration mechanism of the cement particle changes from a *phase boundary reaction* to a *diffusion-controlled reaction*. λ is a coefficient to control the types of reaction (from *phase boundary reaction* ($\lambda = 0$) to *diffusion-controlled reaction* ($\lambda = 1$)).

From the penetration depth of the reaction front in the cement particle the degree of hydration of an individual cement particle is calculated. The resulting degree of hydration α_j of the cement paste at time t_j is calculated as the sum of the contribution of all individual hydrating cement particles at time t_j (for details, see [80]).

Mathematical approximation of the capillary pore structure
The growth process, schematically shown in Figure 6.4, results in a microstructure from which the pore structure can be inferred [11]. This, however, is a tough process with limited accuracy. In HYMOSTRUC the capillary pore structure is approximated with a mathematical expression, viz.:

$$V_{\leq d} = a \cdot (\ln d) + b \tag{6.3}$$

where d is the pore diameter [m], a and b are constants [cm^3], which depend on type and fineness of the cement and the w/c ratio. The pore volume formed by pores smaller than $d =$
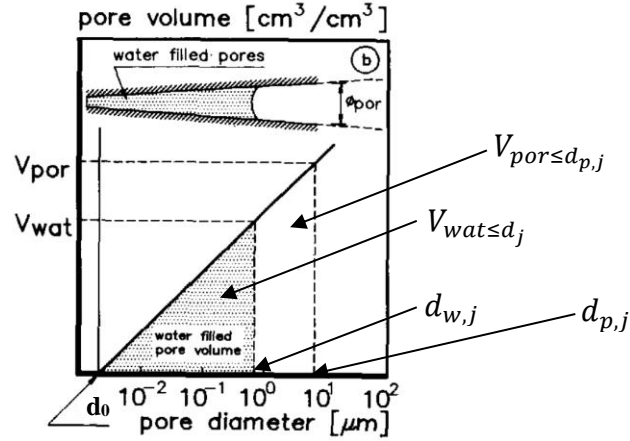
Figure 6.5 Schematization of pore volume and pore size distribution of cement pastes

$d_0 = 2 \times 10^{-9} \, m$ (d_0 is the size of the smallest capillary pore in Figure 6.5), i.e. the gel porosity, is not included in the pore volume $V_{\leq d}$.

Calculation of the relative humidity RH
For a pore size distribution described by Eq. (6.3), the amount of water in the pore system at time t_j, i.e. $V_{wat,j}$, determines the maximum pore $d_{w,j}$ that is still filled with water. Based on Eq. (6.3) it holds:

$$ln \, d_{w,j} = \frac{V_{wat \leq d_{w,j}} - b}{a} \qquad (6.4)$$

where $V_{wat \leq d_{w,j}}$ is the amount of water in capillary pores with diameter $\leq d_{w,j}$ at time t_j (Figure 6.5).

From the diameter of the maximum water-filled pore $d_{w,j}$ at time t_j the relative humidity RH_j in the pore system of cement paste can be calculated by using the Kelvin equation as below:

$$ln \, RH_j = \frac{4\gamma V_m \cos \theta}{d_{w,j} RT} \qquad (6.5)$$

where γ is the surface tension of water ($= 72.86 \times 10^{-3} \, N/m$), V_m is the molar volume of water ($= 1.8 \times 10^{-5} \, m^3/mol$), $d_{w,j}$ is the pore diameter, R is the universal gas constant ($= 8.314 \, J \cdot mol^{-1} \cdot K^{-1}$), T [K] is the temperature, θ is the contact angle, $\cos \theta = 1$ when perfect wetting is assumed.

Numerical simulation of the unsealed-cured cement with HYMOSTRUC
In case the hydration process proceeds under *unsealed* conditions, the HYMOSTRUC program has to be used with adjusted values of the reduction factors $\Omega_1(\alpha)$, $\Omega_2(\alpha, S_{cap})$ and $\Omega_3(\alpha, S_{cap})$ in Eq. (6.2). Those are reduction factors which allow for the effect of the actual state of water in the pore system of the cement paste on the rate of hydration. They are all functions of the degree of hydration α, and during the simulation process they are determined in a step-wise calculation procedure.

The reduction factor Ω_1, also called partition factor, allows for the effect of embedded particles on the rate of hydration. In a cement-RHA blended system some RHA-particles will become embedded in the growing outer shell. However, in this study the cement and RHA particles are assumed to react *independently* from each other and the effect of embedded RHA-particles on the rate of hydration of cement will *not* be considered *explicitly*. Hence, the reduction factor $\Omega_1(\alpha)$ in a cement-RHA blended system is considered the same as in plain cement paste.

The reduction factor $\Omega_2(\alpha, S_{cap})$ describes the influence on the rate of hydration of wetted surface area of the capillary pores compared to the surface area of all capillary pores in the cement paste. In a non-sealed system, additional water may be introduced into the cement paste, resulting in a higher saturation S_{cap} and a larger area of the capillary pores in contact with water, resulting in a higher hydration rate than in a sealed system.

The reduction factor $\Omega_3(\alpha, S_{cap})$ describes the influence of the amount of capillary water in the pore system on the rate of hydration. In an unsealed system the amount of water in the hydration cement paste might be higher (or lower) than in case of sealed curing. This will result in a higher (or lower) rate of hydration.

In Dong's work [147], the rate of hydration $\dot{\alpha}$ in the cement pastes with supply of *additional* water from outside was calculated with HYMOSTRUC [80, 107, 149]. The supply of additional water increases the water saturation level in capillary pores S_{cap} of cement paste, and hence the value of the reduction factors $\Omega_2(\alpha, S_{cap})$ and $\Omega_3(\alpha, S_{cap})$ in Eq. (6.2) (Note: higher values of the reduction factors, i.e. values closer to 1, result in a smaller decrease of the rate of hydration!). In case of simulating internal curing, the water transported from RHA can be seen as supply of additional water to the cement paste. Hence, the approach used by Dong for evaluating the effect of supplying external water on the rate of hydration will also be used for evaluating the effect of water supply from mixed-in water reservoirs, i.e. saturated RHA particles.

6.2.3.2 RHA particles and their pozzolanic reaction (System B)

During mixing of RHA-blended cement paste, the porous RHA particles become filled with water. With the hydration of cement, the amorphous silica of RHA can react with calcium hydroxide, one of the hydration products of cement, resulting in so-called pozzolanic reaction. Part of RHA loses its porous structure and consumes the entrained water in the pozzolanic reaction. The remaining unreacted RHA particles can still hold some water. A particular stage of the hydration process is schematically shown in Figure 6.6.

A hydrating blended cement paste   RHA particle
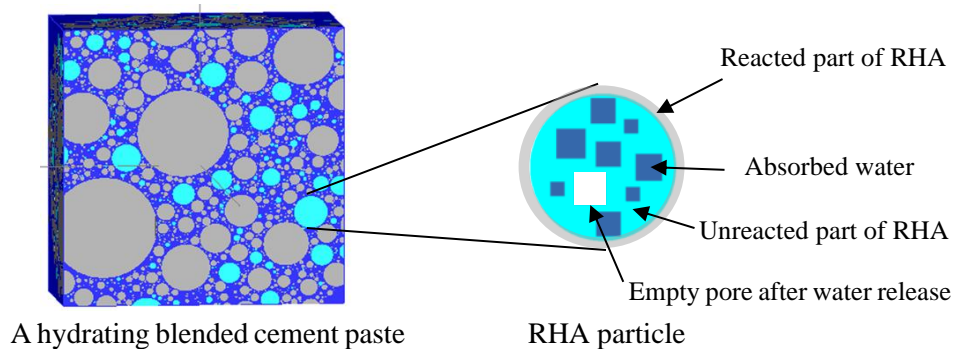
Figure 6.6 Schematic representation of RHA particle in blended cement paste

As discussed in chapter 5, the pozzolanic reaction and mass stoichiometry [53] of RHA can be described as follows:

$$1.1CH + S + 2.8H \rightarrow C_{1.1}SH_{3.9} \tag{6.6}$$

   1.36   1   0.84   3.2

where CH is calcium hydroxide with a molar mass of 74.093 g/mol, S is silica dioxide with a molar mass of 60.08 g/mol and H is water with a molar mass of 18.015 g/mol. Based on Eq. (6.6) the water consumed in the pozzolanic reaction at time t_j, $V_{wat,poz,j}$, can be calculated with:

$$V_{wat,poz,j} = 0.84 \cdot C_{SiO_2} \cdot m_{RHA} \cdot \beta_j / \rho_w \tag{6.7}$$

where C_{SiO_2} is the content (%) of amorphous silica in RHA, m_{RHA} is the initial mass (g) of RHA in cement-RHA mixture, β_j is the degree of pozzolanic reaction of RHA at time t_j, ρ_w is the density of water, i.e. 1 g/cm^3. The silica content of RHA-9 is 88.86%, and most of it is amorphous (Section 4.2). It is assumed that all the silica in the RHA is reactive.

According to Eq. (6.7), the water consumption in the pozzolanic reaction ($V_{wat,poz}$) for 1 g fully reacted RHA can be calculated, viz.:

$$V_{wat,poz} = 0.75 \ (cm^3) \cong 0.75 \ g/g \ RHA \tag{6.8}$$

The water absorption capacity of RHA-9 is 0.58 g/g (see Chapter 5). This is less than the water consumption for the pozzolanic reaction as shown in Eq. (6.8).

The fact that the amount of water absorbed in the RHA particles is less than the amount of water needed for pozzolanic reaction implies that additional water is needed for complete reaction of the RHA. Assuming that the pozzolanic reaction occurs at the surface of the RHA particles, this extra water should be provided by the capillary water in the surrounding cement paste (which implies extra drying of the cement paste and hence an increase of the autogenous shrinkage!), or from the still in-tact RHA-core of the reacting particle. Because the cement and RHA particles are assumed to react *independently* (as discussed in section 6.2.2), the additional water for the pozzolanic reaction is considered to be taken from the amount that is present in the still unreacted part of RHA particles.

For calculating the degree of pozzolanic reaction β_j, an extended version of the HYMOSTRUC program will be used, i.e. HYMOSTRUC-E, developed by Gao [150]. HYMOSTRUC-E can simulate the degree of pozzolanic reaction of pozzolanic materials (silica fume, fly ash or slag) and the DoH of the cement in blended cement systems. Because the chemical composition of RHA is similar to that SF, the RHA will be considered as a kind of coarse silica fume. The input parameters of the model regarding particle size distribution of the powders (cement and RHA), water-binder ratio and density, can be obtained from the experimental results in Chapter 4. Details of the simulation about β_j are presented in section 6.3.2.

6.2.3.3 Moisture transport between cement paste (system A) and RHA (system B)

For simulation of the moisture transport, a stepwise procedure is followed. In each time step the systems A (cement paste) and B (RHA particles) of the blended system are assumed to react independent from each other. Because of the different pore structures and reaction rates the values of RH in the systems A and B will develop differently, suppose the pore systems of A and B are not connected. In reality, however, these pore systems are connected. Hence, moisture will migrate from the system with high RH to that with low RH, until an equilibrium is reached. During the transport process the amount of water received by the system with low RH, i.e. $\Delta V_{wat, rec}$, should be equal to the amount of water released by the system with high RH, i.e. $\Delta V_{wat, rel}$.

To simulate the moisture transport between the systems A and B, the calculation is following the route below (see also Figure 6.7):

Step 1a   Calculate the water decrement in the cement paste due to cement hydration ($\Delta V_{wat, hyd,j+1}$) in time step Δt_{j+1}, and determine the water saturation degree and relative humidity in cement paste at time t_{j+1}.

Step 1b   Calculate the water decrement in RHA particles due to pozzolanic reaction ($\Delta V_{wat, poz,j+1}$) in time step Δt_{j+1}, and determine the water saturation degree and relative humidity in RHA particles at time t_{j+1}.

Step 2   Determine the amount of transported 'exchange water', needed to establish a new RH in the blended paste at time t_{j+1}. To reach this new RH equilibrium, RHA particles release part of entrained water $\Delta V_{wat, rel,j+1}$, and cement pastes receive an amount of water $\Delta V_{wat, rec,j+1}$.

Details of the calculation procedures follow in the sub-sections below.
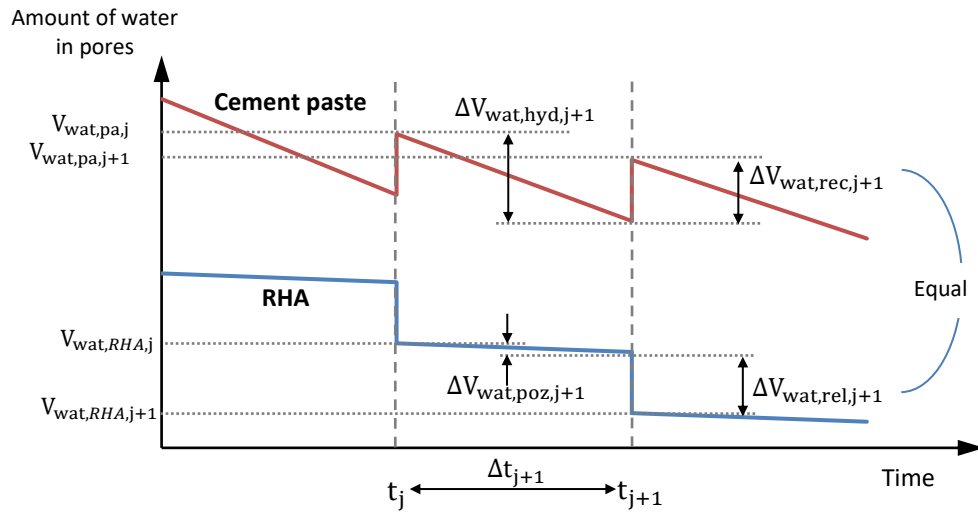
Figure 6.7 Schematic representation of the moisture transport simulation by the water amount change

6.2.3.3a Water saturation degree S and relative humidity RH in cement paste (Step 1a)

In system A (cement paste), at time t_j, the degree of hydration (DoH) of the cement is α_j. In the subsequent time step Δt_{j+1} the degree of hydration will increase by $\Delta \alpha_{j+1}$, resulting in change of the degree of saturation S and of the relative humidity RH in the pore system.

In the time step Δt_{j+1} the water decrement $\Delta V_{wat,hyd,j+1}$ due to cement hydration is:

$$\Delta V_{wat,\,hyd,j+1} = 0.4 \cdot m_C \cdot \Delta \alpha_{j+1} / \rho_w \tag{6.9}$$

where m_C is the mass of cement in a unit volume of cement paste, 0.4 represents the total amount of chemically and physically bound water when 1 g of cement is has completely hydrated [11], ρ_w is the density of water (1 g/cm^3).

Considering the amount of water $\Delta V_{wat,rec,j+1}$ received from RHA particles, the change of amount of water in cement paste $\Delta V_{wat,\,pa,j+1}$ in time step Δt_{j+1} is:

$$\Delta V_{wat,\,pa,j+1} = \Delta V_{wat,hyd,j+1} - \Delta V_{wat,rec,j+1} \tag{6.10}$$

For the amount of capillary water in cement paste after moisture transport $V_{cap\_wat,\,pa,j+1}$ at time t_{j+1}, it holds:

$$V_{cap\_wat,\,pa,j+1} = V_{wat,pa,j} - \Delta V_{wat,pa,j+1} \tag{6.11}$$

where $V_{wat,pa,j}$ is the total amount of water in cement paste at time t_j.

The amount of capillary water $V_{cap\_wat,\,pa}$ is stored in the capillary pore volume and determines the degree of saturation $S_{cap,pa}$ of the cement paste. For the capillary pore volume $V_{por,pa,j}$ at time t_j, when the degree of hydration of the cement is α_j, it holds [9]:

$$V_{por,pa,j} = \frac{\rho_{ce}}{\rho_w + \rho_{ce} \cdot \frac{w}{c}} \cdot \left(\frac{w}{c} - 0.3375 \cdot \alpha_j \right) \tag{6.12}$$

where ρ_{ce} and ρ_w are the densities of cement particles and water, which is 3.15 g/cm^3 and 1 g/cm^3 respectively; w/c is the water-cement ratio and α_j is the degree of hydration of cement at time t_j.

With Eq. (6.10) - (6.12) the water saturation degree in the capillary pores of the cement paste, i.e. $S_{cap,pa,j+1}$, at time t_{j+1} can be described as:

$$S_{cap,pa,j+1} = \frac{V_{cap\_wat,\,pa,j+1}}{V_{por,pa,j+1}} = \frac{V_{wat,pa,j} - \Delta V_{wat,hyd,j+1} + \Delta V_{wat,rec,j+1}}{V_{por,pa,j+1}} \tag{6.13}$$

For the relative humidity in the cement paste $RH_{pa,j+1}$ at time t_{j+1}, i.e. *after* moisture exchange during time step Δt_{j+1}, it holds (Eq. (6.5)):

$$ln\,RH_{pa,j+1} = \frac{4\gamma V_m}{RT} \cdot \left(e^{\frac{b - V_{cap\_wat,pa,j+1}}{a}} \right) \tag{6.14}$$

with γ, V_m, R and T as indicated for Eq. (6.5). The parameters a and b varies with water-cement ratio and degree of hydration of the cement. Values for a and b will be determined in section 6.3.1.

6.2.3.3b Water saturation degree S and relative humidity RH in RHA (Step 1b)

The degree of the pozzolanic reaction of system B (RHA particles) at time t_j is β_j. In the subsequent time step Δt_{j+1} the degree of reaction will increase by $\Delta\beta_{j+1}$, resulting in change of the degree of saturation S_{RHA} and of the relative humidity RH_{RHA} in the pore system of the RHA.

In time step Δt_{j+1} the amount of water in the RHA particles will decrease by the water decrement $\Delta V_{wat,\,poz,j+1}$:

$$\Delta V_{wat,poz,j+1} = \Delta V_{wat,pozC,j+1} - \Delta V_{wat,reRHA,j+1} \tag{6.15}$$

where $\Delta V_{wat,pozC,j+1}$ is the amount of water consumed by chemical reaction (pozzolanic reaction) in time step Δt_{j+1} and $\Delta V_{wat,reRHA,j+1}$ the amount of water entrained in the volume of RHA that has reacted in time step Δt_{j+1}. The amounts of water $\Delta V_{wat,pozC,j+1}$ and $\Delta V_{wat,reRHA,j+1}$ in Eq. (6.15) can be calculated with:

$$\Delta V_{wat,pozC,j+1} = 0.84 \cdot C_{SiO_2} \cdot m_{RHA} \cdot \Delta\beta_{j+1} \tag{6.16}$$

$$\Delta V_{wat,reRHA,j+1} = S_{RHA,j} \cdot V_{RHA} \cdot \emptyset_{pore,RHA} \cdot \Delta\beta_{j+1} \tag{6.17}$$

where C_{SiO_2} the silica content of RHA (88.86%); m_{RHA} the initial mass of RHA in cement-RHA mixture; $S_{RHA,j}$ the water saturation degree in the still unreacted cores or remaining RHA particles at time t_j, V_{RHA} original volume of RHA particles, and $\emptyset_{pore,RHA}$ the porosity of RHA particles, for which a value 0.55 has been measured (see Ch. 5).

In a blended cement-RHA paste the amount of water in the RHA particles does not only change because of the pozzolanic reaction, but also as a result of water transport to the hydrating cement paste. Suppose that in time step Δt_{j+1} the amount of water released to the cement paste is $\Delta V_{wat,rel,j+1}$. For the total decrease of the amount of water in remaining RHA particles, $\Delta V_{wat,\,RHA,j+1}$, it then holds:

$$\Delta V_{wat,\,RHA,j+1} = \Delta V_{wat,poz,j+1} + \Delta V_{wat,rel,j+1} \tag{6.18}$$

with $\Delta V_{wat,\,poz,j+1}$ according to Eq. (6.15).

For the remaining amount of water in RHA particles after moisture transport at time t_{j+1}, i.e. $V_{wat,\,RHA,j+1}$, it holds:

$$V_{wat,\,RHA,j+1} = V_{wat,RHA,j} - \Delta V_{wat,\,RHA,j+1} \tag{6.19}$$

The amount of water $V_{wat,RHA,j+1}$ is stored in the pore volume $V_{por,RHA,j+1}$ of still unreacted RHA particles. For a degree of reaction β_{j+1} of the RHA at time t_j this pore volume is:

$$V_{por,RHA,j+1} = V_{RHA} \cdot (1 - \beta_{j+1}) \cdot \emptyset_{por,RHA} \tag{6.20}$$

where V_{RHA} is original volume of RHA particles and $\emptyset_{por,RHA}$ is the porosity of the RHA.

With Eq. (6.19) and Eq. (6.20) the saturation degree $S_{RHA,j+1}$ of RHA at time t_{j+1} can be determined with:

$$S_{RHA,j+1} = \frac{V_{wat,RHA,j+1}}{V_{pore,RHA,j+1}} = \frac{V_{wat,RHA,j} - \Delta V_{wat,poz,j+1} - \Delta V_{wat,rel,j+1}}{V_{RHA} \cdot (1 - \beta_{j+1}) \cdot \emptyset_{pore,RHA}} \tag{6.21}$$

For a given pore structure and pore volume, the degree of saturation determines the relative humidity. For the relationship between degree of saturation and relative humidity the experimentally obtained moisture isotherm of RHA-9 (Chapter 4) has been adopted. This relationship is shown in Figure 6.8. This figure shows that experimental results can be described with a mathematical expression ($R^2 = 0.99$):

$$lnRH = 0.0172 \cdot (S^{-2.212} - 1)^{0.548} \tag{6.22}$$

Following this expression, the relative humidity of RHA after the moisture transport, $RH_{RHA,j+1}$, at time t_{j+1} can be calculated with (with $S_{RHA,j+1}$ according Eq. (6.21)):

$$ln\,RH_{RHA,j+1} = 0.0172 \cdot \left(S_{RHA,j+1}^{-2.212} - 1\right)^{0.548} \tag{6.23}$$
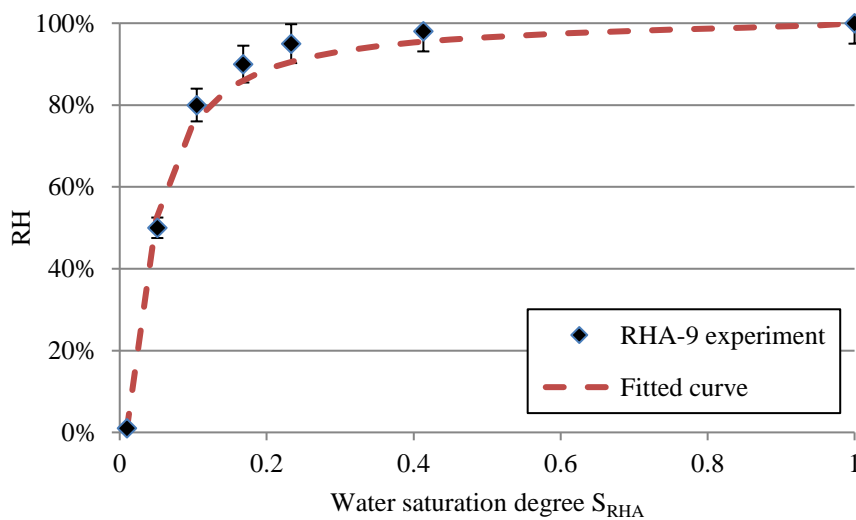
Figure 6.8 Relationship between RH and water saturation degree S_{RHA} in RHA-9 based on desorption isotherm experiments (Chapter 4).

6.2.3.3c Determination of moisture exchange and resulting relative humidity (Step 2)

After cement hydration and pozzolanic reaction in time step Δt_{j+1} new values of the relative humidity in the systems A (cement paste) and B (RHA) are obtained. The differences in RH between system A and B drives the moisture transport to happen. At the end of time step Δt_{j+1} *two* conditions have to be fulfilled, viz.: 1) RH-equilibrium and 2) mass conservation.

First condition: Relative humidity equilibrium. After moisture transport in time step Δt_{j+1}, the relative humidity in the hydrating cement paste and the RHA particles at time t_{j+1} should be equal:

$$RH_{pa,j+1} = RH_{RHA,j+1} \tag{6.24}$$

Second condition: Mass conservation. During the moisture transport in time step Δt_{j+1}, the amount of water $\Delta V_{wat,rec,j+1}$ received by one system should be equal to the amount of water $\Delta V_{wat,rel,j+1}$ released by the other system. In formula form:

$$\left|\Delta V_{wat,rec,j+1}\right| = \left|\Delta V_{wat,rel,j+1}\right| = \Delta V_{wat,j+1} \tag{6.25}$$

For the relative humidity $RH_{pa,j+1}$ and $RH_{RHA,j+1}$ the equations (6.14) and (6.23) it has been derived:

Eq. (6.14): $\quad ln\,RH_{pa,j+1} = \frac{4\gamma V_m}{RT} \cdot \left(e^{\frac{b - V_{cap\_wat,pa,j+1}}{a}} \right)$

Eq. (6.23): $\quad ln\,RH_{RHA,j+1} = 0.0172 \cdot \left(S_{RHA,j+1}{}^{-2.212} - 1 \right)^{0.548}$

With Eq. (6.10) and Eq. (6.11) the term $V_{cap\_wat,pa,j+1}$ in Eq. (6.14) can be rewritten, which leads to the following equation for $RH_{pa,j+1}$:

$$ln\,RH_{pa,j+1} = \frac{4\gamma V_m}{RT} \cdot \left(e^{\frac{b - (V_{wat,pa,j} - V_{wat,hyd,j+1} + \Delta V_{wat,rel,j+1})}{a}} \right) \tag{6.26}$$

With Eq. (6.21) the term $S_{RHA,j+1}$ in Eq. (6.23) can be rewritten, which leads to the following equation for $RH_{RHA,j+1}$:

$$ln\,RH_{RHA,j+1} = 0.0172 \cdot \left(\left(\frac{V_{wat,RHA,j} - \Delta V_{wat,poz,j+1} - \Delta V_{wat,rel,j+1}}{V_{RHA} \cdot (1-\beta_{j+1}) \cdot \emptyset_{pore,RHA}} \right)^{-2.212} - 1 \right)^{0.548} \tag{6.27}$$

At the end of time step Δt_{j+1} the aforementioned conditions (6.24) and (6.25) have to be met. With

$$RH_{pa,j+1} = RH_{RHA,j+1} = RH_{j+1}$$

and

$$\left|\Delta V_{wat,rel,j+1}\right| = \left|\Delta V_{wat,rel,j+1}\right| = \Delta V_{wat,j+1}$$

the two equations (6.26) and (6.27) contain two unknowns, i.c. RH_{j+1} and $\Delta V_{wat,j+1}$. Their values follow from solving these equations, resulting in the new value for the relative humidity RH_{j+1} at time at t_{j+1}. Implicitly also the values for the degree of saturation of the cement paste (system A) and the RHA (system B) are obtained, as well as the amounts of water in cement paste $(V_{wat,\,pa,j+1})$ and RHA particles $(V_{wat,\,RHA,j+1})$ at time t_{j+1}. The latter values are needed for executing the next simulation step.

6.2.4 Flow chart of the Internal Curing Simulation

The Internal Curing Simulation is implemented in MATLAB. A flowchart of the simulation is presented in Figure 6.9.

Initially, the cement paste and RHA both have a water saturation level of 100%. With HYMOSTRUC-E, the hydration increment of cement $\Delta\alpha_{j+1}$ and the reaction increment of RHA $\Delta\beta_{j+1}$ in time step Δt_{j+1} are determined. The hydration process and the pozzolanic reaction go along with consumption of water, i.e. the water decrement in cement paste and in the RHA particles.

By fulfilling the RH equilibrium (Eq. (6.24)) and mass conservation (Eq. (6.25)) the moisture transport process is computed. The amount of exchanged water in time step Δt_{j+1} and the resulting RH_{j+1} at time at t_{j+1} are obtained.

In the stepwise calculation procedure, the evolution of the degree of water saturation in cement paste and RHA are outputted, the development of internal RH in cement paste with RHA is simulated.
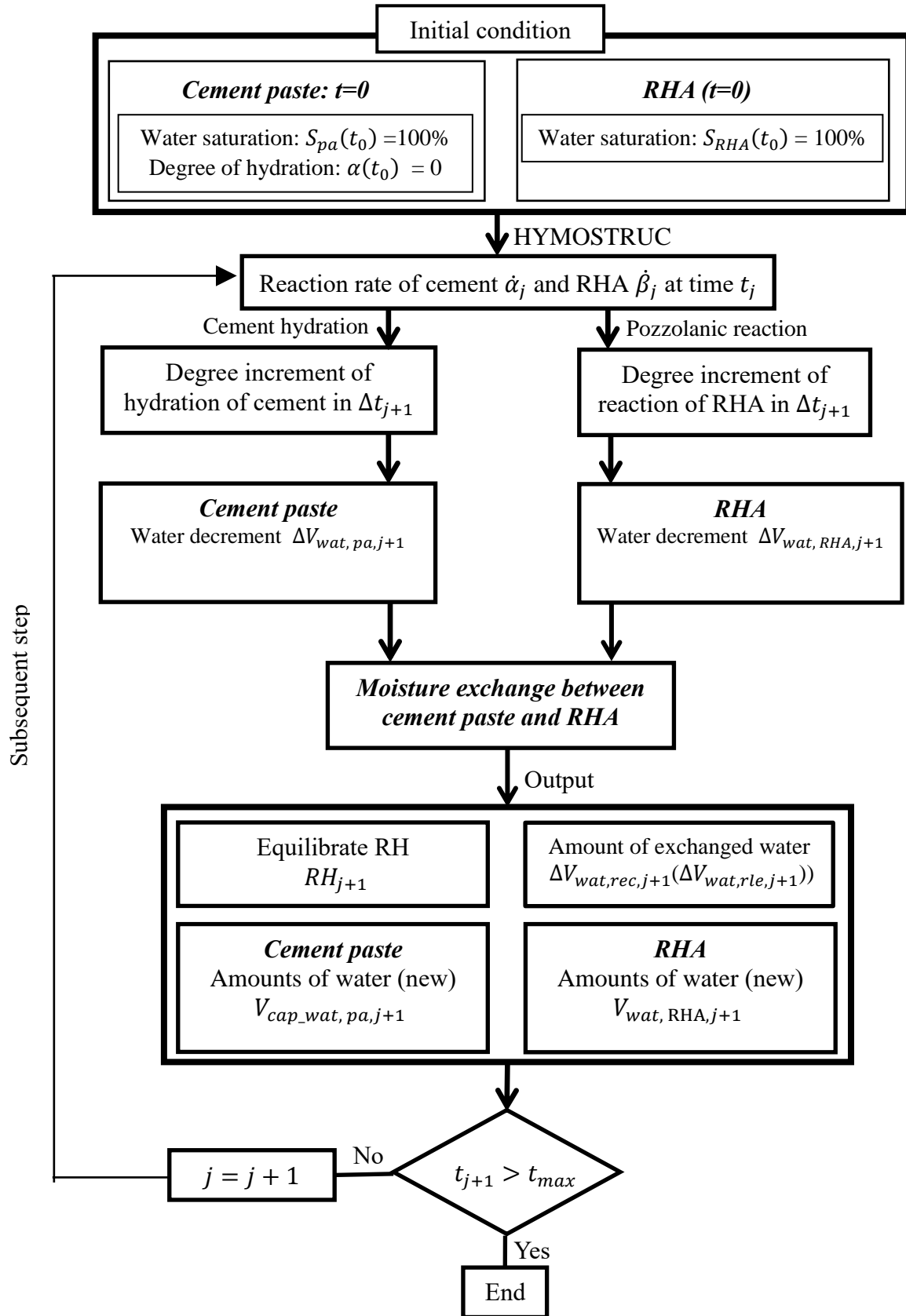
Figure 6.9 Flowchart for the simulation in the Internal Curing Simulation. t_{max} is the maximal time for the simulation.

6.3 Determination of input parameters for HYMOSTRUC-E

6.3.1 Parameters for pore size distribution in cement paste

For running the numerical simulation program HYMOSTRUC-E, the capillary pore size distribution in hydrating cement paste (system A) is approximated by Eq. (6.3). As mentioned in section 6.2.3.1, the parameters a and b in Eq. (6.3) still have to be determined.

For determining the pore size distribution of plain cement paste at different ages, adsorption isotherms of hardened cementitious materials with different water-cement ratio collected by Xi et al. [151] are utilized. Based on the experiment result of Xi et al. [151], the parameters a and b are determined. The details of the calculation are shown in Appendix A.

The parameters a and b for a cement paste (w/c = 0.18) versus degree of hydration are presented in Figure 6.10. The evolution of the parameters is obtained by spline curve fitting on several points. These two curves describe the α-dependency of the parameters a and b of the cement paste, and will be used for the Internal Curing Simulation.
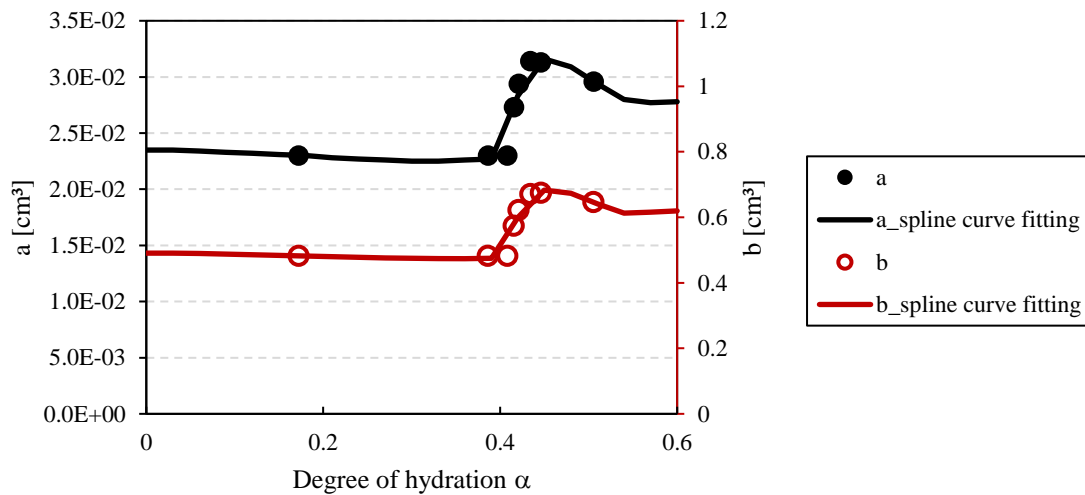
Figure 6.10 Evolution of the parameters a and b of a cement paste with different DoH (w/c = 0.18)

6.3.2 Parameters for pozzolanic reaction of RHA

HYMOSTRUC-E model developed by Gao [150] can simulate the hydration and microstructural development in hardening blend-cement paste. For running the model, the particle size distribution and mineral composition of RHA-9 and cement (relevant data is shown in Chapter 4) are needed. The input data for the cement and RHA for '20% RHA-9' in HYMOSTUC-E is presented in Table 6.1.

Table 6.1 The input data of cement and RHA for '20% RHA-9' in HYMOSTRUC-E

Properties	Value	Properties	Value
Mixing-water/binder ratio*	0.26	Curing temperature [℃]	20
Cement		**RHA-9**	
Percentage in binder	80%	Percentage in binder	20%
n (RRD** parameter)	0.9338	n (RRB parameter)	1.5520
c (RRD parameter)	0.0705	c (RRB parameter)	0.0237
Mean particle size [μm]	13.7	Mean particle size [μm]	9.0
Maximum particle size [μm]	50	Maximum particle size [μm]	50
Minimum particle size [μm]	2	Minimum particle size [μm]	2
Density [kg/m^3]	3150	Density [kg/m^3]	2100
K_0 [$\mu m/h$]	0.05	K_0 [$\mu m/h$]	0.01
δ_{tr} [μm]	0.3	δ_{tr} [μm]	0.016

* The mixing-water/binder ratio is the amount of water added for casting per gram dry powders of binder. Here it includes the water in the superplasticizer.

** RRD is Rosin-Rammler distribution for describing a particle size distribution.

6.4 Simulation results

The Internal Curing Simulation program will be used for simulating the moisture exchange between cement paste and RHA in blended mixtures and the internal RH change in plain cement pastes. Mixture compositions are shown in Table 6.2. First three mixtures are the same mixtures used in Section 4.2. The mixtures Ref 0.225 and Ref 0.18, which respectively have the same water-cement ratio (excluding RHA absorption) with mixtures 10% RHA-9 and 20% RHA-9, are used for studying the effect of internal curing on the hydration of cement.

As reported already in Chapter 5, the absorption capacity of dry RHA-9 particles is 0.58 g/g at RH 100%, and the absorption process is finished in several minutes. The water-cement ratios of blended pastes *after* water absorption by RHA are listed in Table 6.2.

Table 6.2 Proportion of cement-RHA mixtures used for internal curing modelling

Mixture	Mixing-water/binder ratio*	Water-cement ratio (excluding RHA absorption)**	Cement replacement by RHA-9	Superplasticizer-binder ratio
20% RHA-9	0.25	0.180	20%	1.6%
10% RHA-9	0.25	0.225	10%	1.6%
Ref 0.25	0.25	0.260	0	1.6%
Ref 0.225	0.225	0.225	0	0
Ref 0.18	0.18	0.180	0	0

* The mixing-water/binder ratio is the amount of water added for casting per gram dry powders of binder. It does not include the water in the superplasticizer.

** The amount of water in the superplasticizer is considered when water-cement ratio is calculated. The solid mass content of superplasticizer is 35%.

6.4.1 Evolution of hydration of cement and pozzolanic reaction of RHA

The simulated and experimentally observed evolution of cement hydration in mixture 'Ref 0.25' are presented in Figure 6.11 a. The experimentally observed evolution of cement

hydration is determined by measuring the change of non-evaporated water in hydrating cement paste. The simulated hydration curve is performed by HYMOSTRUC-E. The simulated and experimentally observed pozzolanic reaction of RHA-9 in mixture '20% RHA-9' are shown in Figure 6.11 b. The process of pozzolanic reaction determined by experiment is from Section 5.4.2 and the simulated process is from HYMOSTRUC-E. The Figure 6.11 a and b show good agreement between the experimental and modelling results. This illustrates again that HYMOSTRUC-E can well simulate the evolution of the hydration of cement and the pozzolanic reaction of RHA, which is in line with earlier observation in [109, 150].

(a) Degree of hydration   (b) Degree of pozzolanic reaction
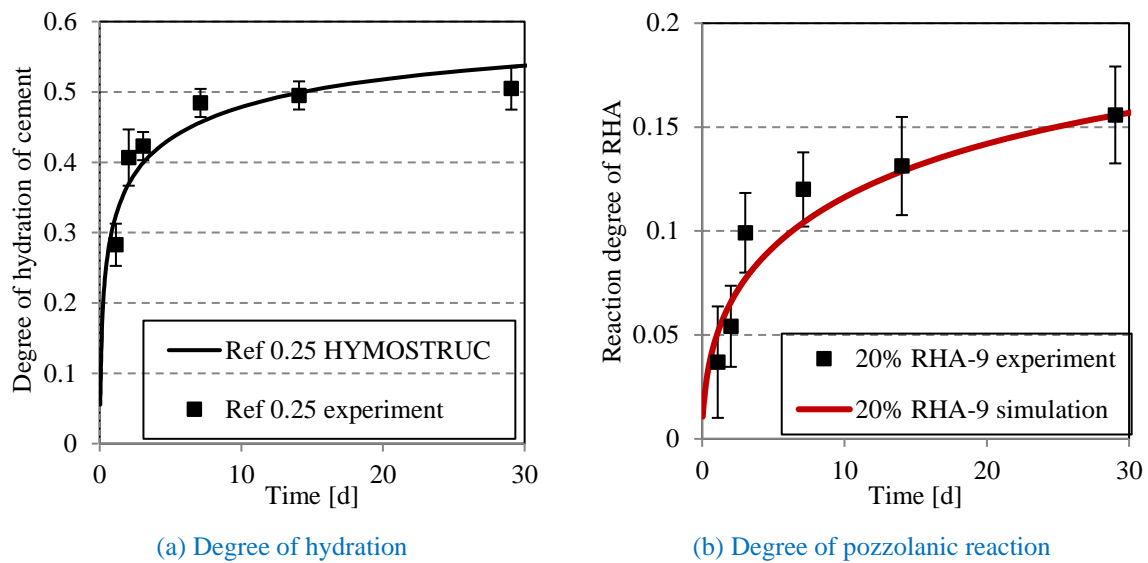
Figure 6.11 Simulated and experimentally observed evolution of the hydration of cement in Ref 0.25 (a) and the pozzolanic reaction of RHA-9 in 20% RHA-9 (b)

6.4.2 Plain cement paste

In the Internal Curing Simulation, the pore size distribution of cement paste is described by Eq. (6.3). To check the validity, the experimental result of the internal RH change in the mixture 'Ref 0.18' and 'Ref 0.25' is utilized for comparison. In the measured result of internal RH, the initial RH drop can be attributed to dissolved salts in the pore solution. The RH drop because of ions in pore solution can be estimated with Raoult's law [57]. The ion concentration of pore solution is not considered in the Internal Curing Simulation. It needs to mention that the experimental result of internal RH shown in Figure 6.12 excludes the influence of dissolved salts by using Raoult's law. The water-cement ratio is 0.18 in mixture Ref 0.18, which is the same as that in mixture 20% RHA-9. The internal RH changes after casting determined by experiment and simulation are presented in Figure 6.12. The start point of curves is the onset of self-desiccation. In Figure 6.12, the simulated RH change is almost identical to the experimental result. This indicates that the internal RH change process in plain cement paste can be well described by the Internal Curing Simulation.
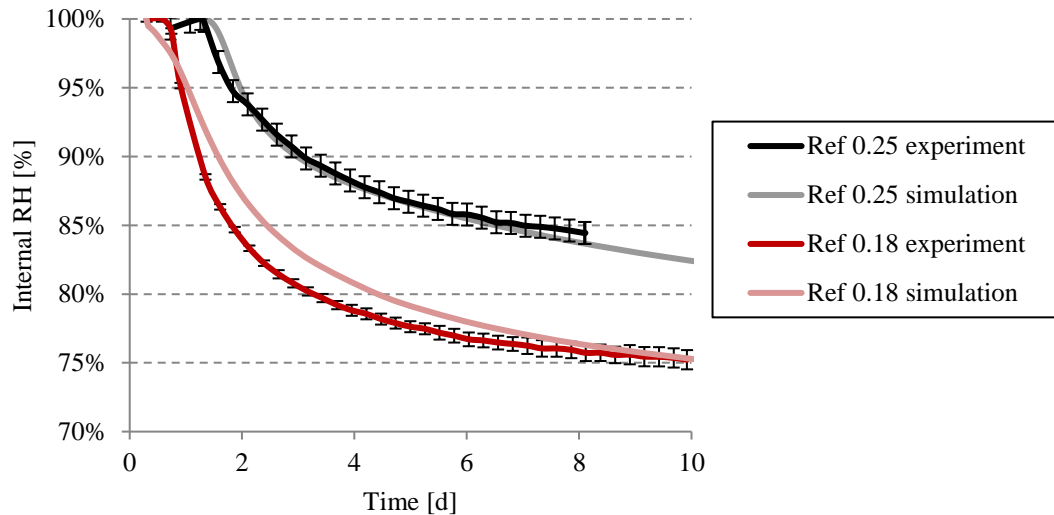
Figure 6.12 Internal RH modelling of the mixture Ref 0.18 and Ref 0.25 by Internal Curing Simulation

6.4.3 Internal curing in cement pastes with RHA

The equilibrated RH and water saturation degrees after moisture exchange are the outputs of the Internal Curing Simulation. The calculated saturation degrees of cement paste and RHA-9 in mixture 10% RHA-9 and 20% RHA-9 are presented in Figure 6.13. The start point of all the curves is the onset of self-desiccation in the mixture.

For the mixture '20% RHA-9', the water saturation degree of cement pastes decreases at a very early age (< 1 day). After 1 day, the saturation degree increases to a high level and maintains there for the following time. For RHA particles, the water saturation degree maintains at a high level in 1 day and then decreases for the later ages. For explaining the reason, the phenomenon is divided into two periods. At the early ages (< 1day), the DoH of cement is small. The pore structure consists of more big pores and less small pores. Besides this, the total water content in the cement paste is more than that in RHA. It means the meniscus in cement paste exists in bigger pore than that in RHA. Based on the Kelvin equation, the bigger radius of meniscus represents a higher RH. The moisture moves from the cement paste to RHA and decreases the water saturation degree of cement paste. At the later ages (> 1day), due to the hydration of cement, the total water content and the pore size is reduced in cement paste. Meanwhile, the water content of RHA does not decrease much because of the low reaction degree. The radius of meniscus in the pores of RHA turns to be bigger than that in cement paste. The transport of moisture is in turn from RHA to the cement paste. Because of the high dosage (20%) in the mixture, RHA particles provide a significant amount of water (big decrease on water saturation degree) to cement paste and maintain its water saturation degree at a very high level.

For the mixture '10% RHA-9', similar increase-period is found in the trend of saturation degree of cement paste as the mixture '20% RHA-9'. However, the saturation degree of cement pastes in the mixture '10% RHA-9' cannot maintain at a high level as it in the mixture '20% RHA-9'. It is evident that RHA particles still released certain amount of water from the big decrease on water saturation degree. However, the total amount of entrained water in RHA particles in '10% RHA-9' is obviously less than that in '20% RHA-9'. The lack of internal curing water leads the saturation degree of cement paste in '10% RHA-9' less than that in '20% RHA-9'.
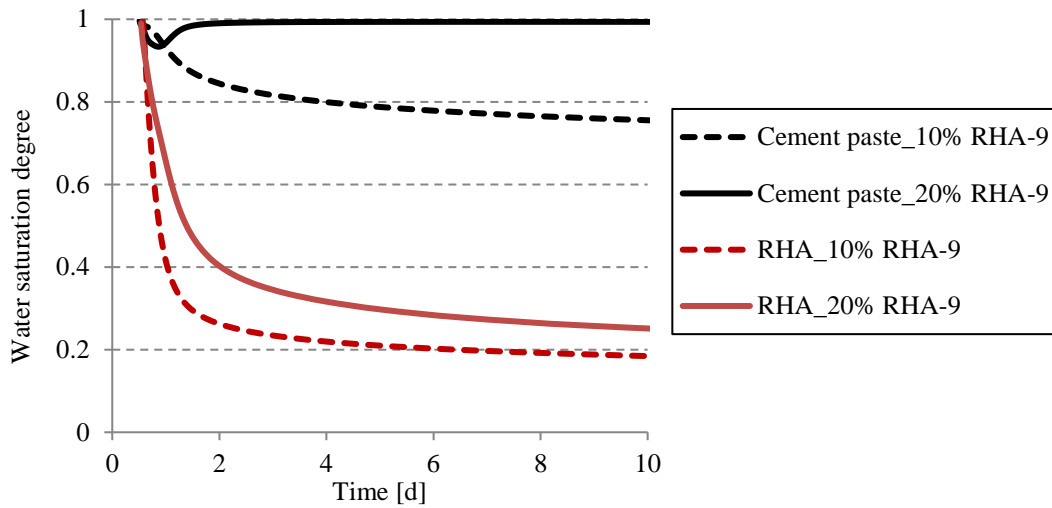
Figure 6.13 Water saturation degrees of cement paste and RHA calculated from the Internal Curing Simulation in the mixture 10% RHA-9 and 20% RHA-9

The hydration processes of cement in mixtures 10% RHA-9 and 20% RHA-9 simulated by Internal Curing Simulation are presented in Figure 6.14. The hydration processes in the plain cement pastes, simulated by HYMOSTRUC, which have the same water-cement ratio as cement-RHA mixtures, are shown in Figure 6.14 for comparison. The reaction curves in Figure 6.14 indicates that the internal curing water from RHA particles enhances the cement hydration in cement-RHA mixtures. Because the total amount of water stored in RHA particles in mixture 20% RHA-9 is larger than in 10% RHA-9, the degree of hydration of cement in 20% RHA-9 increases more than that in 10% RHA-9.
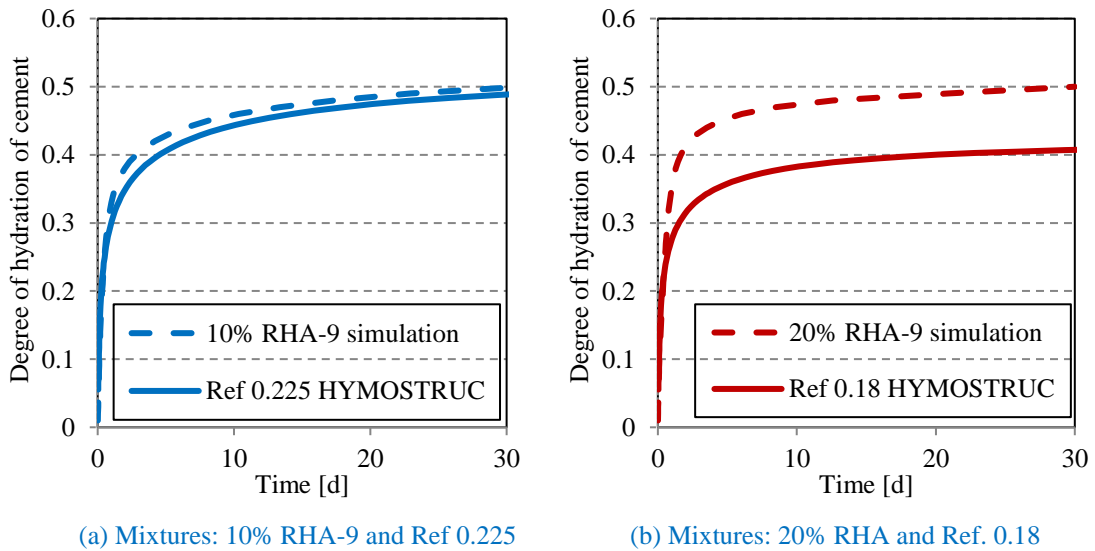
(a) Mixtures: 10% RHA-9 and Ref 0.225 (b) Mixtures: 20% RHA and Ref. 0.18

Figure 6.14 Comparison of hydration process of cement in cement-RHA mixtures and plain cement mixtures with same water-cement ratio

The numerically simulated RHs of the mixture 20% RHA-9 and 10% RHA-9 are compared with the experimental results in Figure 6.15. The start point of all the curves is the onset of self-desiccation.

The simulated RHs in 10% RHA-9 and 20% RHA-9 show a good consistency with the experimental results. This indicates that the internal curing process in the blended cement/RHA system can be well described by the Internal Curing Simulation.
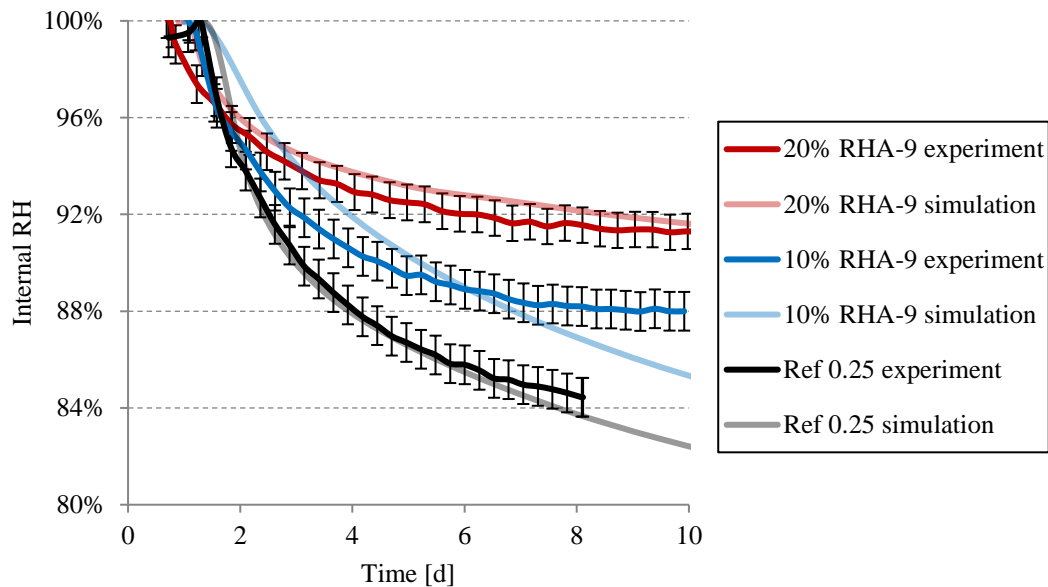
*Figure 6.15 Simulation and experimental results of internal RH in the mixture 10% RHA-9 and 20% RHA-9 and Ref 0.25, measured from the onset of self-desiccation*

The simulation reflects the same trend as experiment, i.e. the internal RH in blended cement paste decreases slowly with the increase of the dosage of RHA. The results also demonstrate that the addition of RHA retards the development of self-desiccation of cement paste.

6.5 Conclusion

For a better understanding of the role of RHA on mitigating autogenous shrinkage, numerical simulations are performed. A model named Internal Curing Simulation is proposed to describe the evolution of the self-desiccation in the cement-RHA mixtures. In this chapter the following conclusions can be drawn:
- By comparing the measured and simulated internal RH, it could be shown that the Internal Curing Simulation describes the moisture exchange between RHA and cement paste quite well.
- From the perspective of retarding the self-desiccation, the effects of pozzolanic reaction and internal curing are competitive phenomena. The pozzolanic reaction of the RHA will intensify the self-desiccation, whereas the release of absorbed water by the RHA will mitigate self-desiccation. With the Internal Curing Simulation the effects of these two phenomena could be evaluated quantitatively and the effectiveness of RHA as internal curing agent was convincingly demonstrated.

Chapter 7

Effectiveness of RHA for mitigating cracking tendency in UHPC

7.1 Introduction

In previous chapters, it has been shown that at the scale of cement pastes, saturated RHA particles act as water reservoirs that can mitigate the autogenous shrinkage of low water-binder ratio cement pastes by internal curing. Because the inert aggregates in UHPC usually won't participate in the chemical reaction of cement or RHA, it can be expected that the autogenous shrinkage in UHPC will be mitigated efficiently by the similar RHA used in cement pastes. The engineering practice, however, will particularly be interested to see whether RHA mitigates not only the autogenous shrinkage in UHPC, but also the shrinkage-induced tensile stresses and the resulting risk of cracking. The cracking tendency of UHPC does not only depend on the magnitude of the autogenous shrinkage, but also on the evolution of the mechanical properties, like stiffness and strength, and the time dependent properties, i.e. creep and relaxation. An in-depth study of RHA on the evolution of mechanical and time-dependent properties is outside the scope of this study. Still it would be worth to give a preliminary indication of the use of RHA on the reduction of the shrinkage-induced cracking tendency of UHPC. For this reason, a simple ring test has been performed and discussed in this chapter to evaluate the effect of RHA on mitigating shrinkage-induced proneness to cracking of UHPC. The autogenous shrinkage, internal RH and compressive strength of UHPC with RHA were also measured.

7.2 Materials

The materials for UHPC specimens, actually mortar specimens, tested in this chapter are Portland cement (CEM I 52.5N), RHA, and a polycarboxylate-based superplasticizer (Solid mass content 35%), the same as used in Chapter 4. One additional constituent, namely silica sand with a particle size ranging from 125 to 250 µm, was added.

Based on the optimization study in Chapter 4, RHA-9 was utilized for the UHPC mixture. The replacement percentage of cement by RHA is 20%. The UHPC composition is listed in Table 7.1.

Table 7.1 UHPC mixture composition of mortar. Values by weight

Mixture	Mixing-water/binder ratio*	Superplasticizer-binder ratio**	Sand-binder ratio	Replacement of RHA [%]	Mean particle size (D_{50}) [µm]
REF	0.25	1.6%	1	0	-
RHA20%	0.25	1.6%	1	20	9.0

* The mixing-water/binder ratio is the amount of water added for casting per gram dry powders of binder. It does not include water in the superplasticizer.

**The 65% mass of superplasticizer is considered as water in this study.

7.3 Methods

7.3.1 Autogenous shrinkage and internal RH

The preparation of UHPC samples and the test procedure for the measurement of autogenous shrinkage and internal RH were the same as described in Chapter 3.

7.3.2 Restrained ring test

The effectiveness of using RHA in UHPC to mitigate the shrinkage-induced susceptibility to cracking was investigated by means of a restrained ring test. The restrained ring test consists of a cylindrical specimen cast around a steel ring. As the specimen shrinks, the steel ring prevents the specimen from deforming, resulting in the development of tensile stress in the specimen [152]. If these tensile stresses exceed the tensile strength of the specimen, cracking will occur.

In order to estimating the induced tensile stress and the time of cracking in the UHPC specimen, the restrained ring test procedure given by ASTM C1581-09 is followed. The test setup and geometry of the ring-shaped specimen are shown in Figure 7.1. Four strain gauges were glued to the interior surface of the steel ring at midheight. The positions of these gauges are opposite each other along the diameter of the inner steel ring. During testing, any moisture exchange with the environment is prevented. It can be done by covering the upper surface with sealing tapes after casting. The contact surface between the steel rings and the steel base was sealed by a sealing gel without adhesion. The test equipment is shown in Figure 7.2.
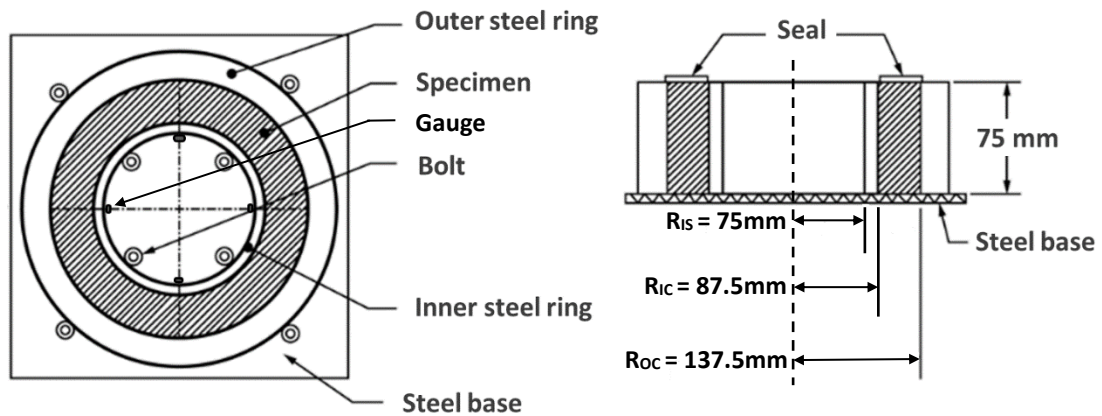
Figure 7.1 Test setup and geometry of the ring specimen
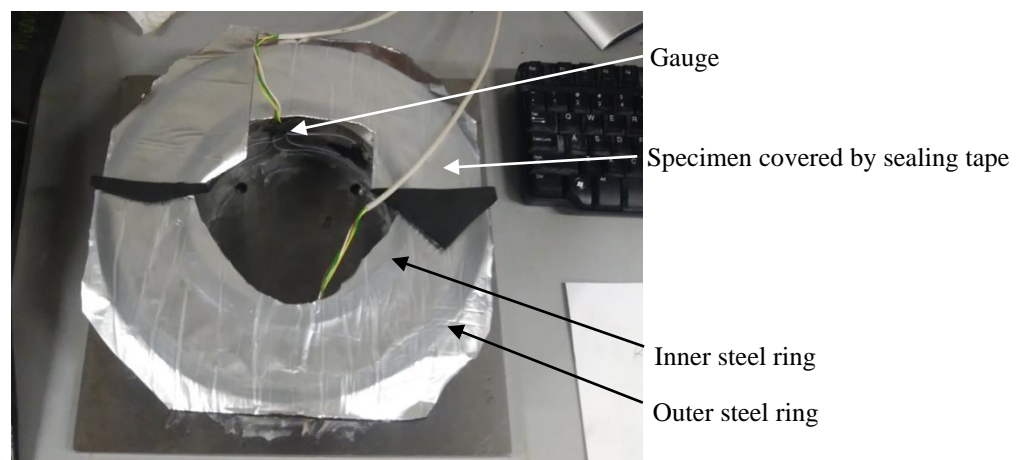
Figure 7.2 Test equipment for the restrained ring test

The strain gauges on the inner surface of the steel ring start to record exerted strains about 30 minutes after casting. The strain of the steel ring was measured with five-minute intervals. With the measured strain of the steel ring the maximum tensile stress in the test specimen $\sigma_{c,max}$ can be derived with equation (7.1) [152].

$$\sigma_{c,max}(t) = -\varepsilon_s(t)E_S\left(\frac{R_{IC}^2+R_{OC}^2}{R_{OC}^2-R_{IC}^2}\right)\left(\frac{R_{IC}^2-R_{IS}^2}{2R_{IC}^2}\right) \qquad (7.1)$$

where $\varepsilon_s(t)$ is the strain measured in the steel ring at time t and E_S is the elastic modulus of the steel ring, i.e. 206 GPa. As indicated in Figure 7.1, R_{IC} is the inner radius of the specimen, R_{OC} is the outer radius of the specimen, and R_{IS} is the inner radius of the steel ring. For the test device used it holds: R_{IC} is 87.5 cm, R_{OC} is 137.5 cm and R_{IS} is 75 cm.

7.3.3 Compressive strength

Compressive strength of UHPC samples at ages of 1d, 3d, 7d and 28d was measured on cubic specimens. The specimen size is $40 \times 40 \times 40$ mm^3. The specimens were cast and cured in the sealed plastic bags for avoiding water loss at 20 ± 1 ˚C until testing. Three samples were measured for each mixture. The test procedure follows EN206.

7.4 Results and discussion

7.4.1 Autogenous shrinkage and internal RH

The autogenous shrinkages of the UHPC mixture with and without RHA are represented in Figure 7.3. The autogenous shrinkages were measured from the onset of self-desiccation as discussed in Chapter 3. Figure 7.3 shows that using RHA significantly reduces the autogenous shrinkage of the UHPC specimen. In mixture RHA20% the autogenous shrinkage measured from the onset of self-desiccation during the first 14 days after casting, is only 80 µm/m. This indicates that the incorporation of sand in UHPC mixtures (compared to the earlier tested RHA-modified pastes, see Figure 4.13) does not affect the effectiveness of RHA
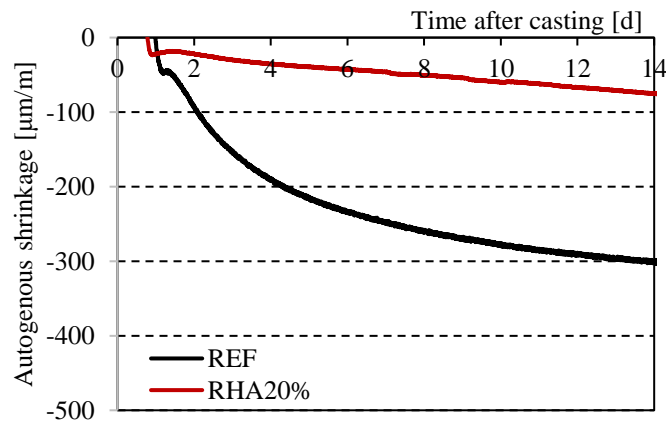
Figure 7.3 Autogenous shrinkage of UHPC with and without RHA. Autogenous shrinkage measured from the onset of self-desiccation

on mitigating autogenous shrinkage. RHA performs as good as it in cement pastes. The similar phenomenon was also found in Tuan's work [6].

Figure 7.4 shows the internal RH change of UHPC during the first 14 days. The addition of RHA reduced the drop of RH in the UHPC specimen. Even after 14 days, the internal RH can be maintained at 90% in UHPC mixture RHA20%. This indicates that even with the incorporatioin of sand, the UHPC specimen still can be internally cured efficiently by the water from RHA.

(a) Internal RH change since casting   *(b) Internal RH decrease since casting*
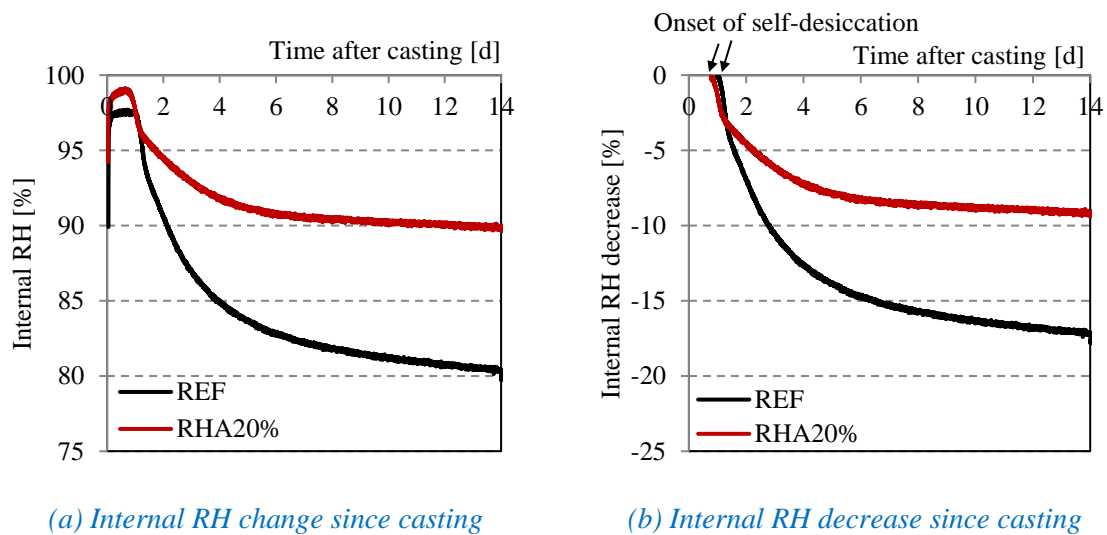
Figure 7.4 Internal RH change of UHPC with and without RHA

7.4.2 Compressive strength

The compressive strength of UHPC with and without RHA is shown in Figure 7.5. Adding RHA to the mixture increases the compressive strength of UHPC at all ages (1d, 3d, 7d, 28d) compared to the reference specimen. The compressive strength of UHPC with RHA reaches 160 MPa at 28d. Due to its porous structure, some of the water is absorbed by RHA during mixing. It leads to a decrease in the initial water binder ratio in the mixture and thus reduces the porosity. For the UHPC mixture RHA20%, the initial water binder ratio is decreased to 0.14 from 0.26 (absorption rate of RHA is 0.58 g/g from section 5.4.1). In the later stage due to the internal curing by the saturated RHA particles, extra water is released (see also Figure 5.13). This amount of curing water increases the water saturation degree of cement paste and facilitates the hydration of cement (see also Figure 6.13 and Figure 6.14), which increases the compressive strength further. Similar phenomenon and explanation can also be found in [114].

A high compressive strength in concrete normally means a high tensile strength. Considering the small autogenous shrinkage of the mixture with RHA, combined with a high tensile strength, the risk of cracking is expected to be low. This will be checked in the next section by the ring test.
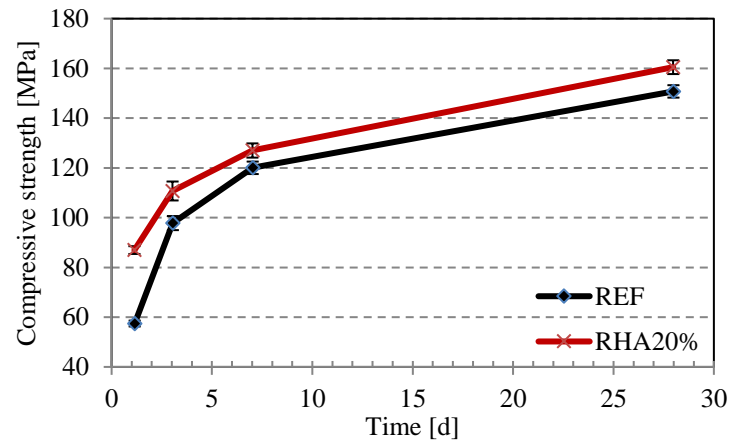
Figure 7.5 Compressive strength of UHPC with and without RHA

7.4.3 Restrained ring test - cracking tendency

The result of the ring test of UHPC specimens with and without the RHA after casting is shown in Figure 7.6. Figure 7.6 b shows that the tensile stress in the mixture RHA20% increases earlier than that in the reference mixture REF without RHA. The setting time of the UHPC mixture with RHA is shorter, the onset of self-desiccation is earlier (Figure 7.6 a), so the tensile stress increases earlier compared to the reference mixture. In both mixtures, after the initial increase, the tensile stress starts to decrease at about 20-24 hours after casting and then increases again. Similar results have also been found by other researchers. Mechtcherine et al. [97] related this decrease of tensile stress to the thermal expansion due to the development of the hydration heat in the cementitious specimens. Park et al. [153] considered this decrease negligible from the engineering point of view because it only takes a very small part of the whole tensile stress change.

When the performance of the two UHPC mixtures during the first 14 days is compared, it seems that the addition of RHA significantly reduces the steel ring strain (Figure 7.6 a) and tensile stress (Figure 7.6 b) of the mortar specimen. The tensile stress of the specimen with RHA is about 2.3 MPa at the age of 14d, which is 3 times smaller than the tensile stress in the reference specimen at the same age. This also indicates that the addition of RHA dramatically reduces the shrinkage-induced susceptibility to cracking in UHPC. The phenomenon can be explained by two reasons. First, the addition of RHA reduces the drop of internal RH in UHPC, leading to small driving force to autogenous shrink. Second, the tensile strength of UHPC with RHA is higher (or similar) than that of the reference, resulting in a higher capacity to resist the tensile stress caused by autogenous shrinkage. These two effects of the addition of RHA together reduce the proneness to cracking of UHPC.

During the ring test, there is no crack happened in 28 days in the mixture RHA20%. The sealing tape of the specimen was removed at about 32 days. The ring-shape specimen was exposed to the environment with 50% RH at 20 °C. The drying shrinkage of the specimen causes the strain of steel ring increases rapidly and the cracking occurs in several days after the removal of sealing (Figure 7.6). This indicates that RHA can maintain the RH at a high level in the UHPC mixture for a long period.

A similar reduction on the tensile stress in a restraint ring test was also found in UHPC with the addition of super absorbent polymers (SAP). Mechtcherine et al. [97] illustrated that at the concrete age 50 days the stresses induced in UHPC specimen containing SAP were approximately 2 MPa, which was 4 times smaller than the corresponding stresses in the
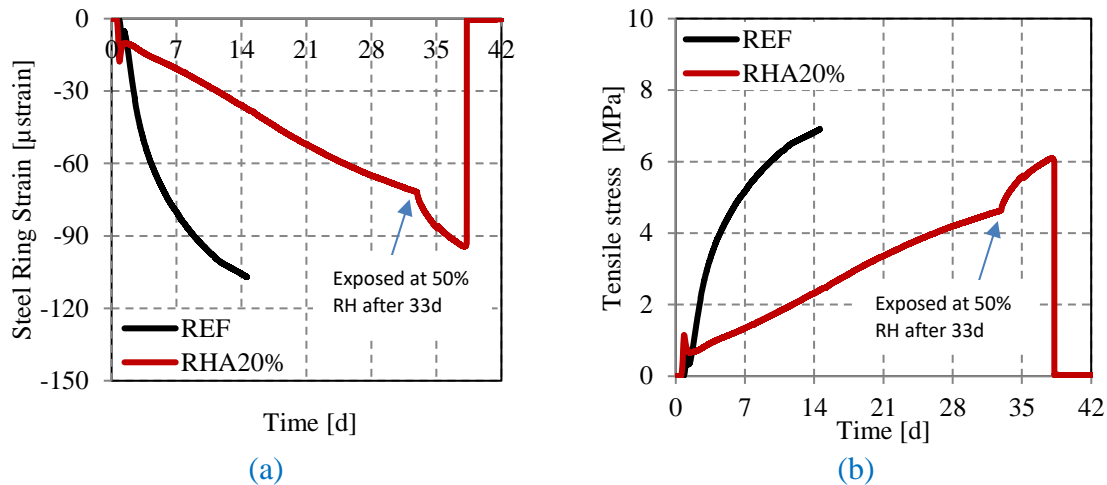
Figure 7.6 Restrained ring test of sealed UHPC specimens after casting (a) Measured steel strain (b) Tensile stress $\sigma_{c,max}$ calculated from the measured steel strain (Eq. (7.1))

reference concrete (w/b=0.19) at the same age. Like the SAP, the addition of RHA can effectively reduce the proneness to cracking of UHPC.

7.5 Conclusions

RHA appears to be a good additive to mitigate autogenous shrinkage and the proneness to cracking in UHPC. It is an effective internal curing agent, even compared to SAP, especially in UHPC application. In this chapter, the following conclusions can be drawn.

1) Incorporating sand in UHPC mixtures does not affect the effectiveness of RHA on mitigating autogenous shrinkage of UHPC at early age. RHA performs as good as it is in cement pastes.
2) The addition of RHA increases the compressive strength of UHPC. From that an increase of the tensile strength might be expected as well, which further contributes to a decrease of the proneness to cracking of RHA-modified UHPC.
3) The proneness to cracking in UHPC at early age is reduced with the addition of RHA, as observed from the restrained ring tests.

Chapter 8

Retrospection, conclusions and prospects

8.1 Retrospection

Ultra-high performance concrete (UHPC) has become one of the promising types of concrete of the 21st century thanks to its ultra-high-strength, low permeability, and excellent durability characteristics. However, the low water/binder ratio and the use of silica fume in UHPC result in high autogenous shrinkage, which significantly increases the cracking potential of UHPC in the first few weeks after casting. Such early-age cracking tends to negate the many advantages of UHPC and limits its utilization in construction.

Autogenous shrinkage, as a major component of early-age shrinkage in UHPC, is a consequence of the self-desiccation during cement hydration. The key to mitigating autogenous shrinkage is to counteract the self-desiccation. The conventional strategy of external moisture-curing has proved to be effective in normal concrete. Nevertheless, this method is not efficient for UHPC. Penetration of moisture from external curing into the interior of the element is hindered due to its dense microstructure. For overcoming this issue, a methodology called internal curing was proposed in the 1990s. Water reservoirs are mixed with cement during casting and then readily release water as needed to replace moisture lost through self-desiccation. Lightweight aggregates and super-absorbent polymers (SAP) are two common-used reservoirs for internal curing in conventional concrete and high strength concrete, while they have drawbacks in UHPC applications. Lightweight aggregates do not meet the requirement of the maximum size of aggregate in UHPC. SAP generates voids in the range of hundreds of micrometers after the release of water, which may negatively influence the durability of UHPC. Therefore, searching for new water reservoirs for internal curing in UHPC remains a motivation for researchers, which is also the principal objective of this research.

After extensively searching and studying, rice husk ash distinguishes itself from its porous structure and pozzolanic reactivity. The effect of rice husk ash on the mitigation of autogenous shrinkage for UHPC mixes was investigated in this research. The mechanisms behind the phenomenon were also studied and revealed. The following analysis and evaluations of these aspects will be given in detail below.

In Chapter 3, the onset of autogenous shrinkage was investigated in cement pastes with low water/cement ratios. The onset of internal RH drop is a more plausible start time of autogenous shrinkage for estimating the (autogenous) shrinkage caused by self-desiccation. This determination of the start time reduces the distraction from the different "time-zero" when autogenous shrinkage is evaluated.

In Chapter 4, RHA was produced by using a drum incinerator and ground to different fineness. The effect of various aspects of RHA on the autogenous shrinkage of cement pastes was studied experimentally. Some influencing parameters were identified:

a) Mean particle size of RHA

When the mean particle size is bigger than 15 μm, a large amount of superplasticizer is required to achieve a certain fluidity for cement pastes containing RHA [6]. When a mean particle size of less than 7 μm is strived at, the required grinding time increases rapidly. Therefore, for obtaining proper workability of the mixtures and saving energy, the mean particle sizes of RHA for the study were chosen to be 7.1 µm, 9 µm and 12.1 µm, respectively.

b) Cement replacement content by RHA

The workability of cement pastes is dramatically reduced with the increase of RHA content when the superplasticizer dosage is fixed. Therefore, the RHA dosage in the

study was limited to a maximum of 25%, which were 10%, 15%, 20% and 25%, respectively.

In Chapter 5, the mixture '20% RHA-9' (mean particle size 9 µm, cement replacement 20%) was defined as the research target since it nearly eliminated the observed autogenous shrinkage. For revealing the mechanism of mitigating the autogenous shrinkage by using RHA, several factors were investigated, respectively:

a) Liquid absorption capacity of RHA
b) Pozzolanic reaction of RHA

In Chapter 6, numerical simulation of internal curing in cement paste with RHA has been performed, aiming for a better understanding of the mechanism of RHA on mitigating autogenous shrinkage. An Internal Curing Simulation was proposed to describe the process of the self-desiccation in the cement-RHA mixtures. Within this model, it was assumed that the drop of saturation of pores in cement paste is instantaneously compensated by the water transported from RHA and redistributed in the cement matrix. The moisture exchange between RHA and cement paste is well described by The Internal Curing Simulation.

In Chapter 7, the effectiveness of RHA on mitigating the autogenous shrinkage of UHPC was evaluated. The cracking probability of UHPC with RHA was also investigated.

8.2 Conclusions

In this thesis, the possibility of using RHA to mitigate the autogenous shrinkage of UHPC was investigated by both experimental studies and numerical simulation. The general conclusions of this study are given as follows:

Onset of autogenous shrinkage

- The onset of internal RH drop is used as the start of autogenous shrinkage, which is more plausible for estimating the (autogenous) shrinkage caused by self-desiccation, comparing to the final setting time.

The optimization of RHA on the fineness and dosage

- The effect of the fineness of RHA, i.e., the mean particle size of 7.1 µm, 9 µm and 12.1 µm, on the autogenous shrinkage and self-desiccation of cement pastes was found to be neglectable. This is because the water absorption capacity and pozzolanic reaction extent of three different RHAs were both close.

- The autogenous shrinkage of cement pastes decreases with the increasing dosage of RHA. A larger dosage of RHA leads to a less significant drop of internal RH in cement pastes.

- With the optimized dosage (20%) and mean particle size (9 µm), the autogenous shrinkage of cement pastes at early age can be eliminated by using RHA.

Mechanism of mitigating the autogenous shrinkage by using RHA

- With the development of cement hydration, the self-desiccation occurs in cement paste, and a RH gradient is created between the RHA particle and the surrounding cement paste. Due to capillary suction and moisture diffusion, water gradually releases from RHA to cement pastes until a new RH equilibrant is reached. This amount of released water provides the internal curing for the mixture, thus counteracts self-desiccation and reduces the driving force of autogenous shrinkage.

- The pozzolanic reaction of RHA can intensify the self-desiccation and negatively affects the mitigation of autogenous shrinkage of cement pastes, but this influence is limited in 7 days.
- Comparing to the SAPs and lightweight aggregates, RHA is a competitive candidate as an internal curing agent.

Numerical simulation of internal curing

- The proposed model - Internal Curing Simulation was proved to be capable to describe the moisture exchange between RHA and cement paste.

Mitigating autogenous shrinkage in UHPC

- The incorporation of RHA dramatically reduces the autogenous shrinkage of UHPC in the first 14 days. The addition of RHA increases the compressive strength of UHPC, as same in the cement paste.
- The proneness to cracking in UHPC at early age is reduced with the addition of RHA, as observed from the restrained ring tests.

8.3 Contributions

The main contributions of this study are listed:

"Time-zero" is a critical terminology in the research field of autogenous shrinkage. The method for determining "time-zero" has been debated for decades, and no consensus has been reached up to date. In this research, an improved hygrometer method was proposed to monitor the internal RH change starting one hour after casting. With the help of this particular experimental result, the onset of internal RH drop is considered as a more plausible start time of autogenous shrinkage for estimating the autogenous shrinkage caused by self-desiccation. It is directly linked to the onset of self-desiccation, which corresponds to the time of initiation of the driving forces leading to autogenous shrinkage.

With the incorporation of optimized RHA, the early-age autogenous shrinkage of both the cement pastes and UHPC can be mitigated to less than 50 microstrains without the jeopardizing of strength.

Comparing to other internal curing agents, RHA has its own characteristics and advantages. Although the water absorption capacity of RHA is smaller than SAP, it can still retain a significant amount of water. Due to the smaller particle size than SAP, RHA is more convenient to distribute in dense concrete, especially in UHPC, for internal curing.

The Internal Curing Simulation is proved as a good numerical tool to study the mechanism of mitigating autogenous shrinkage in blended cement system. From the perspective of retarding the self-desiccation, the effects of pozzolanic reaction and internal curing are competitive phenomena. The pozzolanic reaction will intensify the self-desiccation, whereas the release of absorbed water by the internal curing agent will mitigate self-desiccation. It is hard to separate them and determine their contribution to the self-desiccation from the experimental result. Nevertheless, with the Internal Curing Simulation the effects of these two phenomena could be evaluated quantitatively and the effectiveness of internal curing agent was convincingly demonstrated.

8.4 Prospects

From this study, several aspects are recommended for future research:

- The water absorption capacity and pozzolanic activity are two critical factors that affect the efficiency of mitigating autogenous shrinkage by using RHA. Both aspects are related to the pore structure and amorphous silicate content of RHA, and are strongly influenced by the incineration process of rice husks. The effect of the burning procedure on the properties of RHA needs to be studied. If this effect can be described quantitatively, a customized internal curing agent based on RHA is expected to be manufactured for different purposes.

- The simulation of the moisture exchange between RHA and cement paste in this thesis assumes that the self-desiccation is practically instantaneously compensated by the curing water from RHA. Although the simulated result is consistent with the experimental result, the actual moisture transport is a time-dependent process. The Moisture Exchange & Reaction model can be modified in future to a time-dependent moisture transport model, which can more accurately describe and predict the RH change in cement paste containing RHA.

- Nowadays, global warming is a big challenge for the whole human race. The manufacture of clinker of Portland cement releases a mass of greenhouse gas (CO_2) to the environment. Minimizing the consumption of Portland cement is a possible solution as a response to climate change for the concrete industry. As an agriculture by-product, replacing cement by RHA in concrete can reduces the cost of concrete production and increases environmental benefits. However, the high-water demand constrains the increase of the RHA content in UHPC. In fact, it is known that the addition of some pozzolans like fly ash and blast furnace slag can improve the workability of fresh concrete. This gives an idea that the cement replacement level can be increased further by using RHA combined with these pozzolans. This aspect should be investigated.

Summary

Concrete made with Portland cement has good behaviour under compressive stress, but it is weak in tension. Cracking caused by tension is a typical problem in concrete practice. High autogenous shrinkage at early ages is one of the causes of cracking, especially in high/ultra-high performance concrete. In that stage shrinkage is strongly related to the decrease of relative humidity (RH) inside the concrete. To minimize the probability of cracking induced by autogenous shrinkage at early age, internal curing, which can provide moisture inside the concrete, has been proposed. Several internal curing agents, such as Super Absorbing Polymers (SAP) and saturated lightweight aggregate (LWA), are utilized in high performance concrete and have shown good results for mitigating autogenous shrinkage. The use of these agents, however, also have some drawbacks. Searching for an alternative internal curing methods for ultra-high performance concrete remains a challenge.

A possible candidate for serving as internal curing agent is rice husk ash (RHA). Rice husk ash distinguishes itself by its porous structure and pozzolanic reactivity. When the rice husk is incinerated completely under appropriate conditions, the residue, RHA, contains 90-96% amorphous silica and has a very high specific surface area due to its porous structure. The effect of rice husk ash on mitigating autogenous shrinkage for UHPC mixes was investigated in this research.

In the research field of autogenous shrinkage, there is a continuous debate on the methods for determining the onset of autogenous shrinkage. It was found that the onset of internal RH drop is a more plausible starting point for quantitative description of (autogenous) shrinkage caused by self-desiccation that the often used final setting time.

After determination of the onset of autogenous shrinkage, the effect of the fineness and dosage of RHA on the autogenous shrinkage of blend RHA-cement pastes were determined experimentally. With the optimized dosage (20%) and mean particle size (9 μm), the autogenous shrinkage of cement pastes can be eliminated almost completely by the mixed-in RHA.

Then, the mechanism of mitigating autogenous shrinkage by using RHA is evaluated. RHA, as a porous material, can absorb water during mixing and release it at later ages for internal curing, thus counteracting self-desiccation and reducing autogenous shrinkage. At the same time water is consumed by the pozzolanic reaction of RHA, intensifying self-desiccation. Results of autogenous shrinkage tests reveal that in mixture 20%RHA-9 the degree of pozzolanic reaction of RHA in 28 days is relatively small. This indicates that the effect of the first mechanism, i.e. internal curing by release of water by RHA particles, is more important than the effect of the water-consuming pozzolanic reaction of the RHA.

For a better understanding of these two effects of RHA on mitigating autogenous shrinkage, numerical simulations are performed. A model named Internal Curing Simulation is proposed to describe the evolution of the self-desiccation in the cement-RHA mixtures. The blended system consists of two powders, i.e. cement paste and RHA. For modelling the reaction processes, these two powders are considered, at first, separately. The hydrating cement paste is called system A, and the RHA is called system B. System B exhibits pozzolanic activity. The hydrating system A consumes water and gradually dries out. When this hydration process starts, water will flow from the saturated RHA particles to the drying cement matrix. From that moment on the rate of hydration of system A will be affected by the water coming from the system B (RHA). At the same time, however, the RHA reacts in a pozzolanic reaction. Since this pozzolanic reaction needs water, the water transport from

system B to system A will slow down, stops, or even water is taken from the hydrating cement paste for the pozzolanic reaction, potentially resulting in extra self-desiccation.

By comparing the measured and simulated internal RH, it could be shown that the Internal Curing Simulation describes the moisture exchange between RHA and cement paste quite well. From the perspective of retarding the self-desiccation, the effects of pozzolanic reaction and internal curing are competitive phenomena. The pozzolanic reaction of the RHA will intensify the self-desiccation, whereas the release of absorbed water by the RHA will mitigate self-desiccation. With the Internal Curing Simulation, the effects of these two phenomena could be evaluated quantitatively and the effectiveness of RHA as internal curing agent was convincingly demonstrated.

Finally, after the experimental and numerical study of RHA in cement pastes with low water-cement ratio, the effectiveness of RHA to mitigate autogenous shrinkage was illustrated by performing a classic ring test for studying the proneness to cracking of UHPC. The results showed that RHA is a promising additive indeed to mitigate autogenous shrinkage and proneness to cracking in UHPC.

To summarize, this thesis investigated the possibility of RHA as an internal curing agent in blended RHA-cement mixtures. With the optimized fineness and dosage of RHA, the early-age autogenous shrinkage of both the cement pastes and UHPC can be mitigated to less than 50 microstrains without jeopardizing the strength. The Internal Curing Simulation quantitatively described the effects of internal curing and pozzolanic reaction on mitigating autogenous shrinkage by using RHA quite well. It illustrated that numerical simulations can be most helpful to understand the role of RHA in mitigating autogenous shrinkage in low water-cement ratio mixtures and can be used for optimizing mixture designs of low-shrinkage concrete.

Samenvatting

Beton gemaakt met portlandcement gedraagt zich goed onder drukspanning, maar is zwak onder trekspanning. Scheurvorming als gevolg van trek is een typisch probleem bij het toepassen van beton. Grote autogene krimp bij jong beton is één van de oorzaken van scheurvorming, vooral in beton met (ultra)hoge sterke (UHPC). In jong verhardend beton is krimp sterk gerelateerd aan de afname van de relatieve vochtigheid (RV) in het beton. Om de kans op scheurvorming als gevolg van autogene krimp bij jong beton te minimaliseren, is interne nabehandeling voorgesteld, waarbij vocht in het beton wordt gebracht. Verschillende producten voor interne nabehandeling, zoals superabsorberende polymeren (SAP) en verzadigd lichtgewicht aggregaat (LWA), worden gebruikt in hoogwaardig beton en hebben goede resultaten opgeleverd voor het verminderen van autogene krimp. Het gebruik van deze middelen heeft echter ook een aantal nadelen. Het zoeken naar een alternatieve interne nabehandelingsmethode voor ultrahoogwaardig beton (UHPC) blijft een uitdaging.

Een kansrijke kandidaat voor interne nabehandeling is rijstkafas. Rijstkafas onderscheidt zich door zijn poreuze structuur en puzzolane reactiviteit. Wanneer rijstkaf onder de juiste omstandigheden wordt verbrand bevat het residu, RHA, 90-96% amorfe silica en heeft het door zijn poreuze structuur een zeer hoog specifiek oppervlak. Het effect van rijstkafas op het verminderen van autogene krimp voor UHPC-mengsels werd in dit onderzoek onderzocht.

Met betrekking tot autogene krimp is er een voortdurende discussie over de methoden om het aanvangstijdstip van autogene krimp te bepalen. In het onderzoek bleek dat de start van de interne RV-daling een plausibel uitgangspunt is voor de kwantitatieve beschrijving van (autogene) krimp door zelfuitdroging, beter dan de vaak gebruikte 'einde binding'.

Na het bepalen van het startmoment van de autogene krimp werd het effect van de fijnheid en de dosering van RHA op de autogene krimp van RHA-cementpastas experimenteel onderzocht. Met de geoptimaliseerde dosering (20%) en de gemiddelde deeltjesgrootte (9 μm) zorgt de toegevoegde RHA ervoor dat autogene krimp van cementpastas bijna volledig wordt geëlimineerd.

Vervolgens is het mechanisme van de vermindering van autogene krimp door het gebruik van RHA geëvalueerd. Als poreus materiaal kan RHA tijdens het mengen water opnemen en in latere stadia weer afgeven voor interne nabehandeling, waardoor zelfuitdroging wordt tegengegaan en autogene krimp wordt verminderd. Tegelijkertijd wordt echter ook water verbruikt voor de puzzolane reactie van RHA, waardoor de zelfuitdroging wordt versterkt. Uit de resultaten van de autogene krimpproeven blijkt dat in het mengsel 20%RHA-9 de mate van puzzolane reactie van RHA na 28 dagen nog relatief gering is. Dit wijst erop dat het effect van het eerste mechanisme, dat wil zeggen interne nabehandeling door afgifte van water door RHA-deeltjes, belangrijker is dan het effect van de water verbruikende puzzolane reactie van het RHA.

Voor een beter begrip van deze twee effecten van RHA op het verminderen van autogene krimp worden numerieke simulaties uitgevoerd. Een model met de naam Internal Curing Simulation wordt voorgesteld om de ontwikkeling van de autogene krimp in cement-RHA mengsels te beschrijven. Het gemengde systeem bestaat uit twee poeders, namelijk cementpasta en RHA. Voor de modellering van de reactieprocessen worden deze twee poeders eerst afzonderlijk beschouwd. De hydraterende cementpasta wordt systeem A genoemd en de RHA systeem B. Systeem B vertoont puzzolane activiteit. Het hydraterende systeem A verbruikt water en droogt geleidelijk uit. Wanneer dit hydratatieproces begint, stroomt er water van de verzadigde RHA-deeltjes naar de drogende cementmatrix. Vanaf dat

moment wordt de hydratatiesnelheid van systeem A beïnvloed door het water uit systeem B (RHA). Tegelijkertijd reageert het RHA echter in een puzzolane reactie. Aangezien deze puzzolane reactie water nodig heeft, zal het watertransport van systeem B naar systeem A vertragen, stoppen, of kan het zelfs zo zijn dat er water onttrokken wordt aan de hydraterende cementpasta voor de puzzolane reactie, wat mogelijk leidt tot extra zelfuitdroging.

Door de gemeten en gesimuleerde interne RV te vergelijken kon worden aangetoond dat de vochtuitwisseling tussen RHA en cementpasta vrij goed kon worden gesimuleerd. Vanuit het oogpunt van vertraging van de zelfuitdroging zijn de effecten van de puzzolane reactie en de interne nabehandeling concurrerende verschijnselen. De puzzolane reactie van RHA versterkt de zelfuitdroging, terwijl de afgifte van geabsorbeerd water door RHA de zelfuitdroging vermindert. Op basis van de gesimuleerde interne nabehandeling konden de effecten van deze twee verschijnselen kwantitatief worden geëvalueerd en kon de doeltreffendheid van RHA voor interne nabehandeling overtuigend worden aangetoond.

Na de experimentele en numerieke studie van RHA in cementpasta's met een lage water-cementfactor werd ten slotte de doeltreffendheid van RHA om autogene krimp tegen te gaan geïllustreerd door een klassieke ringtest uit te voeren om de scheurgevoeligheid van UHPC te bestuderen. De resultaten toonden aan dat RHA inderdaad een veelbelovend additief is om autogene krimp en scheurgevoeligheid in UHPC te verminderen.

Samengevat is in dit proefschrift de mogelijkheid van RHA als intern nabehandeling in RHA-cementmengsels onderzocht. Met de geoptimaliseerde fijnheid en dosering van RHA kan de vroegtijdige autogene krimp van zowel de cementpastas als UHPC worden beperkt tot minder dan 50 microrekken zonder dat dit de sterkte in gevaar brengt. De simulatie van interne nabehandeling beschreef kwantitatief de effecten van interne uitharding en puzzolane reactie op het verminderen van autogene krimp door het gebruik van RHA. Het illustreerde dat numerieke simulaties zeer nuttig kunnen zijn om de rol van RHA voor het verminderen van autogene krimp in mengsels met een lage water-cementfactor te begrijpen en kunnen worden gebruikt voor het optimaliseren en ontwerpen van mengsels voor krimparm beton..

Appendix

Parameters a and b determination in cement paste

Based on the best-known isotherm model (Brunauer-Emmett-Teller (BET) model [154]), Xi et al. [151] developed a mathematical model to predict adsorption isotherms of hardened cementitious materials. The adsorption of water in cementitious materials is affected by many parameters, such as type of cement, the water-to-cement ratio w/c, temperature T $[K]$ and curing time t $[d]$. The amount of adsorbed water W (kg in a unit volume of the material) can be calculated according to:

$$W = \frac{V_m' \cdot C \cdot k'' \cdot RH}{(1 - k'' \cdot RH) \cdot [1 + (C-1) \cdot k'' \cdot RH]} \tag{A.1}$$

where RH is the relative humidity, and V_m', C and k'' stand for:

$$C = exp\left(\frac{855}{T}\right), \quad k'' = \frac{(1 - 1/n') \cdot C - 1}{C - 1} \tag{A.2}$$

$$V_m' = \left(0.068 - \frac{0.22}{t}\right) \cdot \left(0.85 + 0.45 \cdot \frac{w}{c}\right) \cdot V_{ct} \tag{A.3}$$

$$n' = \left(2.5 + \frac{15}{t}\right) \cdot \left(0.33 + 2.2 \cdot \frac{w}{c}\right) \cdot N_{ct} \tag{A.4}$$

The value of V_{ct} and N_{ct} depends on the type of cement. For ordinary Portland cement, V_{ct} and N_{ct} are taken as 0.9 and 1.1, respectively. In the calculation, T is 293 [K], w/c is chosen to be 0.3 when w/c is less than 0.3 and t is chosen to be 5 when the age of cement paste is less than 5 days [151]. Note that this formula deals with cement pastes after the age of 0.25 days.

With the determined parameters (Eq. (A.2) - Eq. (A.4)), the adsorption isotherm of a hardened cement paste can be determined according to Eq. (A.1). The adsorption property of cement paste can be converted into the pore size distribution, and then helps to determine the parameters a and b.

A plain cement paste with w/c 0.18 is used as an example to show the calculation process. The pore size distribution of cement paste from adsorption isotherm is shown in Figure A.1.
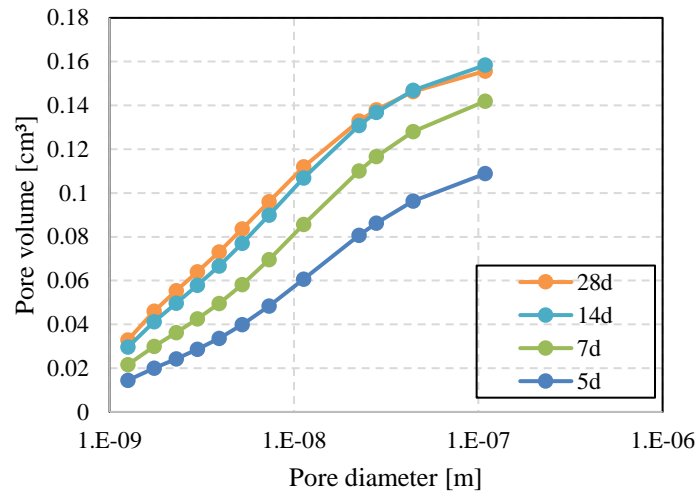
Figure A.1 Pore size distribution of cement paste (w/c=0.18) from the adsorption isotherm in Xi et al. [151]

As discussed in Chapter 6, a simple expression shown below is utilized in Internal Curing Simulation to describe the pore size distribution of cement paste.

$$V_{\leq d} = a \cdot (ln\, d) + b \tag{A.5}$$

Based on the result in Figure A.1, the parameters a and b with different ages can be determined. The ages can be converted to the degree of hydration by using HYMOSTRUC model. An evolution of the parameters a and b is obtained as shown in Figure A.2.
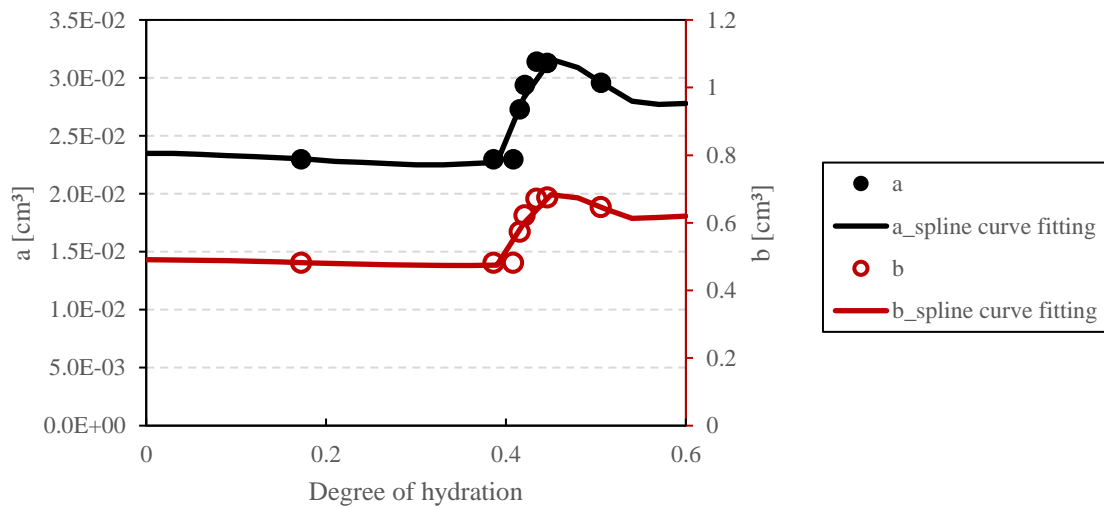
Figure A.2 Evolution of the parameters a and b of a cement paste with different DOH (w/c = 0.18)

Reference

1. Castro, J., et al. *Extending internal curing concepts to mixtures containing high volumes of fly ash*. in *International Bridge Conference*. 2010.

2. Dudziak, L. and V. Mechtcherine. *Mitigation of volume changes of ultra-high performance concrete (UHPC) by using super absorbent polymers*. in *Proceedings of the 2nd international symposium on ultra high performance concrete. Kassel University Press, Kassel*. 2008.

3. Shi, C., et al., *A review on ultra high performance concrete: Part I. Raw materials and mixture design*. Construction and Building Materials, 2015. **101**: p. 741-751.

4. FAO, *Rice market monitor*. Food and Agriculture Organization of the United Nations, 2018. **XXI**(No. 1).

5. Bui, D.D., *Rice husk ash a mineral admixture for high performance concrete*. 2001, Delft University of Technology.

6. Van Tuan, N., *Rice husk ash as a mineral admixture for ultra high performance concrete*. 2011, PhD thesis, Delft University of Technology, Delft, Netherlands.

7. Mehta, P.K., *Pozzolanic and cementitious byproducts as mineral admixtures for concrete-a critical review*. Special Publication, 1983. **79**: p. 1-46.

8. Cook, D., *Rice husk ash concrete technology and design, cement replacement materials, vol. 3*. 1986, London: Surrey University Press.

9. Mehta, P. and R.H.A.A.U. Supplementary, *Cementing Material, in 'Advances in Concrete Technology'*. 1994, CANMET.

10. Schmidt, M., et al., *Ultra-high performance concrete: Perspective for the precast concrete industry*. BETONWERK UND FERTIGTEILTECHNIK, 2003. **69**(3): p. 16-29.

11. Jensen, O.M. and P.F. Hansen, *Water-entrained cement-based materials: I. Principles and theoretical background*. Cement and concrete research, 2001. **31**(4): p. 647-654.

12. Bentz, D.P. and W.J. Weiss, *Internal curing: a 2010 state-of-the-art review*. 2011: US Department of Commerce, National Institute of Standards and Technology Gaithersburg, Maryland.

13. Schmidt, M. and E. Fehling, *Ultra-high-performance concrete: research, development and application in Europe*. ACI Special publication, 2005. **228**: p. 51-78.

14. Resplendino, J. and J. Petitjean, *Ultra high performance fiber reinforced concretes. Interim recommendations*. AFGC-SETRA, Bagneux, France, 2002.

15. Richard, P. and M. Cheyrezy, *Composition of reactive powder concretes*. Cement and concrete research, 1995. **25**(7): p. 1501-1511.

16. de Larrard, F. and T. Sedran, *Optimization of ultra-high-performance concrete by the use of a packing model*. Cement and concrete research, 1994. **24**(6): p. 997-1009.

17. Graybeal, B. *UHPC in the US highway transportation system*. in *Proceedings of the Second International Symposium on Ultra High Performance Concrete, Kassel, Germany*. 2008.

18. Rebentrost, M., G. Wight, and E. Fehling. *Experience and applications of ultra-high performance concrete in Asia*. in *2nd international symposium on ultra high performance concrete*. 2008.

19. Ma, J. and H. Schneider, *Properties of ultra-high-performance concrete*. Leipzig Annual Civil Engineering Report (LACER), 2002. **7**: p. 25-32.

20. Spasojevic, A., *Structural implications of ultra-high performance fibre-reinforced concrete in bridge design*. 2008, Epfl.

21. Long, G., X. Wang, and Y. Xie, *Very-high-performance concrete with ultrafine powders*. Cement and concrete research, 2002. **32**(4): p. 601-605.

22. Rougeau, P. and B. Borys. *Ultra high performance concrete with ultrafine particles other than silica fume*. in *Proceedings of the International Symposium on Ultra High Performance Concrete*. 2004.

23. Le, T.T., *Ultra high performance fibre reinforced concrete paving flags*. 2008, University of Liverpool.

24. Tafraoui, A., et al., *Metakaolin in the formulation of UHPC*. Construction and Building Materials, 2009. **23**(2): p. 669-674.

25. Aïtcin, P.-C., *Cements of yesterday and today: concrete of tomorrow*. Cement and Concrete research, 2000. **30**(9): p. 1349-1359.

26. Wang, D., et al., *A review on ultra high performance concrete: Part II. Hydration, microstructure and properties*. Construction and Building Materials, 2015. **96**: p. 368-377.

27. ASTM, A., *C1698-09 Standard test method for autogenous strain of cement paste and mortar*. ASTM International, West Conshohocken, PA, 2009.

28. Acker, P. and M. Behloul. *Ductal® technology: A large spectrum of properties, a wide range of applications*. in *Proc. of the Int. Symp. on UHPC Kassel, Germany*. 2004.

29. Nair, D.G., K. Jagadish, and A. Fraaij, *Reactive pozzolanas from rice husk ash: An alternative to cement for rural housing*. Cement and Concrete Research, 2006. **36**(6): p. 1062-1071.

30. Singh, B., *Rice husk ash*, in *Waste and Supplementary Cementitious Materials in Concrete*. 2018, Elsevier. p. 417-460.

31. Liou, T.-H. and C.-C. Yang, *Synthesis and surface characteristics of nanosilica produced from alkali-extracted rice husk ash*. Materials science and engineering: B, 2011. **176**(7): p. 521-529.

32. Boateng, A. and D. Skeete, *Incineration of rice hull for use as a cementitious material: The Guyana experience*. Cement and Concrete Research, 1990. **20**(5): p. 795-802.

33. Cook, D., *Rice-husk ash cements: Their development and applications*. 1984: United Nations Industrial Development Organization.

34. Bui, D., J. Hu, and P. Stroeven, *Particle size effect on the strength of rice husk ash blended gap-graded Portland cement concrete*. Cement and concrete composites, 2005. **27**(3): p. 357-366.

35. Zain, M.F.M., et al., *Production of rice husk ash for use in concrete as a supplementary cementitious material*. Construction and building materials, 2011. **25**(2): p. 798-805.

36. Nair, D.G., *Sustainable-affordable Housing for the Poor in Kerala*. 2006.

37. Malhotra, V.M., *Condensed silica fume in concrete*. 2018: CRC Press.

38. Huang, H., et al., *Influence of rice husk ash on strength and permeability of ultra-high performance concrete*. Construction and Building Materials, 2017. **149**: p. 621-628.

39. Chandrasekhar, S., et al., *Review processing, properties and applications of reactive silica from rice husk—an overview*. Journal of materials science, 2003. **38**(15): p. 3159-3168.

40. Sugita, S., et al. *On the semi-industrial production of highly reactive rice husk ash and its effect on cement and concrete properties*. in *International Congress on the Chemistry of Cement, Proceedings, Trondheim ICCC*. 1997.

41. Mehta, P. *Rice Husk Ash-A unique supplementary cementing material Proceeding*. in *International Symposium on Advances in Concrete Technology. Editor. Malhotra, VM Athens, Greece*. 1992.

42. Zhang, M.-H. and V.M. Malhotra, *High-performance concrete incorporating rice husk ash as a supplementary cementing material*. ACI Materials Journal, 1996. **93**: p. 629-636.

43. Bui, D.D., J. Hu, and P. Stroeven, *Particle size effect on the strength of rice husk ash blended gap-graded Portland cement concrete*. Cement and Concrete Composites, 2005. **27**(3): p. 357-366.

44. Ganesan, K., K. Rajagopal, and K. Thangavel, *Rice husk ash blended cement: Assessment of optimal level of replacement for strength and permeability properties of concrete*. Construction and Building Materials, 2008. **22**(8): p. 1675-1683.

45. Siddique, R., *Rice husk ash*, in *Waste materials and by-products in concrete*. 2008, Springer. p. 235-264.

46. James, J. and M.S. Rao, *Reactivity of rice husk ash*. Cement and concrete research, 1986. **16**(3): p. 296-302.

47. Yu, Q., et al., *The reaction between rice husk ash and Ca (OH) 2 solution and the nature of its product*. Cement and concrete research, 1999. **29**(1): p. 37-43.

48. Ordóñez, L., et al., *Reaction of rice husk ash with OPC and portlandite*. Advances in cement research, 2002. **14**(3): p. 113-119.

49. Feng, Q., et al., *Study on the pozzolanic properties of rice husk ash by hydrochloric acid pretreatment*. Cement and Concrete Research, 2004. **34**(3): p. 521-526.

50. Sivakumar, G. and R. Ravibaskar, *Investigation on the hydration properties of the rice husk ash cement using FTIR and SEM*. Applied Physics Research, 2009. **1**(2): p. 71.

51. Van Tuan, N., et al., *Hydration and microstructure of ultra high performance concrete incorporating rice husk ash*. Cement and Concrete Research, 2011. **41**(11): p. 1104-1111.

52. Hwang, C., *The Use of Rice Husk Ash in Concrete. Waste Materials Used in Concrete Manufacturing. Edited: Chandra, S*. 1997, Noyes Publications, USA.

53. Bentz, D.P., et al., *Influence of silica fume on diffusivity in cement-based materials: I. Experimental and computer modeling studies on cement pastes*. Cement and Concrete research, 2000. **30**(6): p. 953-962.

54. Le Chatelier, H., *Sur les changements de volume qui accompagnent le durcissement des ciments*. Bulletin Societe de l'encouragement pour l'industrie nationale, 1900. **5**.

55. Tazawa, E., *Macroscopic shrinkage of hardening cement paste due to hydration*. JCA Proceeding of Cement and Concrete, 1991. **45**: p. 122-127.

56. Jensen, O.M. and P.F. Hansen, *Autogenous deformation and RH-change in perspective*. Cement and Concrete Research, 2001. **31**(12): p. 1859-1865.

57. Lura, P., *Autogenous deformation and internal curing of concrete*. 2003, Delft University of Technology.

58. Breugel, K.v. *Numerical modelling of volume changes at early ages - Potential, pitfalls and challenges*. in *International RILEM Workshop on Shrinkage of Concrete: Shrinkage 2000*. 2000. Paris, France: RILEM Publications SARL.

59. Weiss, J., *Experimental determination of the'Time Zero', t0 ('Maturity-Zero', M0).* Early Age Cracking in Cementitious Systems, RILEM Report, 2003. **25**: p. 195-206.

60. Aitcin, P.-C., *Autogenous shrinkage measurement.* Autoshrink, 1998. **98**: p. 245-256.

61. Bentz, D.P. and O.M. Jensen, *Mitigation strategies for autogenous shrinkage cracking.* Cement and Concrete Composites, 2004. **26**(6): p. 677-685.

62. Lura, P., O.M. Jensen, and K. van Breugel, *Autogenous shrinkage in high-performance cement paste: an evaluation of basic mechanisms.* Cement and Concrete Research, 2003. **33**(2): p. 223-232.

63. Hua, C., P. Acker, and A. Ehrlacher, *Analyses and models of the autogenous shrinkage of hardening cement paste: I. Modelling at macroscopic scale.* Cement and Concrete research, 1995. **25**(7): p. 1457-1468.

64. Soroka, I., *Portland cement paste and concrete.* 1979: Macmillan International Higher Education.

65. Wittmann, F., *Grundlagen eines modells zur beschreibung charakteristischer eigenschaften des betons.* 1977: Ernst.

66. Powers, T.C. *Mechanism of shrinkage and reversible creep of hardened cement paste.* in *Proc. Int. Symp. Concr., London, 1965.* 1965.

67. Buil, M., *Contribution à l'étude du retrait de la pâte de ciment durcissante.* RAPP RECH LPC, 1979(92).

68. Jensen, O.M. and P.F. Hansen, *Autogenous relative humidity change in silica fume-modified cement paste.* Advances in Cement Research, 1995. **7**(25): p. 33-38.

69. Lu, T., *Autogenous shrinkage of early age cement paste and mortar.* 2019, Delft University of Technology.

70. Ferraris, C. and F.H. Wittmann, *Shrinkage mechanisms of hardened cement paste.* Cement and Concrete Research, 1987. **17**(3): p. 453-464.

71. Beltzung, F., F. Wittmann, and L. Holzer, *Influence of composition of pore solution on drying shrinkage.* 2001, Elsevier Science Ltd., Cambridge, MA. p. 39-48.

72. Scovazzo, P. and P. Todd, *Modeling disjoining pressures in submicrometer liquid-filled cylindrical geometries.* Journal of colloid and interface science, 2001. **238**(2): p. 230-237.

73. Israelachvili, J.N., *Intermolecular and surface forces.* 2011: Academic press.

74. Neville, A.M., *Properties of concrete.* Vol. 4. 1995: Longman London.

75. Winkler, E.M. and P.C. Singer, *Crystallization pressure of salts in stone and concrete.* Geological society of America bulletin, 1972. **83**(11): p. 3509-3514.

76. Tezuka, Y., et al. *Hydration characteristics and properties of mixtures of cement and high content of calcium.* in *Proc. Symp. on Chemistry of Cement, Rio de Janeiro, Bresil.* 1986.

77. Mejlhede Jensen, O., *Autogenous deformation and RH-change-selfdesiccation and selfdesiccation shrinkage.* TR, 1993. **284**: p. 93.

78. Vernet, C. and G. Cadoret, *Suivi en continu de l'évolution chimique et mécanique des BHP pendant les premiers jours.* Les Bétons à Hautes Performances-Caractérisation, durabilité, applications, Presse de ENPC, 1992.

79. Budnikov, P. and M. Strelkov, *Some recent concepts on Portland cement hydration and hardening.* Highway Research Board Special Report, 1966(90).

80. Van Breugel, K., *Simulation of hydration and formation of structure in hardening cement-based materials.* 1991.

81. Wittmann, F. *On the interaction of gel particles in hydrating Portland cement.* in *RILEM PROCEEDINGS.* 1992. CHAPMAN & HALL.

82. Mehta, P.K., *Mechanism of expansion associated with ettringite formation.* Cement and concrete research, 1973. **3**(1): p. 1-6.

83. Boivin, S.G., *Retrait au jeune age du béton.* Développement d'une méthode expérimentale et contribution à l'analyse physique du retrait endogène. Etudes et recherches des laboratoires des ponts et chaussées, série Ouvrage d'art OA, 2001. **37**.

84. Bentur, A., *2 Terminology and definitions.* Report 25: Early Age Cracking in Cementitious Systems-Report of RILEM Technical committee TC 181-EAS: Early age cracking shrinkage induced stresses and cracking in cementitious systems, 2002. **25**.

85. Chang-Wen, M., et al., *Water consumption of the early-age paste and the determination of "time-zero" of self-desiccation shrinkage.* Cement and concrete research, 2007. **37**(11): p. 1496-1501.

86. Darquennes, A., et al., *Effect of autogenous deformation on the cracking risk of slag cement concretes.* Cement and Concrete Composites, 2011. **33**(3): p. 368-379.

87. Sant, G., et al. *Examining time-zero and early age expansion in pastes containing shrinkage reducing admixtures (SRA's).* in *Proc., 2nd RILEM Symp. on Advances in Concrete through Science and Engineering.* 2006.

88. Institute, A.C., *ACI concrete terminology.* 2010.

89. Kovler, K. and O. Jensen, *Internal curing of concrete, state-of-the-art Report of RILEM Technical Committee 196-ICC.* RILEM Report, 2007. **41**.

90. Bremner, T. and J. Ries, *Stephen J. Hayde: Father of the Lightweight Concrete Industry.* Concrete international, 2009. **31**(8): p. 35-38.

91. Weber, S. *A blend of aggregates to support curing of concrete.* in *Proceedings of International Symposium on Structural Lightweight Concrete, Sandefjord, Norway, 1996.* 1996.

92. Van Breugel, K., H. de Vries, and K. Takada. *Mixture Optimization of Low Water/Cement Ratio, High-Strength Concretes in View of Reduction of Autogenous Shrinkage.* in *Int. Conf. on High Performance Concretes, Sherbrooke, Canada.* 1998.

93. Bentur, A. *Control of autogenous shrinkage stresses and cracking in high strength concrete, Utilization of high strength/High performance concrete.* in *Proc. of 5^< th> Intl. Symp.* 1999.

94. Jensen, O.M. and P.F. Hansen, *Water-entrained cement-based materials: II. Experimental observations.* Cement and Concrete Research, 2002. **32**(6): p. 973-978.

95. Mohr, B., et al. *Examination of wood-derived powders and fibers for internal curing of cement-based materials.* in *Proceedings of the 4th Interntational Seminar: Self-Desiccation and Its Importance in Concrete Technology.* 2005.

96. Philleo, R., *Concrete science and reality.* Materials Science of Concrete, 1991: p. 1-8.

97. Mechtcherine, V., L. Dudziak, and S. Hempel. *Internal curing to reduce cracking potential of Ultra High Performance Concrete by means of Super Absorbent Polymers.* in *Proceedings of 2nd International RILEM Workshop on Concrete Durability and Service Life Planning (ConcreteLife09).* 2009.

98. Justs, J., et al., *Internal curing by superabsorbent polymers in ultra-high performance concrete.* Cement and Concrete Research, 2015. **76**: p. 82-90.

99. Mechtcherine, V. and H.-W. Reinhardt, *Application of super absorbent polymers (SAP) in concrete construction: state-of-the-art report prepared by Technical Committee 225-SAP.* Vol. 2. 2012: Springer Science & Business Media.

100. Gawin, D., F. Pesavento, and B.A. Schrefler, *Hygro‑thermo‑chemo‑mechanical modelling of concrete at early ages and beyond. Part I: hydration and hygro‑thermal phenomena.* International Journal for Numerical Methods in Engineering, 2006. **67**(3): p. 299-331.

101. Wyrzykowski, M., et al., *Modeling of internal curing in maturing mortar.* Cement and Concrete Research, 2011. **41**(12): p. 1349-1356.

102. Lawrence, M.G., *The relationship between relative humidity and the dewpoint temperature in moist air: A simple conversion and applications.* Bulletin of the American Meteorological Society, 2005. **86**(2): p. 225-234.

103. Taylor, H.F., *Cement chemistry.* Vol. 2. 1997: Thomas Telford London.

104. Jensen, O.M. and P.F. Hansen, *A dilatometer for measuring autogenous deformation in hardening Portland cement paste.* Materials and structures, 1995. **28**(7): p. 406-409.

105. EN, D., *Methods of testing cement—part 3: determination of setting times and soundness.* 2009.

106. Ye, G., et al., *Study on the development of the microstructure in cement-based materials by means of numerical simulation and ultrasonic pulse velocity measurement.* Cement and Concrete Composites, 2004. **26**(5): p. 491-497.

107. Ye, G., *Experimental study and numerical simulation of the development of the microstructure and permeability of cementitious materials.* 2003.

108. *Technical report Isothermal Conduction Calorimetry (ICC) for the determination of heat of hydration of cement: State of Art Report and Recommendations, Ref. No. EUROPEAN COMMITTEE FOR STANDARDIZATION, FprCEN/TR 16632:2013: E.* 2013.

109. Van Breugel, K., *Simulation of hydration and formation of structure in hardening cement-based materials.* 1993.

110. Koenders, E.A.B., *Simulation of volume changes in hardening cement-based materials.* 1997.

111. Zhang, M., *Multiscale lattice Boltzmann-finite element modelling of transport properties in cement-based materials.* 2013.

112. Stauffer, D., *Introduction to Percolation Theory, Francis & Taylor.* 1985, London.

113. Tuan, N.V., G. Ye, and K. van Breugel. *Mitigation of early age shrinkage of ultra high performance concrete by using rice husk ash.* in *3rd International Symposium on UHPC and Nanotechnology for High Performance Construction Materials: Ultra-High Performance Concrete and Nanotechnology in Construction (HIPERMAT-2012).* 2012. Kasse University Press GmbH.

114. Rößler, C., D.-D. Bui, and H.-M. Ludwig, *Rice husk ash as both pozzolanic admixture and internal curing agent in ultra-high performance concrete.* Cement and Concrete Composites, 2014. **53**: p. 270-278.

115. de Sensale, G.R., A.B. Ribeiro, and A. Gonçalves, *Effects of RHA on autogenous shrinkage of Portland cement pastes.* Cement and Concrete Composites, 2008. **30**(10): p. 892-897.

116. Cook, R.A. and K.C. Hover, *Mercury porosimetry of hardened cement pastes.* Cement and Concrete research, 1999. **29**(6): p. 933-943.

117. Ye, G., *Experimental study and numerical simulation of the development of the microstructure and permeability of cementitious materials*. 2003, Delft University of Technology.

118. Diamond, S., *A critical comparison of mercury porosimetry and capillary condensation pore size distributions of portland cement pastes.* Cement and concrete research, 1971. **1**(5): p. 531-545.

119. Cook, R.A. and K.C. Hover, *Mercury porosimetry of cement-based materials and associated correction factors.* Construction and Building Materials, 1993. **7**(4): p. 231-240.

120. Midgley, H., *The determination of calcium hydroxide in set Portland cements.* Cement and Concrete Research, 1979. **9**(1): p. 77-82.

121. Zhao, S., et al., *Expression and Clinical Significance of Sushi Domain- Containing Protein 3 (SUSD3) and Insulin-like Growth Factor-I Receptor (IGF-IR) in Breast Cancer.* Asian Pac J Cancer Prev, 2015. **16**(18): p. 8633-6.

122. Bhatty, J.I. and K.J. Reid, *Use of thermal analysis in the hydration studies of a type 1 portland cement produced from mineral tailings.* Thermochimica acta, 1985. **91**: p. 95-105.

123. Marsh, B.K. and R.L. Day, *Pozzolanic and Cementitious Reactions of Fly-Ash in Blended Cement Pastes.* Cement and Concrete Research, 1988. **18**(2): p. 301-310.

124. Vedalakshmi, R., et al., *Quantification of hydrated cement products of blended cements in low and medium strength concrete using TG and DTA technique.* Thermochimica Acta, 2003. **407**(1-2): p. 49-60.

125. Scrivener, K.L., *Backscattered electron imaging of cementitious microstructures: understanding and quantification.* Cement and Concrete Composites, 2004. **26**(8): p. 935-945.

126. Scrivener, K.L., et al., *Analysis of phases in cement paste using backscattered electron images, methanol adsorption and thermogravimetric analysis.* MRS Online Proceedings Library Archive, 1986. **85**.

127. Mouret, M., E. Ringot, and A. Bascoul, *Image analysis: a tool for the characterisation of hydration of cement in concrete–metrological aspects of magnification on measurement.* Cement and Concrete Composites, 2001. **23**(2-3): p. 201-206.

128. Ma, Y., *Microstructure and Engineering Properties of Alkali Activated Fly Ash-as an environment friendly alternative to Portland cement.* 2013.

129. Lumley, J., et al., *Degrees of reaction of the slag in some blends with Portland cements.* Cement and Concrete Research, 1996. **26**(1): p. 139-151.

130. Escalante, J., et al., *Reactivity of blast-furnace slag in Portland cement blends hydrated under different conditions.* Cement and Concrete Research, 2001. **31**(10): p. 1403-1409.

131. Luke, K. and F.P. Glasser, *Internal chemical evolution of the constitution of blended cements.* Cement and Concrete Research, 1988. **18**(4): p. 495-502.

132. Haha, M.B., K. De Weerdt, and B. Lothenbach, *Quantification of the degree of reaction of fly ash.* Cement and Concrete Research, 2010. **40**(11): p. 1620-1629.

133. Taylor, H.F., K. Mohan, and G. Moir, *Analytical study of pure and extended Portland cement pastes: I, pure Portland cement pastes.* Journal of the American Ceramic Society, 1985. **68**(12): p. 680-685.

134. Kocaba, V., E. Gallucci, and K.L. Scrivener, *Methods for determination of degree of reaction of slag in blended cement pastes.* Cement and Concrete Research, 2012. **42**(3): p. 511-525.

135. Papadakis, V.G., *Experimental investigation and theoretical modeling of silica fume activity in concrete.* Cement and Concrete Research, 1999. **29**(1): p. 79-86.

136. Page, C. and Ø. Vennesland, *Pore solution composition and chloride binding capacity of silica-fume cement pastes.* Matériaux et construction, 1983. **16**(1): p. 19-25.

137. Ghourchian, S., et al., *An investigation on the use of zeolite aggregates for internal curing of concrete.* Construction and Building Materials, 2013. **40**: p. 135-144.

138. Wittmann, J., *Physikalisch-chemische Veränderungen bei der Herstellung und Lagerung von Dosenwürstchen.* 1969, Verlag nicht ermittelbar.

139. Bentz, D.P. and P.E. Stutzman, *Internal curing and microstructure of high performance mortars.* ACI SP-256, Internal Curing of High Performance Concretes: Laboratory and Field Experiences, 2008: p. 81-90.

140. Zhutovsky, S., K. Kovler, and A. Bentur, *Influence of cement paste matrix properties on the autogenous curing of high-performance concrete.* Cement and Concrete Composites, 2004. **26**(5): p. 499-507.

141. Bentz, D.P. and K.A. Snyder, *Protected paste volume in concrete: Extension to internal curing using saturated lightweight fine aggregate.* Cement and concrete research, 1999. **29**(11): p. 1863-1867.

142. Lura, P., et al., *Measurement of water transport from saturated pumice aggregates to hardening cement paste.* Materials and Structures, 2006. **39**(9): p. 861-868.

143. Lura, P., et al., *Kinetics of Water Migration in Cement-Based Systems Containing Superabsobent Polymers*, in *Application of Super Absorbent Polymers (SAP) in Concrete Construction*. 2012, Springer. p. 21-37.

144. Nestle, N., et al., *Water balance and pore structure development in cementitious materials in internal curing with modified superabsorbent polymer studied by NMR.* Microporous and Mesoporous Materials, 2009. **125**(1-2): p. 51-57.

145. Trtik, P., et al. *Neutron tomography investigation of water release from superabsorbent polymers in cement paste.* in *International Conference on Material Science and 64th RILEM Annual Week*. 2010.

146. Wyrzykowski, M., et al., *Modeling of Water Migration during Internal Curing with Superabsorbent Polymers.* Journal of Materials in Civil Engineering, 2012. **24**(8): p. 1006-1016.

147. Hua, D., *Transport Processes in Hydrating Cementitious Coating Systems*. 2018, Delft University of Technology.

148. Trtik, P., et al., *Release of internal curing water from lightweight aggregates in cement paste investigated by neutron and X-ray tomography.* Nuclear Instruments and Methods in Physics Research Section A: Accelerators, Spectrometers, Detectors and Associated Equipment, 2011. **651**(1): p. 244-249.

149. Koenders, E., *Simulation of volume changes in hardening cement-based materials [Ph. D. thesis].* Delft University of Technology, Delft, The Netherlands, 1997.

150. Gao, P., *Simulation of hydration and microstructure development of blended cements*. 2018, Delft University of Technology.

151. Xi, Y., Z.P. Bažant, and H.M. Jennings, *Moisture diffusion in cementitious materials adsorption isotherms.* Advanced cement based materials, 1994. **1**(6): p. 248-257.

152. Shah, H. and J. Weiss, *Quantifying shrinkage cracking in fiber reinforced concrete using the ring test.* Materials and structures, 2006. **39**(9): p. 887.

153. Park, J.-J., et al., *Benefits of using expansive and shrinkage-reducing agents in UHPC for volume stability.* Magazine of concrete research, 2014. **66**(14): p. 745-750.

154. Gregg, S. and K. Sing, *Adsorption, surface area and porosity, Acad.* Press, London, 1982. **3**.

List of publications

Huang, H., & Ye, G. (2017) Examining the "time-zero" of autogenous shrinkage in high/ultra-high performance cement pastes. Cement and Concrete Research, 97, pp.107-114.

Ye G., Huang H., Van Tuan N. (2018) Rice Husk Ash. In: De Belie N., Soutsos M., Gruyaert E. (eds) Properties of Fresh and Hardened Concrete Containing Supplementary Cementitious Materials. RILEM State-of-the-Art Reports, Vol. 25. Cham, Switzerland: Springer.

T. Lu, Z. Li, and H. Huang (2021) Restraining effect of sand on shrinking cement mortar and concrete, Construction and Building Materials, 289, 123166.

T. Lu, Z. Li, and H. Huang (2020) Effect of supplementary materials on the autogenous shrinkage of cement paste, Materials, 13(15), 3367.

Huang, H., Ye, G. (2018) Experimental study on autogenous shrinkage of cement pastes incorporating RHA. In 4th International Conference on Service Life Design for Infrastructures (SLD4), Delft, Netherlands.

Huang, H., Ye, G., Fehling, E., Middendorf, B., & Thiemicke, J. (2016). Use of rice husk ash for mitigating the autogenous shrinkage of cement pastes at low water cement ratio. In Proceedings of the HiPerMat2016 4th international symposium on ultra-high performance concrete and high performance construction materials, Kassel, Germany (pp. 9-11).

Lyu, Y., H. Huang, Ye, G., & De Schutier, G. (2015). Autogenous shrinkage of zeolite cement pastes with low water-binder ratio. In 14th International Congress on the Chemistry of Cement (ICCC 2015) (pp. 1-8).

Huang, H., & Ye, G. (2014) Examining the "Time-Zero" of autogenous shrinkage in cement pastes at low water cement ratio. In International RILEM Conference on Application of Superabsorbent Polymers and Other New Additives in Concrete Construction, Dresden, Germany (pp. 189-200).
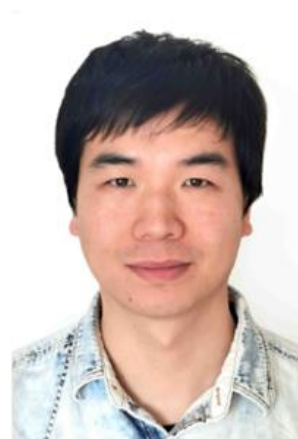
Huang, H., Ye, G., & Van Tuan, N. (2013) Use of rice husk ash for mitigating the autogenous shrinkage of ultra-high performance concrete. International Conference SBE2013 "Sustainable Built Environment for Now and The Future", March 26-27, Hanoi, Vietnam.

Curriculum Vitae

Hao Huang

Date of birth: 10 August, 1986
Place of birth: Xiaogan, China

2011.09 ~ 2023.6

PhD

Delft University of Technology, Delft, The Netherlands

2009.9 ~ 2011.6

Master of Materials Engineering

Wuhan University of Technology, Wuhan, China

2005.9 ~ 2009.6

Bachelor of Materials Science and Technology

Wuhan University of Technology, Wuhan, China